Philipps Universität Marburg

Influence of the *in vivo* half-antibody exchange on the therapeutic efficacy of an IgG4 antibody-drug conjugate

DISSERTATION

zur Erlangung des Doktorgrades der Naturwissenschaften

(Dr. rer. nat.)

dem Fachbereich Biologie

der Philipps-Universität Marburg

vorgelegt von

Peter Herbener

aus Marburg

Marburg an der Lahn, 2018

Vom Fachbereich Biologie der Philipps-Universität Marburg (Hochschulkennziffer: 1180)

als Dissertation angenommen am: 22. Mai 2018

Erstgutachter: PD Dr. Jude Przyborski

Zweitgutachter: Prof. Dr. Uwe Maier

Tag der mündlichen Prüfung: 05. Juni 2018

Major results of this thesis have been published:

Herbener, Peter; Schönfeld, Kurt; König, Martin; Germer, Matthias; Przyborski, Jude M.; Bernöster, Katrin; Schüttrumpf, Jörg (2018): Functional relevance of in vivo half antibody exchange of an IgG4 therapeutic antibody-drug conjugate. In PLoS ONE 13 (4), e0195823. DOI: 10.1371/journal.pone.0195823.

Other topic-related publications:

Schönfeld, Kurt; Herbener, Peter; Zuber, Chantal; Häder, Thomas; Bernöster, Katrin; Uherek, Christoph; Schüttrumpf, Jörg (2018): Activity of Indatuximab Ravtansine against Triple-Negative Breast Cancer in Preclinical Tumor Models. In Pharmaceutical research 35 (6), p. 118. DOI: 10.1007/s11095-018-2400-y.

The present work was conducted in the department of Translational Reseach at Biotest AG, Landsteinerstraße 5, 63303 Dreieich under the supervision of PD Dr. Jörg Schüttrumpf.

Biotest

Zusammenfassung

In den vergangen Jahren ist die Anzahl der in der präklinischen und klinischen Entwicklung befindlichen monoklonalen Antikörper und abgewandelten Derivaten, wie Antikörper-Wirkstoff-Konjugate, zur Behandlung von Krebserkrankungen rapide gestiegen. Abhängig davon, ob Antikörper-Wirkstoff-Konjugate zusätzliche Effektorfunktionen vermitteln sollen, wird häufig der IgG1 oder andernfalls der IgG4 Subtyp verwendet. Letzterer ist bekannt dafür nahezu keine antikörperabhängige zellvermittelte Zytotoxizität oder komplementabhängige Zytolyse zu vermitteln und wird daher hinsichtlich der Patentensicherheit bevorzugt. Eine weitere Besonderheit unveränderter IgG4 Antikörper ist ihre Fähigkeit einen zufälligen Halbantikörperaustausch *in vivo* zu vollziehen, der in der Bildung von bivalenten, bispezifischen Antikörpern resultiert. CD138 ist ein Oberflächenrezeptor, der in Zell-Zell Interaktionen, Proliferation und Migration involviert ist und in verschiedenen Krebsarten, u.a. dem Multiplem Myelom, stark überexprimiert wird. BT062 (Indatuximab Ravtansine) ist ein monoklonaler, Wildtyp IgG4-basierter anti-CD138 Antikörper, an den zytotoxische DM4 Moleküle (ein Derivat des Maytansinoids) gekoppelt sind. Aktuell wird BT062 in einer klinischen Studie zur Behandlung des Multiplen Myeloms getestet. Um die Auswirkungen des Halbantikörperaustausches auf die Funktionalität und Wirksamkeit von Antikörper-Wirkstoff-Konjugaten am Beispiel von BT062 zu untersuchen, wurden folgende Modelantiköper generiert: Ein (I) Wildtyp nBT062; ein (II) stabilisierter nBT062, der durch die Mutationen S228P und R409K nicht mehr in der Lage ist einen Halbantikörperaustauch zu vollziehen; ein (III) halber nBT062, der durch Substitution von Cystein zu Serin an Position 226 und 229 keine kovalente Dimerisierung bilden kann; und ein (IV) bispezifischer nBT062-Natalizumab Antikörper, der jeweils monovalent die Antigene CD138 und CD49d erkennt. Alle vier nBT062 Antikörper wurden in CHO-S Zellen exprimiert und durch Affinitätschromatographie mit Protein A aufgereinigt. Die analytische Charakterisierung durch elektrophoretische Methoden, Western Blot und Größenausschlusschromatographie bestätigte die Reinheit und durch die Mutationen eingefügten strukturellen Eigenschaften der Antikörper. Analysen mit NCI-H929 ($CD138^+/CD49d^+$), Ba/F3-hCD138 ($CD138^+/CD49d^-$) und Jurkat ($CD138^-/CD49d^+$) Zellen zeigten, dass alle Modelantikörper spezifisch und mit nanomolarer Affinität an CD138 binden konnten und anschließend in die Zellen internalisiert wurden. Nach erfolgreicher Konjugation mit dem zytotoxischen Agens DM4 wurde mittels *in vitro* Zellzytotoxizitätsversuchen gezeigt, dass alle nBT062-DM4 Varianten das Wachstum von Tumorzellen inhibieren konnten (IC_{50}: ~80-460 pM). Der direkte Einfluss des Halbantikörperaustauschs auf die Wirksamkeit wurde *in vivo* in einem Xenograft-Mausmodel getestet. nBT062-Natalizumab-DM4 zeigte dabei nur ohne zusätzliche Anwesenheit von humanen IgG4 Antikörpern eine geringe Wirksamkeit. Wildtyp, stabilisierter und halber nBT062-DM4 hatten eine sehr gute antitumorale Wirkung. Allerdings wurde die Wirksamkeit

des Wildtyp und halben nBT062-DM4 in einer niedrigen Dosierung durch die Anwesenheit von humanem IgG4 reduziert. In Mausplasmen konnte für diese beiden Modelantikörper der Halbantikörperaustausch nachgewiesen werden, wohingegen der stabilisierte nBT062-DM4 diesem Mechanismus nicht unterlag. Die Ergebnisse zeigen, dass sich der Einbau von Mutationen zur Unterbindung des IgG4 Halbantikörperaustausches positiv auf die antitumorale Wirksamkeit von Antikörper-Wirkstoff-Konjugaten ausübt.

Abstract

A high number of therapeutic antibodies and their derivates *e.g.* antibody-drug conjugates (ADC) are under preclinical or clinical evaluation for the treatment of cancer. Most of those ADCs are based on the IgG1 or IgG4 subtype, depending on whether additional effector functions are desired or not. In contrast to IgG1, IgG4 is hardly capable to induce antibody-dependent cell-mediated or complement-dependent cytotoxicity and thus IgG4-based ADCs with cytotoxic payloads targeting only proliferating cells may have a preferred safety profile. Another unique property of the IgG4 subtype is the *in vivo* exchange of half-antibodies, resulting in random bispecific antibodies. BT062 (indatuximab ravtansine) is an ADC composed of an anti-CD138 IgG4 antibody conjugated to the highly cytotoxic maytansin derivate DM4. BT062 is currently evaluated in a clinical trial for the treatment of multiple myeloma. To investigate the influence of IgG4 half-antibody exchange on the functional properties and efficacy of ADCs, the following BT062 model antibodies mimicking the different process-derived antibody species were generated: (I) Wildtyp (WT) nBT062; (II) stable nBT062, comprising S228P and R409K mutations to prevent IgG4 shuffling *in vivo*; (III) half nBT062, serving as a model of the transistant state as C226S and C229S amino acid substitutions lead to the lack of covalent half antibody dimerization; and (IV) bispecific nBT062-natalizumab monovalently recognizing CD138 and CD49d antigens. All nBT062 variants were produced in FreeStyle CHO-S cells and purified by protein A affinity chromatography. Electrophoresis, western blotting and size exclusion chromatography were used to confirm the purification quality and provide first evidence on the aimed characteristics of each antibody due to the introduced mutations. *In vitro* analyses on NCI-H929 ($CD138^+/CD49d^+$), Ba/F3-hCD138 ($CD138^+/CD49d^-$) and Jurkat ($CD138^-/CD49d^+$) cells demonstrated nanomolar binding activities of all nBT062 variants towards CD138 followed by antigen-mediated internalization. After successful conjugation with model-corresponding quanities of DM4, resulting ADCs were investigated by an *in vitro* cytotoxicity assay. All nBT062-DM4 variants were capable to inhibit tumor cell proliferation by picomolar quanitities (IC_{50}: ~80-460 pM). The MAXF 1322 xenograft mouse model was used to directly assess the influence of IgG4 shuffling *in vivo*. Bispecific nBT062-natalizumab-DM4 was the least potent model demonstrating only a boarderline efficacy even without the presense of human IgG4. WT nBT062-DM4, stable nBT062-DM4 and half nBT062 were highly effective against the tumor cells. At a low dosage, the efficacy of WT nBT062-DM4 and half nBT062-DM4 was reduced by the presence of human IgG4, while stable nBT062-DM4 was hardly affected. Analysis of mouse plasma samples confirmed the formation of bispecific antibodies out of WT nBT062-DM4 and half nBT062-DM4, but no half-antibody exchange was detected within samples of stable nBT062. These data clearly demonstrate an advantage of incorporating half-antibody exchange-preventing mutations into IgG4-based ADCs.

Contents

Abbreviations

Short term	Long term
ADC	Antibody-drug conjugate
ADCC	Antibody-dependent cellular cytotoxicity
ADCP	Antibody-dependent cell-mediated phagocytosis
AML	Acute myeloid leukemia
APC	Antigen-presenting cell
APLP2	Amyloid Precursor Like Protein 2
BCR	B cell receptor
Bs	bispecific
BWL	Body weight loss
C	Constant
CD	Cluster of differentiation
CD138/ hCD138	Human Syndecan-1
CD49d	Integrin α4
CDC	Complement-dependent cytotoxicity
CDR	Complementarity-determining region
CF	Correction factor
CHO	Chinese Hamster Ovary
CHO-S	Suspension Chinese Hamster Ovary (cells)
CIP	Cleaning-in-place
CMV	Cytomegalovirus
CNS	Central nervous system
CTLA-4	Cytotoxic T lymphocyte antigen-4
CV	Column volume
Da	Dalton
DAR	Drug-to-antibody ratio; DM4-to-antibody ratio
DC	Dendritic cell
DF	Dilution factor
DHFR	Dihydrofolate reductase
DM4	N2′-deacetyl-N2′-(4-mercapto-4-methyl-1-oxopentyl)-maytansine
DMA	Dimethylacetamid
DPBS	Dulbecco's Phosphate-Buffered Saline
DTT	Dithiothreitol
DVD	Double-variable domain
ECL	Electrochemiluminescence
EDTA	Ethylenediaminetetraacetic acid

ELISA	Enzyme-linked immunosorbent assay
FA	Formic acid
Fab	Fragment antigen binding
FACS	Fluorescence-activated cell sorting
Fc	Fragment-crystallizable
FcRn	Neonatal fragment-crystallizable receptor
FCS	Forward scatter
FcγR	Fragment-crystallizable gamma receptor
FDA	US Food and Drug Administration
FGF-2	Fibroblast growth factor 2
Fr	Variable framework
FRET	Förster resonance energy transfer
Fv	Variable fragment
GSH	Reduced glutathione
GSSG	Oxidized glutathione
H	Heavy
HAT	Hypoxanthine-aminopterin-thymidine
HEK-293	Human Embryonic Kidney-293
HEPES	4-(2-hydroxyethyl)-1-piperazineethanesulfonic acid
HER2	Human epidermal growth factor receptor 2
HESI	Heated electrospray ionization
HGF	Hepatocyte growth factor
HGPRT	Hypoxanthine:guanine phosphoribosyl transferase
HLA-DR	Human leukocyte antigen-DR
HPLC	High performance liquid chromatography
i.v.	intravenous
IAA	Iodoacetic acid
IC50	Half-maximal inhibitory concentration
IEF	Isoelectric focusing
Ig	Immunoglobulin
IgSF	Immunoglobulin superfamily
IRES	Internal ribosome entry site
IVIg	Intravenous immunoglobulin
KiH	Knobs-into-holes
L	Light
LAMP-1	Lysosomal-associated membrane protein 1
LBA	Ligand binding assay

LC-ESI-MS	Liquid chromatography - electrospray ionization time-of-flight mass spectrometry
LC-MS	Liquid chromatography - mass spectrometry
LPAM	Lymphocyte Peyer patch adhesion molecule
LpL	Lipoprotein lipase
mAb	Monoclonal antibody
MAC	Membrane attack complex
MAdCAM-1	Mucosal addressin cell adhesion molecule-1
MAXF	Mammary cancer xenograft Freiburg
MFI	Median fluorescence intensity
MHC	Major histocompatibility complex
MOI	Multiplicity of infection
MTX	Methotrexate
MWCO	Molecular weight cut off
nBT062	Naked BT062
NEM	N-Ethylmaleimide solution
NHS	N-hydroxysuccinimide
NK	Natural killer
NMRI	Naval Medical Research Institute
NMRI nu/nu	Athymic immunodeficient mutant on NMRI background
NS/0	Non-immunoglobulin secreting
PDX	Patient-derived tumor xenograft
PE	R-Phycoerythrin
pI	Isoelectric point
PK	Pharmacokinetics
PPIA	Peptidylprolyl isomerase A
PVDF	Polyvinylidene fluoride
qRT-PCR	Quantitative real time polymerase chain reaction
RPMI	Roswell Park Memorial Institute
RTV	Relative tumor volume
SANC	Sample negative control
sCD138	Soluble Sydecan-1
SCID	Severe combined immunodeficient
SCNC	Standard curve negative control
SDS-PAGE	Sodium dodecyl sulfate polyacrylamide gel electrophoresis
SEC	Size exclusion chromatography
SPDB	N-succinimidyl-4-(2-pyridyldithio)butanoate

SSC	Sideward scatter
TCR	T cell receptor
TFA	Trifluoroacetic acid
TGF-ß1	Transforming growth factor ß1
T_H cell	$CD4^+$ T-lymphocyte
TPA	Tripropylamine
V	Variable
VCAM-1	Vascular cell adhesion molecule-1
VEGF	Vascular endothelial growth factor
VLA-4	Very-late antigen 4, consisting of integrin α4β3
VSVG	Vesicular stomatitis virus glycoprotein
WST-1	(4-[3-(4-Iodophenyl)-2-(4-nitrophenyl)-2H-5-tetrazolio]-1,3-benzene disulfonate)
WT	Wild type

List of Figures

List of Tables

1 Introduction

1.1 The human immune system

The immune system consists of a variety of effector cells and molecules that protect the body from four categories of disease-causing microorganisms: Viruses, fungi, bacteria and parasites (Murphy, Weaver 2017; Male et al. 2007). It can be subdivided into the innate and adaptive immune system. Innate immunity represents the first line of defense against pathogens: It reacts in an antigen-unspecific manner within minutes after pathogen entry. Neutrophils, eosinophils, basophils, monocytes, macrophages, natural killer (NK) cells and dendritic cells (DCs) are the major cell types of the innate immune response. Antigen-presenting cells (APCs) like DCs bridge the innate and adaptive immunity by activating the latter one, including B and T cells. These cells are mainly responsible for the characteristics of the adaptive immune system: It reacts antigen-specific *e.g.* by antibodies (immunoglobulins) or $T_{effector}$ cells and it features immunological memory, leading to a more effective response at a repeated antigen exposure (Male et al. 2007). These properties render the adaptive immunity highly effective against pathogens.

1.2 Cancer evolves when the immune system fails

Cancer is one of the major causes of death worldwide besides cardiovascular diseases in industrialized nations (World Health Organization (WHO) 2017). The most common deathly cancers are female breast, lung, liver, stomach, colorectal, and prostate cancer (Torre et al. 2015). Hanahan and Weinberg described eight major hallmarks of cancer, namely sustaining proliferative signaling, evading growth suppressors, resisting cell death, reprogramming of energy metabolism, enabling replicative immortality, inducing angiogenesis, activating invasion and metastasis, and evading immune destruction (Hanahan, Weinberg 2011). Genome instability, fostering genetic diversity, seems to be the major underlying cause of these hallmarks (Hanahan, Weinberg 2011). As single mutations are rarely unable to induce tumor development, multiple alterations in several tumor-related genes are necessary for malignant tumor growth (Croce 2008). Besides protecting the host from pathogens, the immune system does also survey transformed cells which may induce cancer (Smyth et al. 2001). A number of different immune cells can be involved by several mechanisms: Cluster of differentiation (CD) 4^+ and $CD8^+$ T cells are able to recognize either tumor specific antigens or overexpressed, non-mutated proteins on the cell surface (*e.g.* p53 and Her2/neu) due to their T cell receptors (TCR) and induce apoptosis of those cells (Igney, Krammer 2002). As cells of the innate immune system macrophages and neutrophils are involved in cancer immunosurveillance by either destruction of tumor vessels, inhibition of angiogenesis

or even by direct cell killing. Furthermore, macrophage s and neutrophils are capable to stimulate cytotoxic T cells, NK cells and APCs by tumor antigen presentation (Elgert et al. 1998; Di Carlo et al. 2001; Igney, Krammer 2002). NK cells survey body cells for appropriate expression of self-antigens. If no self-antigen is expressed on the surface of a cell, it will by lyzed by the NK cell (Kärre 2008). Tumor cells have evolved several mechanisms to escape the immune response: The tumor stroma can serve as physical barrier between tumor and immune cells (Igney, Krammer 2002). Furthermore, tumor cells are able to downregulate the tumor antigens or mutate them to escape from an initial immune response (Kim et al. 1975; Stackpole et al. 1980). In addition, major histocompatibility complex (MHC) I is downregulated to prevent presentation of foreign antigens to T cells. Cancer cells could also express MHC surrogates to prevent NK cell activation (Farrell et al. 1997; Cretney et al. 1999). By the expression of cytokines (*e.g.* TGF-ß and IL-10) malignant cells are able to suppress the immune response. The expression of anti-apoptotic molecules and or downregulation of pro-apoptotic molecules saves the tumor from apoptosis (Torre-Amione et al. 1990; Matsuda et al. 1994; Medema et al. 1999; Igney, Krammer 2002). Tumors might also induce apoptosis through CD95L expression of CD95-sensitive immune cells as reported by Walker and coworkers (Walker et al. 1998). To stop malignant tumor growth, there are several types of cancer treatments, including surgery, chemotherapy, radiation therapy, stem cell transplantations, immunotherapy and others. As one type of the immunotherapy, monoclonal immunoglobulins are one of the most successful therapeutic strategies for hematologic and solid tumors (Scott et al. 2012a).

1.3 Immunoglobulins

In the 1890s, immunoglobulins (Igs) were first discovered by Emil von Behring and Shibasaburo Kitasato as an agent in the serum of animals which was able to induce a short-lived protection in humans against diphtheria or tetanus toxin (Murphy, Weaver 2017; Schroeder, Cavacini 2010). Igs or frequently designated as antibodies are glycoproteins of the immunoglobulin superfamily which further includes for example MHC proteins, antibody receptors, many lymphocyte cell-surface proteins, but also growth factor receptors and others (Lander et al. 2001). Igs are able to bind specifically to particular surface structures referred to as epitopes present on foreign, native proteins, glycoproteins, polysaccharides, bacteria, and viral particles. They can be membrane-bound to B cells as B cell receptors (BCR) or are present as soluble proteins in the blood and tissue fluids (Male et al. 2007). Due to their binding, soluble Igs can participate in host defense either by direct neutralization of these foreign objects or by inducing effector functions such as activating the classical complement pathway or effector cells depending on the type of Ig. This Ig mediated immunity is known as humoral immunity (Navolotskaya 2014; Murphy, Weaver 2017).

1.3.1 B lymphocytes produce antibodies

In response to a foreign antigen, antibodies are secreted by differentiated B cells. To initiate antibody production, APCs have to internalize respective pathogens at the place of infection. During the APCs migration to the lymphatic tissues, *e.g.* lymph nodes, the pathogen is processed within the endosome due to acid-dependent proteases. Pathogen-specific peptides are loaded intracellularly onto the MHC II and the resulting complex is further presented on the APC's surface. Naïve $CD4^+$ T-lymphocytes (T_H cells) recognize those MHC II peptide complexes and become activated. In parallel, circulating naïve B cells must encounter their specific pathogen and bind it by their BCR. Antigen-mediated crosslinking of the BCRs induces internalization followed by pathogenic proteolyzation. While migrating to lymphatic tissues, pathogenic peptides are presented in complexes with MHC II molecules on the B cell surface. Those MHC II antigen complexes are recognized by TCRs of T_H cells. Additionally, co-stimulatory signals are required and induced by interactions of CD28 and CD40 on the surface of the B cell with B7 and CD154 expressed on the T_H cell's surface. This induces cytokine secretion by the T_H cell, causing B cell proliferation and differentiation into either antibody-secreting plasma cells or memory cells (Murphy, Weaver 2017) (see Figure 1-1).

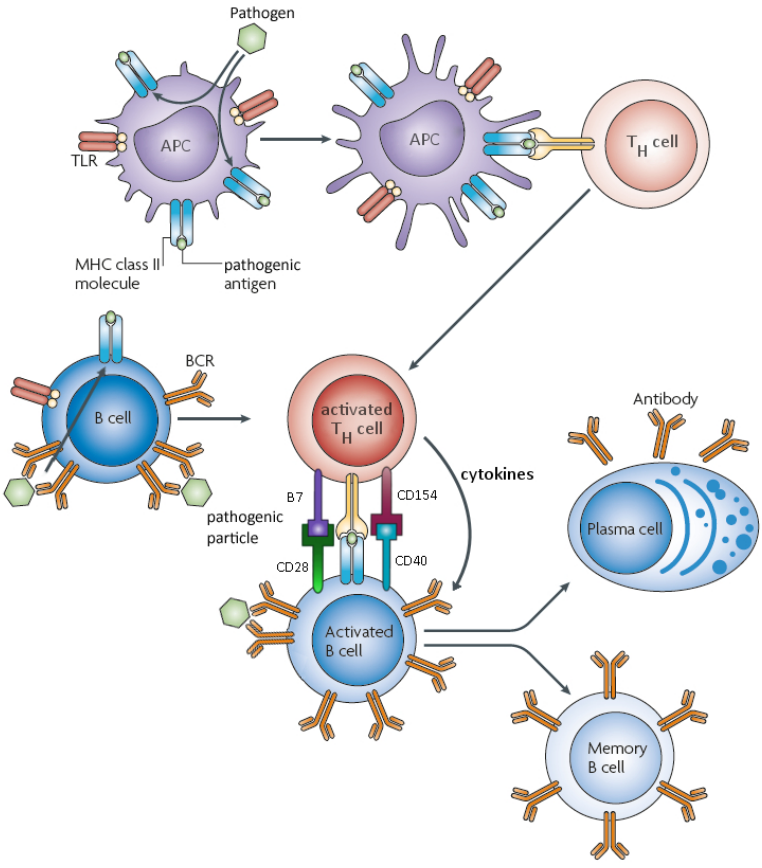

Figure 1-1: Activation of humoral immunity.
Pathogens are internalized and processed by antigen presenting cells (APCs). Respective antigens are presented in complex with MHC II molecules. Naive T_H cells become activated by recognizing those antigen-MHC II complexes. Naive B cells bind pathogens by their B cell receptors (BCR) and process them upon internalization for MHC II antigen presentation. This MHC II antigen complex is bound by activated T_H cells, while CD40/CD154 and B7/CD28 interactions mediate a co-stimulatory signal. Cytokine secretion of the T_H cells results in B cell activation leading to differentiation into either antibody-secreting plasma cells or memory B cells, depending on the cytokine milieu (adapted from Bachmann, Jennings 2010).

1.3.2 Antibody isotypes and structure

Igs belong to the immunoglobulin superfamily (IgSF) (Williams, Barclay 1988). Five different classes, referred to as isotypes, are known in humans: IgA, IgD, IgE, IgG and IgM. IgA is further divided into IgA1 and IgA2, while IgG is separated in four subtypes, namely IgG1, IgG2, IgG3, and IgG4. Serum IgA, IgD, IgE and IgG are present as monomers, but IgA is also available as dimer in secretions. IgM is the only multimeric antibody, present as pentamer or hexamer (Male et al. 2007; Rojas, Apodaca 2002; Navolotskaya 2014) (see Figure 1-2 A). The monomeric structure represents a Y-shaped molecule which is based on two identical heavy (H) and two identical light (L) chains (Berlot et al. 2015). Five different H chain molecules α, γ, δ, ε or μ define the immunoglobulins isotypes. L chains are separated in κ or λ. Within one immunoglobulin neither the isotype, subclass nor the light chain classification is mixed (Bayry et al. 2007). Each H and L chain comprises a variable domain (V) on the N-terminal protein site and a C-terminal constant region (C). While L chains are built up of one C domain, H chains have three to four. Both, V and C domains consist of 110 to 130 amino acids, resulting in a molecular weight of approx. 12,000 to 13,000 Da. Each of both domains contains two sandwiched ß-pleated sheets linked by a disulfide-bond of two conserved cysteines (Williams, Barclay 1988; Schroeder, Cavacini 2010)(see Figure 1-2 B). L chains are attached and covalently bound by a disulfide bond to the V and first C (CH1) domain of the H chain, thereby creating the fragment antigen binding (Fab) region. Within this, the dimerized variable domains of the H and L chain create the variable fragment (Fv) mediating the antigen-specific binding (Inbar et al. 1972). This distinct specificity is mediated by three hyper-variable complementarity-determining regions (CDR) within the V domains. These CDRs are surrounded by four conserved framework regions (Schroeder, Cavacini 2010). The Y-shape results from dimerization of two heavy chains. H chains comprising only 3 C domains tend to have a space region, referred to as hinge, between the CH1 and CH2 domains which is absent in H chains comprising 4 C domains (Schroeder, Cavacini 2010). Cysteins in the hinge region stabilize H chain dimerization by covalent disulfide bonds. The dimerized C domains of the H chain result in the fragment-crystallizable (Fc) region. The Fc portion mediates effector functions by interacting with Fc receptors on several immune cells, induces the complement system due to C1q binding and influences the antibodies' half-life by neonatal Fc receptor (FcRn) recycling mechanisms (Morea et al. 2000; Bayry et al. 2007; Murphy, Weaver 2017).

Immunoglobulins are expressed by B lymphocytes upon interaction with T_H cells and cytokine secretion due to the latter cell type (see 1.3.1). The cytokine milieu defines the expression of the Ig isotype and subclass based on nine CH genes. During B cell differentiation, the antigen specificity of the Ig's V domain is defined by complex

recombination of V, D and J gene cluster downstream to the CH genes (Honjo 1983; Schroeder, Cavacini 2010).

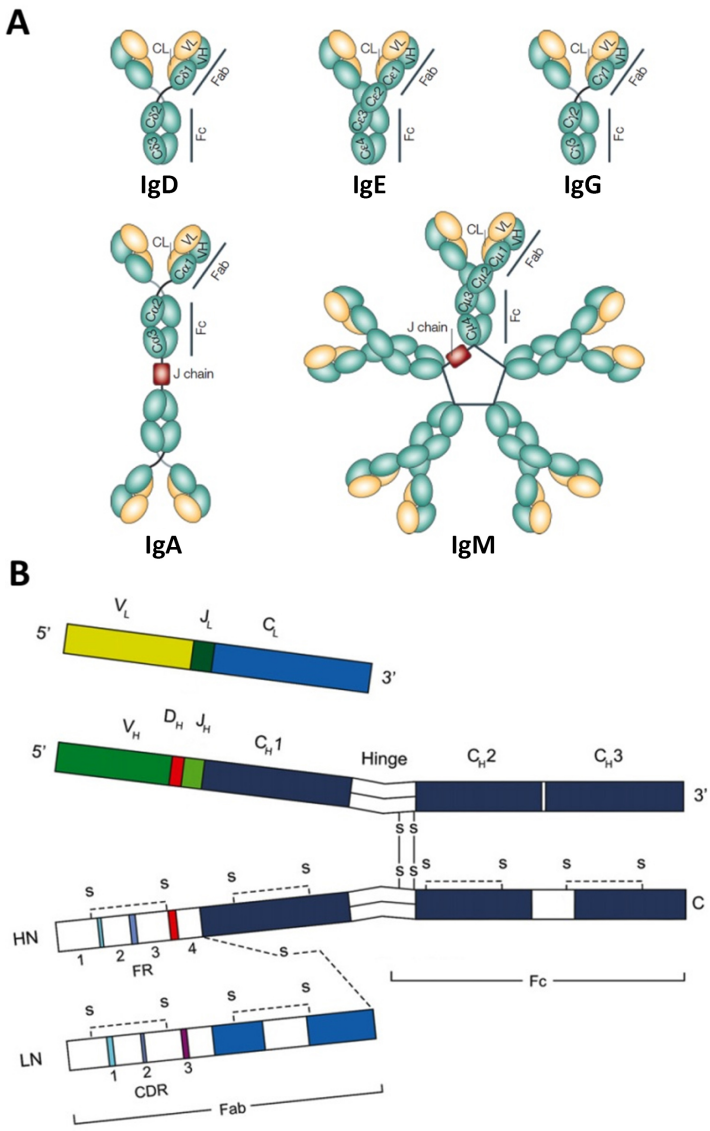

Figure 1-2: Antibody isotypes and basic IgG structure.
A: Humans have five different immunoglobulin isotypes: IgD, IgE and IgG are monomeric, IgA is a dimer in secretions and IgM is typically a pentamer. Each monomeric backbone is composed of two heavy (H, green) and two light chains (L, yellow), while the number of constant domains within the H chains differs between isotypes. Multimeric antibodies incorporate an associated J chain (polypeptide, red box) (adapted from Rojas, Apodaca 2002).
B: Typical structure of an IgG molecule. The two upper boxes represent L and H chains structured into regions encoded by specific genes. Variable (V) and constant (C) domains are marked as well as regions expressed by D and J genes. The two boxes at the bottom represent the IgG's protein domains. Antibodies contain a fragment-crystallizable (Fc) region mediating an immune response (e.g. receptor binding) and a fragment antigen-binding (Fab) region. Three complementarity-determining regions (CDR) define the antigen specificity surrounded by four sections of the framework region (Fr). Both H chains are covalently bound by two disulfide bonds in the hinge region (Adapted from Schroeder, Cavacini 2010).

1.4 Effector functions of IgG

The IgG isotype accounts for approx. 70-75% of all antibodies in human serum and approx. 10-20% of all plasma proteins, thus it is one of the most abundant proteins besides albumin. The four IgG subclasses IgG1, IgG2, IgG3 and IgG4 split in proportions of approx. 60, 32, 4, and 4 %, respectively (Male et al. 2007; Vidarsson et al. 2014). In contrast to other IgG subclasses, the serum concentration of IgG4 has a high variability in the human population ranging from less than 10 µg/ml to > 2 mg/ml (Aucouturier et al. 1984). IgG antibodies have several mechanisms to inactivate invading microorganisms and foreign pathogens. They can bind to receptors or their ligands, thereby inhibit their interactions or neutralize infectious agents such as bacterial toxins by blocking their function sites (Capra 1997). However, most

effector functions are mediated by the antibodies' Fc interacting with certain innate receptors or adaptor molecules. The major adaptor molecule is C1q, inducing complement-dependent cytotoxicity (CDC). Upon IgG binding to antigens on cellular surfaces, C1q attaches to the antibody resulting in a disposition of C3b to enable further phagocytosis of the target (opsonization), while simultaneously the formation of the membrane attack complex (MAC), C5-C9, is initiated. The latter one is a transmembrane channel inducing osmotic lysis of the target cell. Neither IgG2 nor IgG4 antibodies are able to induce the complement pathway as they lack C1q binding activities (Tao et al. 1993; Nirula et al. 2011; Vidarsson et al. 2014; Murphy, Weaver 2017). Another major effector function is antibody-dependent cellular cytotoxicity (ADCC). For its activation, IgG antibodies specifically bound to target cells, are detected by fragment crystallizable gamma receptors (FcγR) expressed on the surface of effector cells. Upon binding, these cells release several molecules such as cytokines and cytotoxic enzymes *e.g.* perforines, inducing membrane damage, and granzymes leading to apoptosis induction. ADCC is mainly mediated by IgG1 or IgG3 antibodies activating NK cells, but neutrophils, macrophages and eosinophils are also compatible (Woof, Burton 2004; Murphy, Weaver 2017). Antibody-dependent cell-mediated phagocytosis (ADCP) is a further important mode of action induced by antibodies. It is primarily guided by IgG3 and IgG1 antibodies interacting with FcγRIIa on macrophages. However, monocytes, neutrophils and DCs are also capable to phagocytose antibody-bound microorganisms or particles (Weiskopf, Weissman 2015).

In general, the IgG1 and IgG3 subtypes interact with high affinity and efficiently with most of the FcγR, while IgG2 and IgG4 have a diminished affinity to several of those receptors. For example, FcγRI is bound by IgG1, IgG3 and IgG4 but the latter one demonstrates a reduced binding resulting in decreased phagocytic activity and subsequent degradation of antibody-antigen complexes (Nimmerjahn, Ravetch 2008; Vidarsson et al. 2014). FcγRIII is mainly responsible for NK cell activation during ADCC and has a very low affinity for IgG4. Thus, this subtype is hardly capable to induce this effector function. Nevertheless, the allotype of the receptor and the glycoform of the antibody can influence this binding (Jefferis 2012). In addition, IgG4 has a minor binding activity to the inhibiting FcγRIIb/c making them hardly able to reduce active immune responses (Murphy, Weaver 2017). The binding affinity to FcRn is similar among the four IgG subclasses (Jefferis 2005, 2007; Nirula et al. 2011). FcRn mediates bidirectional IgG transcytosis across epithelial cells (Kuo, Aveson 2011). This very weak affinity for FcγRs and the lack of C1q binding results in reduced effector functions and the lack of CDC due to IgG4 antibodies, which might be the reason why IgG4 antibodies are a preferred subclass for immunotherapy, where host's effector functions are undesired (Nirula et al. 2011).

1.5 IgG4 is exchanging half-antibodies

Besides demonstrating strongly limited effector functions, the IgG4 subclass possesses a further unique property: They are able to exchange half-antibodies (H+L) *in vivo* leading to the formation of bispecific antibodies (see Figure 1-3A). This phenomenon was disabused by several findings: While blood-derived, polyclonal IgG4 antibodies are not capable to crosslink two identical antigens and thus act functionally monovalent, chimeric, monoclonal IgG4 antibodies are able to do so (Aalberse et al. 1983; Schuurman et al. 1999). In 1999, Schuurman and colleagues have demonstrated the existence of bispecific antibodies: In human sera of patients containing IgG4 antibodies against house dust mites and grass pollen, they found antibodies crosslinking both, radiolabeled house dust mite and sepharose-coupled grass pollen allergens (Schuurman et al. 1999; Nirula et al. 2011). Furthermore, non-reducing sodium dodecyl sulfate polyacrylamide gel electrophoresis (SDS-PAGE) of IgG4 antibodies has obtained half-antibody fractions (Aalberse, Schuurman 2002). The presence of IgG4 half-antibody exchange was finally proven by injecting anti-Betv1 and anti-Feld1 IgG4 antibodies into immunodeficient nude mice: Administration of equal amounts of anti-Betv1 and anti-Feld1 antibodies resulted in approx. 50% bispecific anti-Betv1/Feld1 antibodies. Administration of both antibodies in combination with 20-fold excess of an IgG4 with irrelevant specificity strongly decreased the detection of bispecific anti-Betv1/Feld1 antibodies in the antigen crosslinking assay, indicating a random exchange of half-antibodies (van der Neut Kolfschoten, Marijn et al. 2007). Young et al. additionally demonstrated in 2014 that endogenous polyclonal IgG4 antibodies undergo half-antibody exchange in humans as they detected antibodies containing both, one κ and one λ light chain (Young et al. 2014).

The sequence and structure of IgG4 and IgG1 are highly similar but two important amino acid changes are mainly responsible for the ability of IgG4 to perform half-antibody exchange: P228 and K409 in IgG1 are changed to S228 and R409 in IgG4. S228 is located in the IgG4 hinge region and constitutes a CXXC motif, which contains two cysteines building the two covalent disulfide bonds linking the two half-antibodies. IgG1 molecules comprise a CPPC motif creating sufficient space between the two cysteines, that they are only able to form interchain disulfide bonds with a second IgG1 half antibody. In contrast, IgG4 antibodies comprise a CPSC motif resulting in a decreased distance between the two cysteines allowing the formation of either inter- or intrachain disulfide bonds (Aalberse, Schuurman 2002; Schuurman et al. 2001)(see Figure 1-3B). R409 is the crucial residue at the CH3-CH3 interface, weakening the non-covalent interactions between these domains and allowing half-antibody exchange (Labrijn et al. 2011; Davies et al. 2014). Incorporation of S228P and R409K mutations into IgG4 antibodies separately prevent IgG4 shuffling, while P228S and K409R mutations in IgG1 antibodies result in half-antibody exchange (Labrijn et al. 2011).

However, the function of naturally occurring half-antibody exchange of endogenous IgG4 antibodies has not yet been fully clarified. It has been proposed that bispecific IgG4 antibodies may dampen inflammatory responses, as they lack antigen cross-linking besides lacking major effector functions (van der Neut Kolfschoten, Marijn et al. 2007).

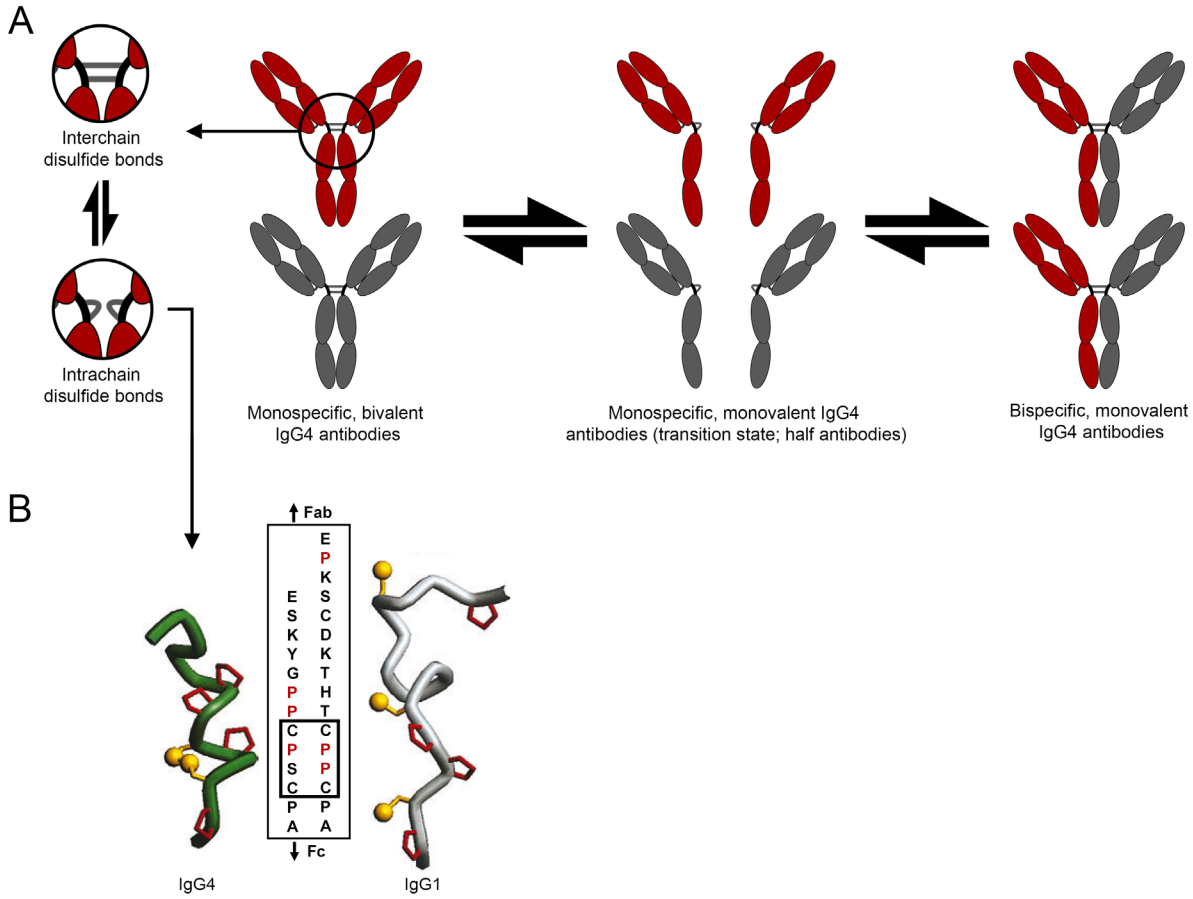

Figure 1-3: Mechanism of IgG4 half-antibody exchange.

A: Schematic illustration of the dynamic half-antibody exchange process *in vivo*. **B:** 3D peptide models of the hinge region of IgG4 (left) and IgG1 (right) with respective amino acids indicated. Demonstrated is the reduced distance of the two cysteines by the IgG4's CPSC motif resulting in intrachain disulfide bonds. In contrast, IgG1 is only capable of H interchain disulfide bond bridging based the CPPC motif. Cysteines are shown in yellow, prolines in red (B adapted from Aalberse, Schuurman 2002).

1.6 Generation of monoclonal antibodies

A method for the unlimited production of antibodies with a known antigen specificity was published by Köhler and Milstein in 1975. Apart from minor changes, it is still the most commonly used technique for antibody production today. It is based on the immunization of mice with an antigen of interest to produce spleen cells secreting antibodies with the respective specificity. These spleen cells are isolated and fused with polyethylene glycol to immortal, antibody non-secreting myeloma cells lacking the enzyme hypoxanthine:guanine phosphoribosyl transferase (HGPRT) to generate hybrid cells referred to as hybridoma. For

hybridoma selection, the cells are grown in hypoxanthine-aminopterin-thymidine (HAT) medium. HGPRT metabolizes hypoxanthine to purines, which are necessary for DNA synthesis, while aminopterin blocks purine as well as thymidine synthesis. Therefore, non-fused myeloma cells die due to the lack of HGPRT and non-fused spleen cells die after a few days because of their limited lifespan. Antibody-producing hybridoma cells are isolated and single clones are used to produce monoclonal antibodies (Murphy, Weaver 2017). Application of murine monoclonal antibodies induces immune responses in humans (Sgro 1995; Mak, Saunders 2006; Harding et al. 2010). To reduce this risk chimeric or humanized antibodies are used. For chimerization, murine genes encoding the constant H and L regions are replaced in the hybridoma genome by homologous human genes through homologous recombination (Fell et al. 1989). For the generation of humanized antibodies, CDRs within an expression vector containing the sequence of a fully human antibody are replaced by the antigen specific, murine CDRs. Transfection of cell lines (*e.g.* CHO, HEK-293, SP2) with these vectors results in the secretion of humanized, antigen-specific antibodies. Since both antibody types, chimeric and humanized, still have a likelihood to induce an immune response against the administered therapeutic antibody, it is also possible to create fully human therapeutic antibodies by the use of transgenic mice. These mice are generated by introducing human immunoglobulin loci segments into the germlines of mice deficient in murine antibody production. After immunization with an antigen and the use of the hybridoma technique fully human, monoclonal antibodies can be produced *in vitro* (Green et al. 1994; Jakobovits 1995).

1.6.1 Isotype selection of therapeutic monoclonal antibodies

Currently, most of the approved therapeutic monoclonal antibodies (mAb) are based on the IgG class, mainly because of practical and functional concerns (Salfeld 2007; Jefferis 2012; Irani et al. 2015). Beside the antigen specificity, the isotype selection is an important aspect during the generation of therapeutic mAbs as it defines effector functions (see section 1.4) and antibody half-life. If effector functions like ADCC and CDC are desired, IgG1 and IgG3 are suitable as they bind all FcγRs with high affinity. However, IgG3 has not been used for therapeutic mAb development so far, probably due to the reduced serum half-life, lack of protein A binding for purification or the high number of IgG3 allotypes across populations (Irani et al. 2015). For neutralization of soluble antigens, where effector functions are less relevant, IgG1, IgG2 and IgG4 are suitable. In contrast to other IgG subclasses, IgG4 has superior anti-inflammatory activity which is preferred for targeted delivery of therapeutic conjugates or receptor blocking without cell depletion (Labrijn et al. 2009). The strongly diminished effector functions of IgG4 antibodies reduce the risk of side effects by undesired immune reactions. However, several mutations for each IgG subclass are known to further

enhance or diminish interactions with FcγRs or extending the half-life by increasing FcRn binding (Wang et al. 2017).

1.6.2 Generation of bispecific antibodies

Within recent years, bispecific antibody formats capable to bind two distinct antigens have gained high interest for therapeutic or diagnostic approaches (Brinkmann, Kontermann 2017). First, recombinant bispecific antibodies were produced in the 1980s by simple coexpression of both different IgGs due to the fusion of two different hybridoma cells, referred to as hybrid hybridomas or quadroma cells (Milstein, Cuello 1983). This resulted in up to 9 unwanted H and L chain pairings leading to only up to 10-50% of the desired bispecific species (Milstein, Cuello 1983; Suresh et al. 1986a, 1986b). Since then, several approaches for heterogenic H chain – H chain interactions were developed *e.g.* (I) disulfide bond pairing by introduction of cysteine pairs into the CH3 domains, (II) salt bridges by oppositely charged residues for each of the different H chains, and (III) the knobs-into-holes (KiH) strategy based on the substitution of either smaller or respectively bigger amino acids in the opposite H chains (Ridgway et al. 1996; Merchant et al. 1998; Carter 2001). The heterogenic H chain pairing of the letter KiH strategy was further improved by phage display and incorporation of cysteine based disulfide bridging resulting in up to 95% heterodimers (Atwell et al. 1997; Carter 2001). However, all attempts of heterogenic H chain pairing suffered from random L chain pairing resulting in approx. 25% of the desired bispecific antibody. If possible, this was avoided by the use of a common light chain (Kontermann, Brinkmann 2015). The first genetic solution for this issue was provided by the CrossMab technology (Schaefer et al. 2011): The CH1 domain of the H chain was exchanged with the C domain of the respective L chain leading to mostly correct H-L chain pairing. Another elegant method for overcoming the H-L chain pairing problem is based on the introduction of several mutations within the respective C and V regions of each H and L chains, termed orthogonal Fab interface leading to nearly 100% correct pairing (Lewis et al. 2014). However, beside classical bispecific antibodies comprising two H and two L chains several other bispecific formats have been developed making it possible to choose from a pool of up to 50 different approaches *e.g.* double-variable domain (DVD)-Igs, double svFcs, diabodies, SEEDbodies and so on (Kontermann 2012; Brinkmann, Kontermann 2017).

1.7 Immunotherapy: monoclonal antibodies for cancer treatment

For the treatment of solid tumors and hematological malignancies antibody-based immunotherapy is one of the most promising strategies. These antibodies can mediate tumor cell killing by several mechanisms: (I) Indirectly by mediating ADCC or ADCP, (II) by inducing the complement pathway (CDC), (III) by activation and regulation of T cells, or (IV) directly by the antibody (see Figure 1-4). In the latter case, the therapeutic antibody might cause receptor blockade, induction of apoptosis or target-mediated delivery of a drug. Several antibodies having effects on tumor vasculature and stroma have been successfully applied in the clinic (Scott et al. 2012b). Tumor antigens bound by therapeutic monoclonal antibodies can be separated into several categories: Hematopoietic differentiation antigens, cancer/testes antigens, glycoproteins expressed by solid tumors, glycolipids, carbohydrates, anti-angiogenic targets, growth factors or receptors and stromal and extracellular matrix antigens (Scott et al. 2012b). Today, there are 23 therapeutic monoclonal antibodies approved by the US Food and Drug Administration (FDA) against different tumor-associated antigens and many more are under investigation (Cai 2016). In 1997, the first monoclonal antibody referred to as rituximab was approved by the FDA to treat B-cell non-Hodgkin lymphomas which were resistant to other chemotherapy regimens (Grillo-López et al. 2002). Rituximab binds to CD20 expressed on B cells, induces effector functions like ADCC and CDC and decreases the number of malignant B cells in the circulation (Weiner et al. 2010). Trastuzumab, the second approved monoclonal antibody, inhibits breast tumor growth by preventing the activation of human epidermal growth factor receptor 2 (HER2) on the tumor cells (Hudis 2007). The first approved IgG4 therapeutic antibody was gemtuzumab ozogamicin. The antibody was conjugated to calicheamicin, an antitumor anthracycline antibiotic. It was used for the treatment of CD33-positive acute myeloid leukemia (AML) after the first relapse. However, it was withdrawn in 2010 after a post approval clinical trial, because no sufficient benefit was provided for the patients (Rowe, Lowenberg 2013). In 2017 it was re-approved by the FDA to treat AML patients above 60 years of age. The newest approach of monoclonal antibodies leading to a breakthrough in the clinic is designated as immune checkpoint inhibitors. Immune checkpoints are immunologic surface proteins mediating co-stimulatory or inhibitory signals for regulation and activation of T cells (Pardoll 2012). The anti-cytotoxic T lymphocyte antigen-4 (CTLA-4) antibody ipilimumab was the first FDA approved immune checkpoint inhibitor for the treatment of melanoma (Traynor 2011). Due to antibody binding to CTLA-4 on the T cell's surface, it inhibits the immunosuppressive signal between CTLA-4 and B7 expressed on an APC. Thus, B7 is free to bind CD28 on the T cell leading to T cell activation and proliferation. Thereby, T cell-mediated immunity is amplified (Tarhini et al. 2010; Lipson, Drake 2011).

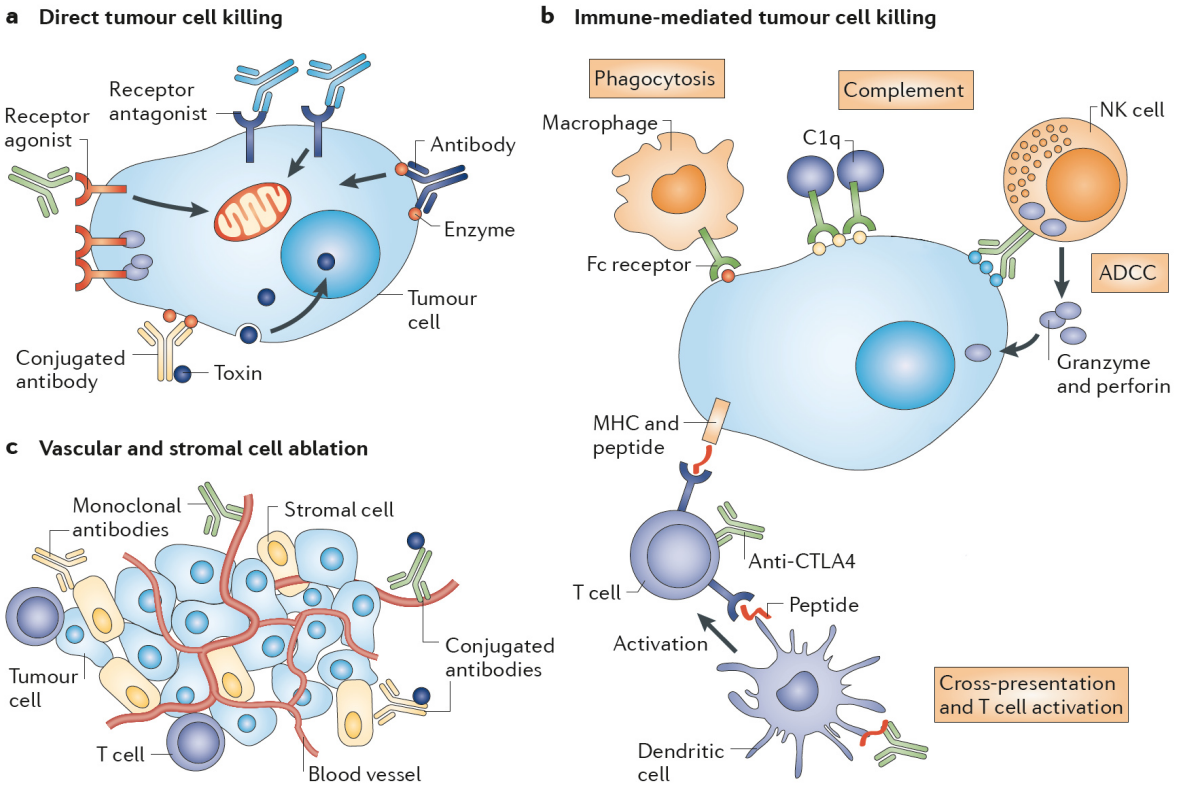

Figure 1-4: Tumor cell killing mechanisms of therapeutic antibodies.

A: Direct tumor cell killing can be mediated by antibody binding to receptor antagonists *e.g.* surface receptors for kinase activation leading to reduced proliferation and apoptosis or agonist binding leading directly to apoptosis. Tumor cell death can also occur by enzyme neutralization due to antibody binding or target-orientated toxin transfer. **B:** Immune-mediated tumor cell killing can be realized either through antibody induced phagocytosis by macrophages, the activation of the classical complement pathway by C1q binding, antibody-dependent cellular cytotoxicity (ADCC) by the activation of NK cells or activation of T cells by immune checkpoint inhibitors. **C:** The death of vascular and stromal cells is mediated either by antibodies delivering toxins to stroma cells, the vasculature or directly by inhibition of stroma cells by antibodies (adapted from Scott et al. 2012b).

1.7.1 Antibody-drug conjugates

Despite antibody-drug conjugates (ADCs) have been investigated for decades, they have just become successful within the recent years due to the development of new linker and conjugation technologies. Based on the complex structure consisting of the three main units antibody, cytotoxic agent and the linker, ADC design includes a lot of challenges to gain the different properties and desirable characteristics of each unit (Diamantis, Banerji 2016). The antibody's target antigen should be exclusively expressed or highly up regulated on tumor cells without down regulation during treatment and promote a fast internalization of the ADC. To prevent a loss of efficacy it is an advantage if the antigen is not shed from the cells' surface or the antibody binds a membrane-bound specific epitope on the antigen (Mack et al. 2014). However, there is no minimal threshold of antigen expression since many variables like internalization rate, binding affinity and cytotoxic potential of the drug need to be

considered (Diamantis, Banerji 2016). For efficient tumor cell killing, potent cytotoxic payloads are necessary. Today those drugs are targeting either the inhibition of microtubule or induce DNA damage. For example, microtubule assembly is interrupted by maytansinoids and auristatins leading to cell cycle arrest in the G2/M phase during cell proliferation (Sapra, Shor 2013; Bouchard et al. 2014). Duocarmycin and calicheamicin act independently from the cell cycle leading to rapid cell death by alkylating the minor groove of the DNA or cause double-strand DNA breaks at the minor groove, respectively (Diamantis, Banerji 2016). Specific linkers are used to attach those drugs in an optimal manner. They directly influence the ADC's pharmacokinetics (PK) and the efficacy and should ensure that the drug is released only once the ADC is internalized but not during circulation (Teicher, Chari 2011; Shefet-Carasso, Benhar 2015). Two categories of linkers are currently used: cleavable and non-cleavable linkers. During lysosomal ADC degradation non-cleavable linkers remain intact and cytotoxic drugs are acting when still attached to the linker and amino acid residues from the antibody. Cleavable linkers can be either pH-, lysosomal protease- or glutathione-sensitive (Shefet-Carasso, Benhar 2015; Senter, Sievers 2012; Sapra et al. 2011). Since resulting active drugs are smaller due to the lack of amino acids and linker residues, cleavable linkers increase the potential of bystander effects when the cytotoxic agents diffuse into neighboring cells. This gives an advantage for the treatment of heterogenic antigen-expressing tumors (Diamantis, Banerji 2016).

1.8 BT062 for treatment of multiple myeloma

Multiple myeloma is a malignant disease and a distinct type of B cell lymphoma. It is defined by an uncontrolled clonal proliferation of plasma cells in the bone marrow, resulting in the production of complete Igs (typically IgA or IgG) or immunoglobulin L chains (plasmacytosis) which are detectable in the urine or serum of the patient (Kyle, Rajkumar 2004). Multiple myeloma increases the risk of organ damage and infection diseases and it potentially leads to bone structure destructions (osteolysis) (Longo et al. 2012). The disease is responsible for approx. 10% of hematologic cancers and 1% of all cancers (Harousseau, Moreau 2009). CD138, also referred to as Syndecan-1, is a transmembrane heparin sulfate proteoglycan and belongs to the syndecan proteoglycan family. Surface expression of CD138 is restricted to endothelial cells and distinct hematopoietic cells: While CD138 is present on precursor B cells and antibody-producing plasma cells, the surface protein is absent on mature B cells and $CD34^+$ stem cells (Sanderson et al. 1989; Wijdenes et al. 2002; O'Connell et al. 2004). In comparison to healthy plasma cells, CD138 expression is highly upregulated on multiple myeloma cells and it is therefore used as a reliable biomarker for diagnosis (Wijdenes et al. 1996; Bayer-Garner et al. 2001). Besides this, the surface receptor can also be found on

distinct solid tumors including bladder, lung, pancreatic, breast and prostate cancer (O'Connell et al. 2004). CD138 is participating in many cellular functions, such as cell-matrix interactions, cell-cell adhesion, migration, signaling and proliferation. It interacts with a variety of growth factors all also known to be involved in tumor development including fibroblast growth factor 2 (FGF-2), transforming growth factor β 1 (TGF-β1), hepatocyte growth factor (HGF) and vascular endothelial growth factor (VEGF) (Bernfield et al. 1992; Bernfield et al. 1999; Derksen et al. 2003; Ramani et al. 2013; Lee et al. 2013). BT062, also termed indatuximab ravtansine, is an ADC. It is composed of the anti-CD138 antibody nBT062 (naked BT062) covalently conjugated to the cytotoxic agent DM4. nBT062 is a chimeric IgG4 antibody based on the murine B-B4 precursor. The latter one is shown to bind to the linear epitope between residues 90 to 93 of the CD138 core protein (Ikeda et al. 2009; Dore et al. 1998). Since nBT062 is an IgG4 antibody, it is not capable to induce ADCC or CDC. DM4 is a highly toxic maytansinoid, a chemical derivate of maytansine, which was first isolated from the bark of the Ethiopian shrub *Maytenus ovatus* (Kupchan et al. 1972). An average of 3.5 DM4 molecules are attached to one nBT062 via N-succinimidyl-4-(2-pyridyldithio)butanoate (SPDB) linkers. Currently BT062 is evaluated in clinical trials for the treatment of multiple myeloma, breast and bladder cancer. Upon administration to patients, BT062 is supposed to bind CD138 on the target tumor cell and gets internalized by endosomal uptake (see Figure 1-5). Within the lysosome, the ADC is proteolytically degraded leading to the release of DM4. Those free maytansinoids diffuse through the lysosomal membrane, bind to the microtubule, inhibit tubulin polymerization and thereby induce cell cycle arrest during the G2/metaphase. Finally, this results in the apoptosis induction of the tumor cell (Lopus et al. 2010). An additional antitumor effect might be mediated by the diffusion of free DM4 molecules into the surrounding tumor cells. In contrast, antibody-conjugated DM4 is not able to diffuse through plasma membranes (Weill et al. 2008). Thus, in line with the restricted CD138 expression pattern in healthy cells and high upregulation in a variety of tumors, BT062 should possess low systemic toxicity.

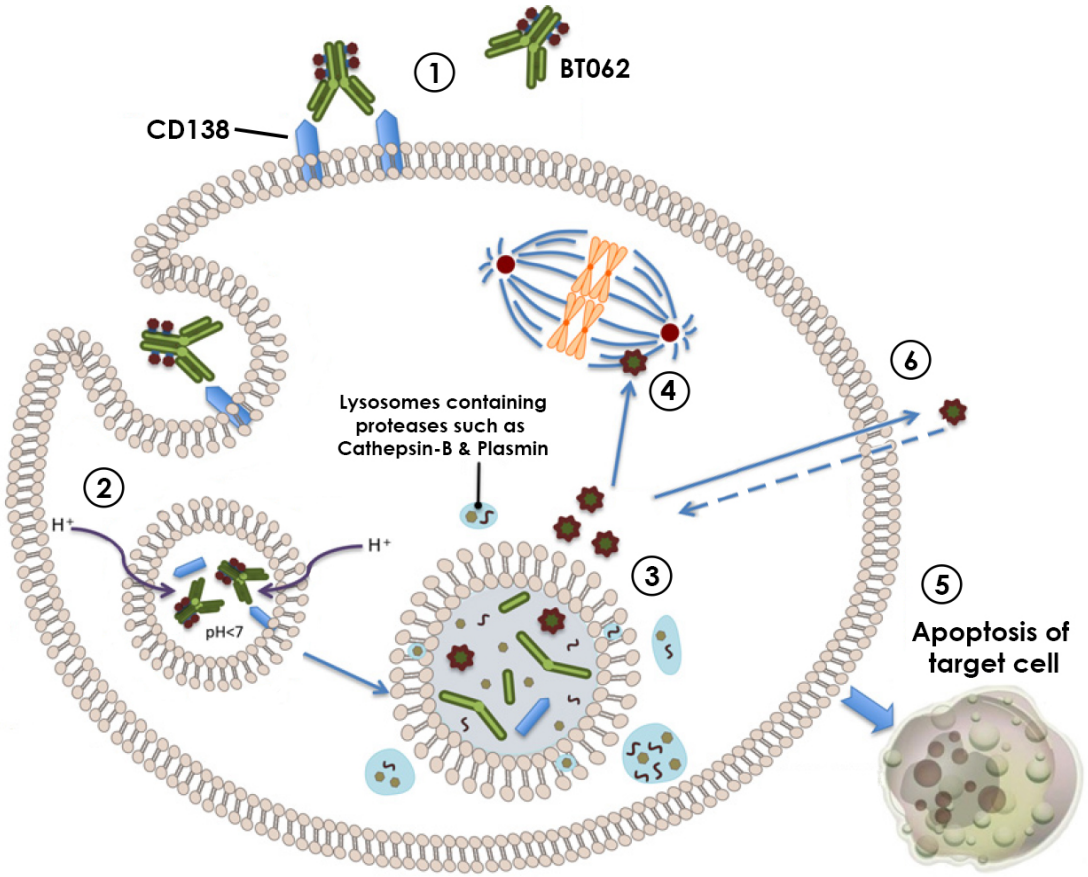

Figure 1-5: BT062's proposed mode of action for tumor cell killing.

Blood circulating BT062 attaches to membrane-bound CD138, highly overexpressed on the tumor cell's surface (1). Once bound, the antibody-drug conjugate (ADC) is internalized by endocytosis (2) and followed by entering the lysosome. Proteolytic degradation of BT062 releases the cytotoxic, maytansine-derivate DM4 (3). During cell proliferation, DM4 inhibits polymerization of tubulin leading cell cycle arrest within the metaphase (4) and thereby inducing tumor cell apoptosis (5). An additional bystander effect may be achieved by diffusion of DM4 molecules into surrounding tissue leading to further killing of tumor cells (6) (adaped from Peters, Brown 2015).

1.9 Natalizumab as α4-integrin binding therapeutic antibody

Natalizumab, commonly known under its trade name Tysabri, is a commercially available therapeutic antibody approved for the treatment of multiples sclerosis and Crohn's disease. It is a humanized monoclonal antibody against integrin α_4, based on the IgG4 subtype containing κ light chains and produced by Biogen Inc. in non-immunoglobulin secreting (NS/0) murine myeloma cells (Baldo 2016). Yu et al. have shown that natalizumab binds a non-linear epitope of integrin α_4 involving the amino acids Gln-152, Lys-201 and Lys-256 (Yu et al. 2013). Integrin α_4 (CD49d) is a subunit present in integrin $\alpha_4\beta_1$, termed Very Late Antigen 4 (VLA-4) and in integrin $\alpha4\beta_7$, named Lymphocyte Peyer patch adhesion molecule (LPAM). Both cell surface receptors are expressed on leukocytes with the exception of neutrophils. They are involved in migration of these cells across the endothelium towards an

inflamed tissue by interactions with vascular cell adhesion molecule-1 (VCAM-1) and mucosal addressin cell adhesion molecule-1 (MAdCAM-1), respectively (Yu et al. 2013; Cavaliere et al. 2017). Multiple sclerosis is an autoimmune disease affecting the central nervous system (CNS) due to infiltration of mononuclear leukocytes leading to myelin and axon damage. Initially, it is characterized by transient inflammation and durable remyelination afterwards. Over time, extensive and chronic neurodegradation occurs (Compston, Coles 2002, 2008). Natalizumab can prevent activated lymphocyte migration across the blood brain barrier into the CNS by blocking integrin $\alpha_4\beta_1$ from interactions with VCAM-1 expressed on activated vascular endothelial cells and thereby protects neuronal cells from damage of inflammatory responses (Yu et al. 2013). Crohn's disease is a relapsing systemic inflammatory disease mainly affecting the gastrointestinal tract by inducing immune responses against commensal microbiota (Baumgart, Sandborn 2012). MAdCAM-1 is expressed on vascular endothelial cells of the gastrointestinal tract and mediates homing of lymphocytes to Peyer's patches and their recruitment to sites of inflammation (Ruiz-Velasco et al. 2000). By blocking the interaction of MAdCAM-1 on gut endothelial cells with lymphocyte-expressed integrin $\alpha_4\beta_7$, natalizumab decreases the recruitment and migration of lymphocytes towards the site of infection (Biogen Idec 2013).

Since natalizumab comprises a wild type IgG4 hinge region without stabilizing mutations, it was demonstrated by Labrijn et at. that the therapeutic antibody exchanged half-antibodies with endogenous IgG4 in patients affected with multiple sclerosis. Those bispecific antibodies were observed by the detection of natalizumab antibodies containing both, λ-L chains beside original κ-L chains. Additionally, bispecific natalizumab/IgG4-CD20 antibodies were found *in vitro* after reduced glutathione treatment by online electrospray ionization time-of-flight mass spectrometry (LC-ESI-MS) and enzyme-linked immunosorbent assay (ELISA) as well as *in vivo,* after monospecific antibody administration into severe combined immunodeficient (SCID) mice (Labrijn et al. 2009). Based on the IgG4 shuffling characterization of natalizumab and availability of its DNA sequence, it was used in this study for the recombinant generation of a bispecific IgG4 antibody model.

2 Aims of this work

It is known that endogenous human IgG4 antibodies as well as unstabilized therapeutic IgG4 such as natalizumab undergo half-antibody exchange *in vivo* and are thus able to form bispecific antibodies (Labrijn et al. 2009; Young et al. 2014). Biotest is currently evaluating BT062, an ADC consisting of an unstabilized anti-CD138 IgG4 antibody conjugated to the cytotoxic agent DM4 in clinical trials. In this thesis it was examined if potential *in vivo* derived IgG4 species of BT062 -as example for unstabilized IgG4-based ADCs- were still functional in terms of specific antigen binding, receptor-mediated cellular internalization and induction of apoptosis via DM4 release. Furthermore, the direct influence of IgG4 shuffling on the therapeutic efficacy was evaluated *in vivo*.

To address those issues, beside wild type (WT) nBT062 three further model antibodies mimicking potential IgG4-shuffling related variants were recombinantly generated: stable nBT062, half nBT062 and bispecific nBT062-natalizumab. All nBT062 variants were expressed, purified and characterized by analytical methods. Questions on the antibodies' functionality were investigated by fluorescence-activated cell sorting and fluorescence microscopy using human and transgenic, murine cell lines. The nBT062 model variants were conjugated to DM4 and resulting CD138-specific ADC models were studied on their cytotoxic potency *in vitro*. The influence of endogenous IgG4 antibodies on the efficacy of the different nBT062 variants was assessed in a xenograft mouse model and blood samples of mice were analyzed to draw qualitative conclusions with respect to IgG4 half-antibody exchange.

3 Methods and Materials

3.1 Cultivation of mammalian cells

3.1.1 General cultivation conditions

NCI-H929, Jurkat, Ba/F3 and Ba/F3-hCD138 cell lines were cultured at 37°C, 5% CO_2 and 100% atmospheric humidity in a static Thermo Scientific Incubator. FreeStyle CHO-S cells were cultured at 37°C, 8% CO_2 and 100% atmospheric humidity under shaking conditions of 125 rpm with 3 cm orbit (Kuhner). Cell operations were performed under sterile conditions using a lamina flow hood (Thermo Scientific). Cell line specific media are listed in section 3.8.1.

3.1.2 Thawing of frozen cells

Frozen cells were retrieved from liquid nitrogen stocks and were thawed in a 37°C water bath. Cells were transferred into a centrifugal tube containing 10 ml of pre-warmed cell culture medium and centrifuged at 306 x g for 8 min. The supernatant was discarded, the cell pellet was resuspended in 10 ml of the respective growth medium (see section 3.8.1) and the cell suspension was transferred into 25 cm^2 culture flasks (Sarstedt).

3.1.3 Passaging for maintenance of suspension cells

Cell suspensions were split every 3 to 4 days depending on their density. Clustered cells were separated by gentle pipetting. The cell number and viability was determined by mixing 10 µl cell suspension with 10 µl of 0.2% trypan-blue. The solution was transferred to a Neubauer cell counting chamber, cells were counted under the microscope and the cell number was determined using to the following formula:

$$cells/_{ml} = \frac{counted\ viable\ cells * 10^4}{dilution\ factor} \quad \textbf{(I)}$$

The viability was calculated according to the following formula:

$$\%\ viable\ cells = \frac{counted\ viable\ cells}{total\ cells} * 100 \quad \textbf{(II)}$$

The respective cell number was adjusted (see Table 3-1) and the cells were centrifuged at 300 x g for 8 min. The supernatant was discarded, the cells were resuspended in pre-warmed growth medium and transferred into a cultivation flask (25 or 75 cm^3). FreeStyle CHO-S cells were transferred into shaking flasks (125 or 250 ml).

Table 3-1: Doubling time and cell counts of suspension cells.

Cell line	Species	Doubling time	Cell number before splitting [cells/ml]	Adjustment of cell number for passaging [cells/ml]
FreeStyle CHO-S	Hamster	~ 19 h	1 – 1.5 x10^6	3 x 10^5
NCI-H929	Human	~ 70 h	1 – 1.5 x10^6	4 x 10^5
Jurkat	Human	~ 25-30 h	1 – 1.5 x10^6	1.5 x 10^5
Ba/F3	Mouse	~ 21 h	1.2 – 1.8 x 10^6	0.8 x 10^5
Ba/F3-hCD138	Mouse	~ 21 h	1.2 – 1.8 x 10^6	0.8 x 10^5

3.1.4 Freezing of cells

Suspension cells were harvested and counted as described in section 3.1.3. Cells were centrifuged at 306 x g for 8 min and the cell pellet was resuspended in freezing medium (90% respective growth medium, 10% DMSO) to adjust the cell number to 2x10^6 cells/ml. 1 ml of the cell suspension was transferred into each cryovial (Life Technologies), which were placed into a Nalgene freezing container (Thermo Fisher Scientific) containing 2-propanol for constant cooling to -80°C. After 3 days the cryovials were transferred to liquid nitrogen for long-term storage.

3.1.5 Generation of transgenic Ba/F3-hCD138 cells

A stable genetically modified murine Ba/F3 cell line expressing human CD138 was generated by Sirion Biotech GmbH (Martinsried, Germany). The coding region of human CD138 (933 bp, reference sequence NM_002997) was cloned into the multiple cloning site (MSC) of the lentiviral vector pcLV-CMV-MCS-IRES-Puro. The vector contains a cytomegalovirus (CMV) promotor for transgene expression, an internal ribosome entry site (IRES) as bicistronic element and a puromycin (Puro) resistance gene for positive selection of transfected cells. Cloning of the hCD138 into the lentiviral vector was verified by DNA sequencing. Lentiviral packaging plasmids and the generated expression vector were co-transfected into HEK293TN cells to produce lentiviral HIV-based, vesicular stomatitis virus glycoprotein (VSVG) pseudotyped, self-inactivating particles for transduction. Ba/F3 cells were incubated with these particles at a multiplicity of infection (MOI) of 50. After 72 h, puromycin was added to a final concentration of 0.75 µg/ml and cells were selected for 12 days.

For quantification of CD138 expression, transgenic cells were analyzed via semi-quantitative real time polymerase chain reaction (qRT-PCR) by Sirion Biotech GmbH. Total RNA of Ba/F3-hCD138 cells was isolated and 1 µg was reverse transcribed using a mixture of random hexamer and oligo-dT primers. A Light Cycler 480 (Roche) qRT-PCR system was used to determine the relative expression level of human CD138 in Ba/F3-hCD138 cells.

Murine peptidylprolyl isomerase A (PPIA) was used as housekeeping gene and parental Ba/F3 cells were tested as negative control. Results are shown in Table 3-2.

Table 3-2: qRT-PCR results for CD138 expression in Ba/F3-hCD138 cells.

Cell line	Cp* human CD138	Cp* PPIA
Ba/F3-hCD138	18.36	15.84
Ba/F3, parental	no detection	16.28

*Cp: crossing point.

Since Ba/F3-hCD138 cells were tested negative for lentiviral particles (< 1 x 10^3 genomic copies/ml) by qRT-PCR using a Lenti X qRT-PCR Titration Kit (Clontech), cells were handled under biosafety level 1.

3.2 Generation of different CD138-specific nBT062 antibodies

3.2.1 Plasmid generation of nBT062 antibody variants

The protein sequence of WT nBT062 as disclosed in patent WO2009080829, SEQ No. 1 and 2 (Kraus et al. 2008) was used as basis for the generation of stable nBT062, half nBT062 and bispecific nBT062-natalizumab molecules. All mutations were introduced *in silico* into the DNA sequence using VectorNTI (Thermo Fisher Scientific) followed by full length DNA synthesis and subsequent cloning into pEF expression vectors at Thermo Fisher Scientific, Germany.

3.2.1.1 Sequence design of stable nBT062

For the generation of stable nBT062 DNA sequence, the stabilizing amino acid mutations S228P and R409K (Labrijn et al. 2011) were introduced into respective DNA sequence of the WT nBT062 heavy chain. Further, a L235E mutation was introduced into this variant to reduce FcγR binding.

3.2.1.2 Sequence design of half nBT062

The cysteines building up the disulfide bonds of the hinge region were exchanged by serines (C226S + C229S) to create half nBT062. Respective DNA sequences of WT nBT062 heavy chains were modified.

3.2.1.3 Sequence design of bispecific nBT062-natalizumab

For the generation of the bispecific nBT062-natalizumab antibody, the available CDR and framework regions of natalizumab H and L chains as disclosed in patent US5840299 (Bendig

et al. 1995) were used. The regions were aligned to the stable nBT062 amino acid sequence by SIM tool (Swiss Insitute of Bioinformatics) to identify the respective amino acid sections at the DNA level. To ensure correct H - H chain pairing during eukaryotic co-expression of the two different H and two different L chains, the 'knobs-into-holes' technology was used (Carter 2001). It is based on the introduction of sterically complementary regions in the CH3 domains of both H chains *e.g.* by exchanging larger amino acids with smaller ones in the one H chain and exchanging smaller amino acids with larger ones in the second H chain. S354C and T366W 'knob'-mutations were introduced into the CH3 domain of the nBT062 H chain, while Y349C, T366S, L368A, and Y407V 'hole'-mutations were inserted into the CH3 domain of the natalizumab H chain. To ensure correct H to L chain pairing, orthogonal Fab interfaces were used (Lewis et al. 2014). The nBT062 Fab of the bispecific nBT062-natalizumab was modified with D1R and Q38D mutations in the L chain and Q39K and K62E mutations in the variable region of the H chain. Q38R, S176W and L135Y mutations were introduced into the L chain of the natalizumab Fab of bispecific nBT062-natalizumab, while Q39Y, F174G and H172A mutations were applied to the H chain. An overview of the introduced mutations is shown in Figure 3-1.

3.2.1.4 Plasmid cloning

Full length DNA sequences of the model antibodies were synthesized and cloned into pEF expression vectors (Biotest adapted, see appendix 7.1). These vectors contain an origin of replication and an ampicillin resistance for prokaryotic replication, a cytomegalovirus (CMV) promotor for eukaryotic transgene expression, and a puromycin or methotrexate (MTX) resistance gene for positive selection of transfected cells. Puromycin is able to inhibit protein translation by binding the A site of the ribosome instead of tRNA and is thus transferred to the assembling peptide chain causing its premature release. MTX selection is used in cell lines which lack dihydrofolate reductase (DHFR), a protein essential in purine metabolism. The DHFR gene is located on the vector and as MTX inhibits DHFR activity it is forcing the cells to produce more DHFR and conditionally more recombinant protein of interest. Site-directed cloning of the antibodies coding regions was performed by insert and vector digestion with *HindIII* and *NotI* restriction enzymes and subsequent ligation. H and L chains of monospecific antibodies WT nBT062, stable nBT062 and half nBT062 were cloned into separate vectors containing either a puromycin or a MTX resistance and used for co-expression.

To co-express two individual H and two individual L chains of the bispecific nBT062-natalizumab antibody from two plasmids, a T2A elements was used. The first T2A element was originally derived from *thosea asigna* virus and was shown to enable the expression of two proteins from one mRNA (Szymczak, Vignali 2005). This was achieved at the

translational level by inducing ribosome skipping (Donnelly et al. 2001a; Donnelly et al. 2001b). The addition of an N-terminally furin cleavage site leads to the deletion of any C-terminally introduced spacer residues from the T2A element. The performed cloning procedure was as follows: H and L chain sequences of the nBT062 part were synthesized as one DNA molecule containing a furin cleaving site and a T2A element (Chng et al. 2015) between the individual chains (see Figure 3-1). The DNA was cloned into the pEF vector containing a puromycin resistance. H and L chains of the natalizumab part, also separated by a furin recognition site and a T2A element, were cloned into the pEF vector harboring a MTX resistance.

The sequences were synthesized and plasmids were delivered in TE buffer by Thermo Fisher Scientific as 500 µg plasmid preparations.

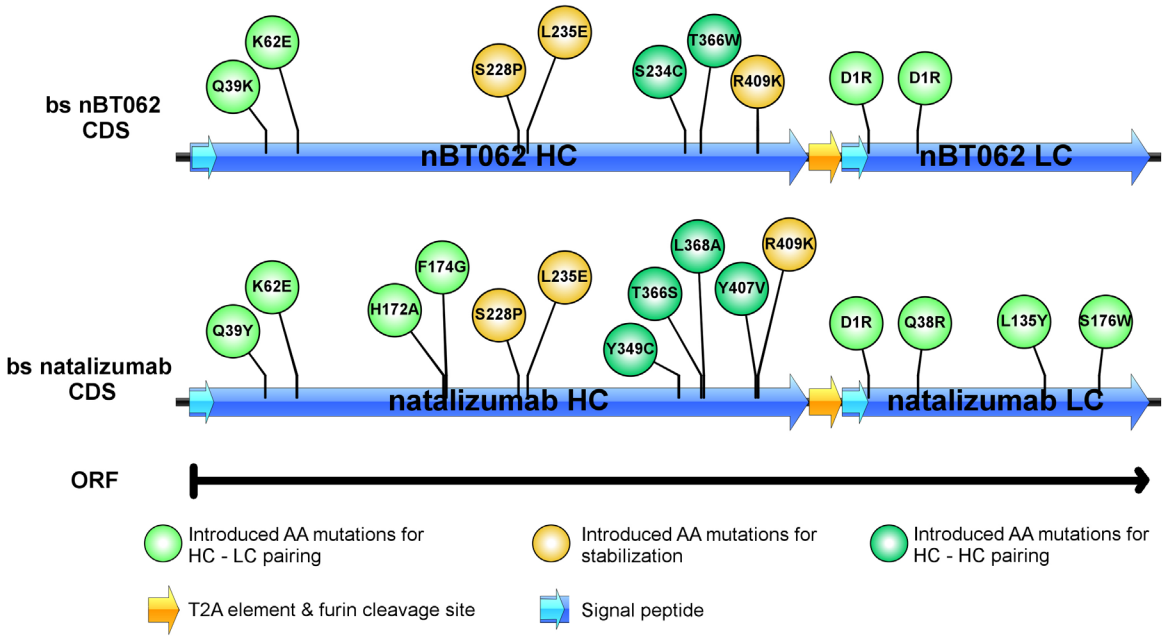

Figure 3-1: Modified nBT062 and natalizumab DNA constructs for coexpression to generate bispecific nBT062-natalizumab.

The coding regions (CDS) of the synthetic inserts of modified nBT62 and modified natalizumab are shown. Heavy chain (HC) and light chain (LC) of each antibody part are transcripted into one mRNA and separation is done on the translational level due to a T2A element. For antibody stabilization and to enable correct chain pairing, several amino acid substitutions were introduced (highlighted).

3.2.2 Expression of different nBT062 antibody variants

3.2.2.1 Nucleofection of FreeStyle CHO-S cells

For transfection of WT nBT062, stable nBT062, half nBT062 and bispecific nBT062-natalizumab plasmid DNA (see section 3.2.1) into FreeStyle CHO-S cells the SG Cell Line 4D-Nucleoctor X Kit (Lonza) was used. Two days prior to transfection cells were split (see section 3.1.3) to ensure that they were in the growth phase. Cells were counted as described in section 3.1.3 and $1x10^6$ cells per antibody were centrifuged at 90 x g for 10 min. The supernatant was discarded by pipetting and the cell pellet was resuspended carefully in 90 µl per $1x10^6$ cells in room temperature, fully supplemented Nucleofector Solution (Lonza, included in the kit). 5 µg of each plasmid were gently mixed with 90 µl cell suspension, the volume was adjusted to 100 µl with Nucleofector Solution and the cells were subsequently transferred into nucleofection cuvettes. Cells were nucleofected using program FF-137 on Lonzas 4D-Nucleofector. Subsequently, the nucleofected cells were diluted with 1.5 ml of pre-warmed CHO-S expression medium and seeded in one well of a 6 well plate under static conditions.

3.2.2.2 Selection of stable expressing cells

For the generation of stable cell pools expressing the different nBT062 variants via spontaneous plasmid DNA integration into the genome, selection pressure was applied. Two days after nucleofection, cells were counted and split into two samples: $2x10^5$ cells/ml were seeded into CHO-S expression medium supplemented with either 10 µg/ml puromycin (Life Technologies) and 100 nM methotrexate (MTX, Sigma-Aldrich) or 20 µg/ml puromycin and 200 nM MTX as selection markers. The cells were seeded in 800 µl/well in 12-well plates and transferred into a CO_2 incubator without shaking. The viability was monitored twice weekly. A full media exchange was performed once per week. When the cells entered growth phase, they were expanded up to 20 ml cultures and transferred to shaking conditions (see section 3.1.1). The supernatant of the cell culture was occasionally tested for CD138 specific antibody production via electrochemiluminescence assay (see section 3.6.3). Once the viability of the cells was stable above >90 %, cells were transferred in CHO-S expression medium containing either 30 µg/ml puromycin and 500 nM MTX or 50 µg/ml puromycin and 1000 nM MTX to boost protein expression in a second selection phase. As soon as the viability was stable above 95%, cell pools expressing CD138-specific antibodies were frozen to create a master cell bank.

3.2.2.3 Batch cultivation for antibody production

Stable cell pools expressing the different antibody variants were cultured as described in section 3.1 in their respective selection medium. For batch production 3x 300 ml cells were seeded in puromycin- and MTX-free FreeStyle CHO-S Expression Medium at a density of

$3x10^5$ cells/ml in 1L shaking flasks (Corning). Cells were cultured for 8 days and their viability was checked at least three times a week. On day 3 and day 6, 21 ml of complex feed #1 (Biotest) were added to each culture flask. On day 8, cell suspensions were transferred into centrifugation tubes (Corning) and centrifuged for 30 min at 2000 x g. Subsequently, the supernatant was sterile filtered using a Mini Kleenpak Fluorodyne II 0.2µm (Pall) filter connected to a Watson Marlow 323 Pump. The harvest was stored at -20°C until purification.

3.2.3 Purification of nBT062 variants from cell harvest

3.2.3.1 Affinity purification with HiTrap MabSelect column

For purification of antibodies from cell harvests, HiTrap MabSelect 5 ml Protein A affinity columns (GE Healthcare) connected to an Äkta Avant 150 system with Unicorn 6.2 software (GE Healthcare) were used.

Supernatants from batch productions were thawed over night at room temperature, the pH value was checked and if necessary adjusted to pH ~7 with 1 M NaOH or 1 M HCl. After start-up, the tubes of the Äkta system were applied to the respective solutions as described in Table 3-3, the pump wash program was performed to remove any air bubbles. The whole system was equilibrated with ~25 ml DPBS at a system flow rate of 20 ml/min. The S1 tube was carefully transferred from DPBS into the harvest solution and the sequence for purification (Table 3-4) was initiated using a system flow rate of 3 ml/min. After the elution step, the 50 ml tube containing the purified antibody in 0.1 M citrate buffer pH 3.75 was removed from the fractionator and the pH was neutralized to pH ~7 with 1 M Tris base pH 8.0. Subsequently, buffer exchange against nBT062 formulation buffer was performed using Slide-A-Lyzer dialysis cassettes (Thermo Fisher Scientific). The process was carried out at 4°C for 2 h, the dialysis buffer was changed and the protein was dialyzed for another 2 h. A last dialyzing step was done overnight.

Table 3-3: Äkta Avant 150 connection settings for antibody purification.

Insert connection tubes	Solution
A1	DPBS
A2	DPBS + 1M NaCl
B1	0.1 M citrate pH 3.75
B2	0.1 M citrate pH 2.7
S1	System equilibration: DPBS; Purification: Harvest

Outlet connection tubes	Target vial
Outlet 1	Empty bottle for flow through
Fractionator A1	Empty tube for column wash
Fractionator A2	Empty tube for elution
Fractionator A3	Empty tube for post elution wash

Table 3-4: Sequence for antibody purification.

Step	Buffer	Volume
Equilibration	DPBS	10x CV*
Sample loading	Harvest	Total (until air)
Wash 1	DPBS	3x CV*
Wash 2	DPBS + 1 M NaCl	3x CV*
Wash 3	DPBS	3x CV*
Elution	0.1 M citrate pH 3.75	6x CV*
Post elution wash	0.1 M citrate pH 2.7	3x CV*

*CV = Column volume

3.2.3.2 Cleaning-in-place (CIP) of HiTrap MabSelect column

To remove very tightly bound, precipitated or denatured substances and to recover the affinity resin in the column, a cleaning protocol was used. Directly after the purification run, the insert connection tubes A2, B1, B2, and S1 were transferred into H_2O and air bubbles were removed by pump wash. B1 was connected to 0.01M NaOH pH 12.0 and a second pump wash was performed. A system wash with ~25 ml DPBS using insert connection tube A1 was applied and the CIP sequence according to Table 3-5 was initiated with a flow rate of 3 ml/min. For system and column storage, all insert connection tubes were transferred into a 20% ethanol solution and the whole system including the column was rinsed.

Table 3-5: CIP sequence for HiTrap MabSelect column.

Buffer	Volume / Time
DPBS	3x CV*
0.01 M NaOH pH 12.0	4x CV*
Incubation break	30 min
DPBS	10x CV*

*CV = Column volume

3.3 Analytical characterization of nBT062 variants

3.3.1 SDS-PAGE and Coomassie Brilliant Blue staining

To separate antibodies according to their molecular weight and determine half-antibody proportions, sodium dodecyl sulfate polyacrylamide gel electrophoresis (SDS-PAGE) was performed. It is based on the potency of proteins to move within an electrical field. The intrinsic charge of the proteins is covered by SDS to achieve a proportional ratio of negative charge to protein length. Denatured, reducing SDS-PAGE is used to separate the single subunits of a protein. For this purpose, a reducing agent is used to disrupt disulfide bonds after boiling the samples. Under non-reducing conditions, proteins retain their secondary and tertiary structures.

3.3.1.1 Sample preparation

Reducing sample preparation

Antibodies were used at a concentration of 2 mg/ml. Reducing sample buffer was produced by combining 2.5 parts of NuPAGE LDS Sample Buffer (4x, Thermo Fisher Scientific) with 1 part of NuPAGE Sample Reducing Agent (10x, Thermo Fisher Scientific). 15 µl of an antibody sample were mixed with 15 µl of reducing sample buffer in a 1.5 ml vial and heated for 10 min at 70°C using a thermoshaker (Eppendorf).

Non-reducing sample preparation

For production of the non-reducing sample buffer, 1 part of 400 mM N-Ethylmaleimide solution (NEM) was mixed with 1 part of NuPAGE LDS Sample Buffer (4x, Thermo Fisher Scientific). 15 µl of this solution was transferred into a vial with 15 µl of antibody solution (stock concentration 2 mg/ml), mixed by vortexing and incubated for 30 s at 70°C using a thermoshaker (Eppendorf).

3.3.1.2 Electrophoresis procedure

A Novex 4-12% Tris-Glycine Mini Protein Gel was inserted into the XCell SureLock Mini-Cell Electrophoresis System (Thermo Fisher Scientific) and inner and outer chambers were filled with 1x MOPS Running buffer (Thermo Fisher Scientific). 7.5 to 10 µl of the prepared sample (7.5 – 10 µg) and 10 µl of SeeBlue Plus2 Pre-stained Protein Standard (Thermo Fisher Scientific) were loaded onto the gel. The sample separation was achieved by running the gel at a constant voltage of 200 V for 45 to 60 min.

3.3.1.3 Coomassie Brilliant Blue Staining

Immediately after the run, the gel was transferred into a staining tray filled with approximately 50 ml of fixation solution and was incubated for 45 min on an orbital shaker (Heidolph) to prevent diffusion of the proteins within the gel. To visualize the protein bands, the fixation

solution was discarded, 50 ml final staining solution (see section 3.8.4) was added and incubated for 2 - 4 h on an orbital shaker. For destaining the background of the gel, the fast-destaining solution was added for 30 s. Afterwards the gel was destained twice for 10 min and once for 16 h with slow-destaining solution. It was scanned using the Argus software on Epson Perfection V700 photo. For storage, the gel was transferred into 1% glycerol for 1 h, clamped between two cellophane sheets and dried for 3 h in a Gel Air Dryer (Bio-Rad).

3.3.2 Isoelectic focusing and Western Blotting

Isoelectric focusing is used to separate proteins within a gel matrix based on their relative amount of acidic and basic amino acid moieties. Since the protonation status of amino acid moieties is pH dependent, proteins are either positively, negatively or not charged. A protein net charge of zero is reached at a specific pH-value: the isoelectric point (pI). By loading proteins onto a pH-gradient electrophoresis gel and by applying a constant voltage, proteins in a pH-range below their pI move within the electric field towards the cathode. Proteins in a pH range over their pI migrate towards the anode. All molecules move within the electric field until they reach their pI.

3.3.2.1 Isoelectric focusing procedure

Isoelectric focusing was performed using the XCell SureLock Mini-Cell electrophoresis system (Thermo Fisher Scientific). For sample preparation, antibodies were diluted to a concentration of 2 mg/ml with water, subsequently mixed with 50% Novex IEF Sample Buffer pH 3-10 (Thermo Fisher Scientific) and 20 µl (5 µg) were applied to a Novex pH 3-10 IEF gel. For pH identification, 10 µl of the Serva IEF Marker 3-10 were pipette into a gel pocket. The inner system chamber was filled with chilled 200 ml IEF Cathode Buffer (Thermo Fisher Scientific) and the outer chamber was filled with chilled 600 ml IEF Anode Buffer (Thermo Fisher Scientific). Antibodies were separated in a stepwise process: 100 V for 60 min, 200 V for 60 min and 500 V for 30 min. IEF gels were further processed by Coomassie Brilliant Blue staining or Western Blotting.

3.3.2.2 Coomassie Brilliant Blue Staining

Protein visualization on IEF gels was carried out as already described for Tris-Glycine Mini Protein Gels in section 3.3.1.3. The procedure was identical except for the fixation step: IEF gels were fixed for 30 min at room temperature in 50 ml 12% trichloroacetic acid/ 3.5% sulfosalicylic acid.

3.3.2.3 Western Blotting

To further investigate the separated proteins, they were transferred onto a polyvinylidene fluoride (PVDF) membrane (Thermo Fisher Scientific) by using the XCell II Blot module

(Thermo Fisher Scientific) for semi-wet protein transfer. The PVDF membrane was directly applied to the IEF gel and the system was filled with Novex Tris-Glycine Transfer Buffer (25x, Thermo Fisher Scientific) according to the manufacturer's instructions. Protein blotting was performed for 1 h at 25 V. After protein transfer, the membrane was blocked over night at 4°C in Odyssey Blocking buffer (Licor) and incubated afterwards simultaneously with 1 µg/ml anti-BT062-Biotin (Biotest) and anti-natalizumab-HRP (Bio-Rad) for 2 h at room temperature. Binding of anti-idiotypic antibodies was visualized after 2 h of simultaneous incubation with anti-HRP-800CW (Licor) and Streptavidin-680RD (Licor) on Licors Odyssey Imager.

3.3.3 Size exclusion chromatography

Size exclusion chromatography (SEC) is used to separate proteins based on their hydrodynamic radii. SEC columns have a defined pore size, wherein large molecules are not retained. In contrast, smaller molecules fit into these pores and are retained. Thus, molecules are eluted from the column in reverse order of their molecular weight. Unretained compounds are released in the column's void volume defined as the space between particles in the resin bed. A fully retained molecule is eluted at the column's included volume defined as the sum of the void volume and pore volume. SEC analysis can be performed under different buffer conditions, which might either maintain or interrupt covalent and non-covalent associations.

3.3.3.1 Non-denaturing SEC

To analyze the ability to form aggregates, antibody samples were analyzed by non-denaturing SEC. A TSKgel G3000 column (Tosoh Bioscience) was connected to the Ultimate 3000 nano HPLC system (Thermo Fisher Scientific) and used for protein separation. nBT062 SEC buffer (see section 3.8.6) was applied to the HPLC system on position "buffer A". Antibody samples were diluted with DPBS to a concentration of 1 mg/ml in a final volume of 100 µl and put into the system's autosampler. 100 µl of nBT062 SEC buffer were used as negative control. System parameters are listed in Table 3-6 and the program defined in Table 3-7 was applied for the sample run. Data evaluation was done with Chromelion Software (Thermo Fisher Scientific).

Table 3-6: System parameters for non-denaturing SEC.

System parameter	Set value
Column temperature	30°C
Autosampler temperature	5 ± 3°C
Lower pressure limit	5 bar

Upper pressure limit	50 bar
Flow rate	0.25 ml/min
Injection volume	50 µl
Detection	Absorption at 280 nm

Table 3-7: Program for non-denaturing SEC.

Step	Retention time	Pump device
Injection	0 min	50 µl; Autozero
Isocratic elution	60 min	100% buffer A
End	60 min	n/a

3.3.3.2 Denaturing SEC

This test method was used to denature any non-covalently paired half-antibodies by isopropanol in the SEC buffer. The percentage of half-antibodies present was determined by relating the peak areas of full and half-antibodies obtained by UV detection at 280 nm.

The experiment was performed on the same system and column as described in section 3.3.3.1. Denaturing SEC buffer (see section 3.8.6) was applied to the instrument on position “buffer A”. Antibody samples were diluted first to a concentration of 1.2 mg/ml with DPBS and were further mixed 1:2 with denaturing SEC buffer to a final volume of 100 µl. The samples were loaded into the instrument’s autosampler and the run was initiated using the system parameters and program settings as indicated in Table 3-8 and Table 3-9. Data evaluation was done with Chromelion Software (Thermo Fisher Scientific).

Table 3-8: System parameters for denaturing SEC.

System parameter	Set value
Column temperature	30°C
Autosampler temperature	5 ± 3°C
Lower pressure limit	5 bar
Upper pressure limit	50 bar
Flow rate	0.25 ml/min
Injection volume	50 µl
Detection	Absorption at 280 nm

Table 3-9: Program for denaturing SEC.

Step	Retention time	Pump device
Injection	0 min	50 µl; Autozero
Isocratic elution	60 min	100% buffer A
End	60 min	n/a

3.3.4 *In vitro* half-antibody exchange testing

To qualitatively evaluate the prevention of half-antibody exchange due to the incorporation of stabilizing S228P and R409K mutations into the IgG4 backbone, antibodies were exposed to mild reducing conditions to potentially enable half-antibody formation followed by oxidization for random H chain dimerization.

nBT062 variants were mixed with natalizumab, DPBS and reduced glutathione (GSH) to produce a 200 µl solution containing 2 mg/ml of each antibody and 10 mM GSH. The antibodies were reduced at 37°C over night at 300 rpm in a thermoshaker (VWR). GSH was removed by dialysis against DPBS (2x 4 h) using Slide-A-Lyzer MINI Dialysis Device (Pierce) with a 10 kDa molecular weight cut off. The solution was transferred into a 1.5 ml vial and oxidized glutathione (GSSG) was added to a final concentration of 5 mM. Random reoxidization of half-antibodies was carried out over night at 37°C and 300 rpm.

3.4 Biological characterization of nBT062 variants

3.4.1 Antibody labeling with Dylight fluorescent dyes

For direct detection of antibodies during flow cytometric analysis or fluorescence microscopy, nBT062 model antibodies and natalizumab were labeled with fluorescent dyes using the Dylight 488 (Dy488) antibody labeling kit (Thermo Fisher Scientific) according to the manufacturer's instructions. The conjugation with Dylight dyes is based on activated N-hydroxysuccinimide (NHS) esters reacting with primary amines within the protein and forming stable, covalent amide bonds, while NHS groups are released. Antibody solutions were diluted with DPBS to a concentration of 2.2 mg/ml in a final volume of 500 µl and 40 µl of 0.67 M borate buffer were added. The prepared protein solution was transferred into the vial containing the Dylight dye powder and mixed gently by vortexing. The labeling reaction was carried out for 60 min at RT in the dark and unbound dye was subsequently removed by kit-containing dye-removal spin columns. Final antibody concentrations and the antibody-to-dye ratios were determined by photometric absorption: 20 µl of the dye-conjugated antibody were mixed by pipetting up and down with 180 µl of DPBS and transferred into a UV-transparent F-bottom plate (Cell star, Greiner). The absorption was measured at 280 and 493 nm on a

POLARstar Omega photometer (BMG Labtech) using DPBS as blank. As indicated in the manual, the following formulas were used to calculate the protein concentration and dye-to-protein ratio:

$$Protein\ concentration\ \left(\frac{g}{l}\right) = \frac{A_{280} - (A_{max} * CF)}{\varepsilon_{protein}} * DF * m \quad \textbf{(III)}$$

$$ratio\ dye{:}protein = \frac{A_{max} * DF}{\varepsilon_{Dye} * c_{Protein}} \quad \textbf{(IV)}$$

DF (dilution factor)	10
$\varepsilon_{protein}$	210,000 for IgG
m (specific mass)	150,000 Da
A_{max} (Excitation wavelength in nanometers)	493
CF (Correction factor (A_{280}/A_{max}))	0.147
ε_{Dye} (Molar extinction coefficient ($M^{-1}\ cm^{-1}$) at A_{max})	70,000

Table 3-10: Determined antibody concentration and dye to protein ratio.

Antibody	Concentration [mg/ml]	Dye-to-protein ratio
WT nBT062-Dy488	1.92	2.6:1
Stable nBT062-Dy488	2.17	2.6:1
Half nBT062-Dy488	1.82	2.8:1
Bispecific nBT062-natalizumab-Dy488	1.99	2.7:1
Natalizumab-Dy488	2.05	2.8:1

3.4.2 Fluorescence-activated cell sorting

Fluorescent-activated cell sorting (FACS) is based on the principle of flow cytometry. Cells are separated and can be individually analyzed for their size, granularity, viability and the expression of specific proteins or even proteins' phosphorylation status. The cell size is measured by the forward scatter, while the sideward scatter detects the granularity. The viability and the presence of specific surface proteins is determined by DNA-intercalating dyes or fluorescent labeled antibodies, respectively. Intracellular proteins can be investigated by cell fixation and membrane permeabilization prior to antibody staining. Fluorescent dyes are excited by a specific wavelength and subsequently emit light of a longer wavelength. The resulting emission spectrum is compared to control cells. By the amount of specifically bound antibodies, conclusions can be drawn for expression pattern of proteins.

3.4.2.1 Procedure for flow cytometric analysis

Cell density and viability was determined by trypan blue staining as described in section 3.1.3. The required amount of cells was centrifuged at 300 x g for 8 min, the supernatant was

discarded and cells were adjusted to a density of $1.5x10^6$ cells/ml. 100 µl cell suspension (100,000 to 150,000 cells) were pipetted into each well of a 96-well U bottom plate and the plate was centrifuged at 450 x g for 5 min. The supernatant was discarded.

Surface binding

To compare the binding activity of the different nBT062 antibody variants and natalizumab, the cells were resuspended in 100 µl of antibody solution containing the respective antibodies in a serial dilution ranging from $5x10^{-7}$ to $2.82x10^{-12}$ mol/L in DPBS/3%FCS. Cells were incubated for 30 min at 4°C and subsequently washed twice with DPBS/3%FCS by centrifugation at 450 x g for 5 min. The supernatant was discarded by vacuuming and pelleted cells were resuspended in 150 µl DPBS/3%FCS. 100 µl of a 10 µg/ml concentrated Alexa Fluor 647-labeled goat anti-human secondary antibody was added and cells were incubated again for 30 min at 4°C. To remove unbound antibodies, cells were washed twice with DPBS/3%FCS, resuspended in 150 µl DPBS/3%FCS and analyzed using a BD FACS Canto II flow cytometer (Beckton Dickinson) with FACSDiva Software. Data evaluation was done using Flowjo and GraphPad Prism.

Flow cytometric internalization analysis

To analyze CD138-mediated antibody internalization, cells were resuspended in 100 µl of a 15 µg/ml concentrated Dylight-488 labeled antibody solution containing nBT062 variants or natalizumab in DPBS/3%FCS (see section 3.4.1). Cells were either incubated for 0.5 h at 4°C or for 24 h at 37°C to analyze either antibody surface binding or internalization, respectively. Cells expressing CD49d were also co-incubated with a 50-times excess of natalizumab to block potential CD49d-mediated internalization. After incubation, cells were washed once with DPBS/3%FCS and incubated either for 10 min at 4°C with DPBS/3%FCS or for 10 min at 37°C with Trypsin to digest CD138 surface receptors including bound antibodies. Cells were washed twice with DPBS/3%FCS and analyzed with a FACS Canto II flow cytometer with FACSDiva Software. Flowjo and GraphPad Prism were used for further data processing.

3.4.3 Fluorescence microscopy

To investigate the internalization of nBT062 model variants by fluorescence microscopy, $1.5x10^5$ Ba/F3 ($CD138^+/CD49^-$) and Ba/F3-hCD138 ($CD138^+/CD49^-$) cells/well were seeded into 96-well U-bottom plates (see section 3.4.2.1). Cells were centrifuged at 450 x g for 5 min and the supernatant was discarded. Cell pellets were resuspended in 100 µl of the respective fluorescently labeled nBT062 antibody variant (see section 3.4.1; 10 µg/ml) in DPBS/3%FCS

and incubated for 30 min at 4°C for antibody surface binding. Unbound antibodies were washed away by pelleting the cells at 450 x g for 5 min, discarding of the supernatant, resuspension of the cells in 150 µl DPBS/3%FCS and another centrifugation and resuspension step in 150 µl DPBS/3%FCS. To study internalization of cell surface bound antibodies, cells were incubated for 3 h at 37°C. Subsequently, cells were centrifuged at 450 x g, the supernatant was discarded and the cell pellet was resuspendend in 100 µl Trypsin (PAA) to digest surface-anchored CD138 including bound antibodies during incubation for 10 min at 37°C.

Cells were washed once and fixed for 10 min at 37°C in paraformaldehyde (4% in PBS, Santa Cruz). After another washing step the cells were permeabilized in 100 µl 0.02% Saponin (Sigma-Aldrich) for 30 min at RT. To avoid further unspecific antibody binding, intracellular blocking was performed in 1x BMB/DPBS (Boehringer Blocking Agent, Roche) for 10 min at RT. Cells were washed twice with DPBS/3%FCS. To investigate the type of internalization, lysosomal-associated membrane protein-1 (LAMP1) was costained by resuspending the cells with 100 µl of a rabbit anti-LAMP1 antibody solution (Abcam, 1:500 in 1x BMB/DPBS) and incubation for 30 min at 4°C. Cells were washed twice and incubated for 30 min at 4°C with 100 µl of a Cy3-labeled goat anti-rabbit H+L secondary antibody (Jackson ImmunoResearch, 1:500 in 1xBMB/DPBS). To finalize the samples, cells were washed twice with DPBS/3%FCS, resuspended in 40 µl of Prolong Gold Antifade Mountant with DAPI (Thermo Fisher Scientific) and transferred onto glass microscopy slides. Samples were cured for 24 h in the dark. Fluorescence microscopy and data evaluation was performed using an Olympus IX53 inverted fluorescence microscope (Olympus) and cellSens Software (Olympus).

3.5 Generation and characterization of DM4-conjugated nBT062 variants

3.5.1 DM4-conjugation of nBT062 variants

To generate CD138 specific ADCs, the different anti-CD138 antibodies WT nBT062, stable nBT062, half nBT062 and bispecific nBT062-natalizumab were conjugated to the tubulin-inhibiting maytansinoid DM4 using the conjugation technology developed by Immunogen (USA; Figure 3-2).

In a first step, the antibody formulation buffer was exchanged to buffer A (see section 3.8.9) by using illustra NAP-25 columns (GE Healthcare). According to the manufacturer's instructions, columns were pre-equilibrated with 25 ml buffer A. 2.5 ml per antibody variant were applied onto the middle of the resin bed followed by an elution step by applying 3.5 ml buffer A. The eluate was collected. The procedure was repeated until approx. 25 mg of the respective CD138-specific antibody were obtained. Antibody concentrations were determined by photometric absorption at 280 nm as described in section 3.5.2 using formula (II). Subsequently, antibody solutions were concentrated to approx. 10 mg/ml by using 0.5 ml Amicon Ultra 30 kDa molecular weight cut off (MWCO) centrifugation filters (Merck). The N-succinimidyl-4-(2-pyridyldithio)butanoate (SPDB) linker (Immunogen, solved in 100% Ethanol) was added in a 6.5-times molar quantity to the antibody. Buffer A and ethanol were added resulting in a final antibody concentration of 8 mg/ml and 5% ethanol. The antibody-linker conjugation reaction was carried out for 4 h at RT under stirring conditions. Unconjugated SPDB linker was removed by the use of illustra NAP-25 columns and the concentration was measured by photometric absorption. To conjugate DM4 (N2′-deacetyl-N2′-(4-mercapto-4-methyl-1-oxopentyl)-maytansine) with the unmodified, functional group of the antibody-attached SPDB linker, DM4 (Immunogen, 15 mM in Dimethylacetamid (DMA, Merck)) was added in a 7.1-times molar quantity to the antibody. Buffer A and DMA were added to a final antibody concentration of 5 mg/ml and 6% DMA. The reaction was performed under stirring conditions for 16 h at RT. Unconjugated DM4 was removed and buffer was exchanged to BT062 formulation buffer (Biotest) in a single step by using the illustra NAP-25 columns as mentioned before. ADC samples were sterile filtered (0.2 µm) and the protein concentration and DM4-to-antibody ratio was measured as described in section 3.5.2. The half nBT062 was conjugated on the calculation of a full length antibody. To mimic the situation of a shuffled antibody *in vivo*, the bispecific nBT062-natalizumab was conjugated with 50% of SPDB and 50% of DM4.

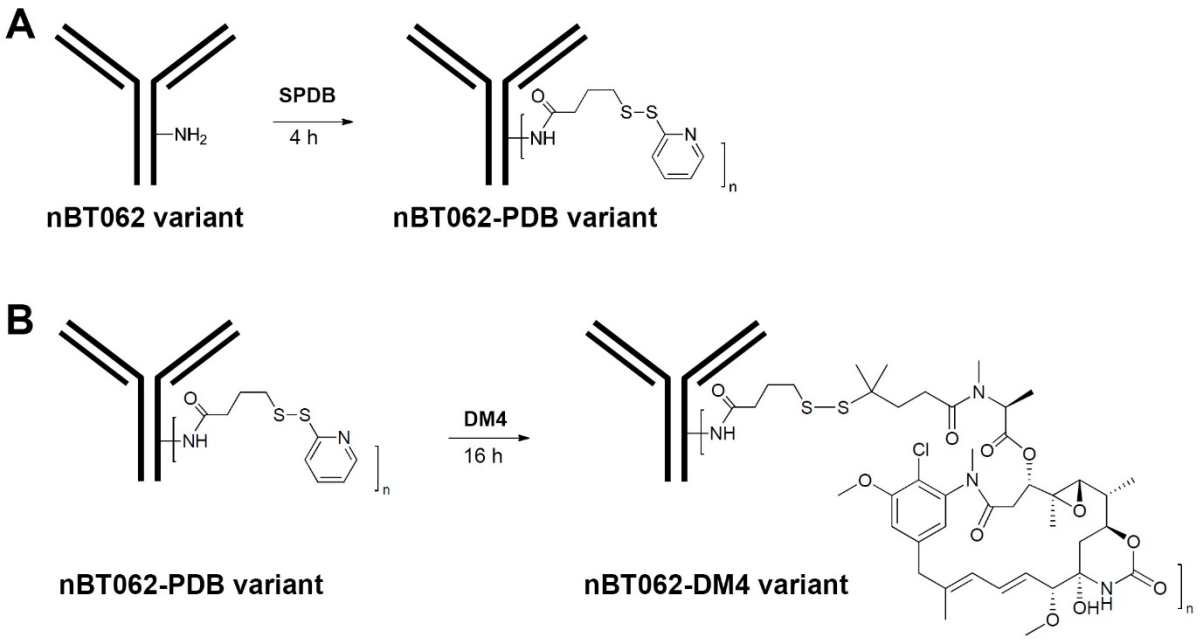

Figure 3-2: SPDB modification and DM4 conjugation reactions

Generation of ADCs by two separated reactions: **A**: ε-amino groups of lysines in nBT062 variants were randomly conjugated with an SPDB linker by acylation and release of N-hydroxysuccinimide (NHS). **B**: DM4 was conjugated to the second functional group of the antibody-attached SPDB linker.

3.5.2 Determination of DM4 to antibody ratio

To determine the antibody concentration and total amount of DM4 within nBT062-DM4 variants, 50 to 100 µl of a sample were added to a final volume of 1 ml with BT062 formulation buffer. Samples were mixed by gentle vortexing, transferred into 1 ml cuvettes and the absorbance was measured in duplicates at 252 and 280 nm using an Ultrospec 2100 pro photometer (Amersham Biosciences). BT062 formulation buffer was used as blank.
The molar concentration of DM4 was calculated as follows:

$$DM4\ [\mu M] = \frac{\left((A_{252} * DF) - (0.344 * A_{280} * DF)\right) * 1000000}{24377} \quad \textbf{(V)}$$

Molar BT062 concentration was calculated:

$$BT062\ [\mu M] = \frac{(1000000 * A_{280} * DF) - (5180 * DM4\ [\mu M])}{216060} \quad \textbf{(VI)}$$

The DM4-to-antibody ratio (DAR) was calculated:

$$DAR = \frac{DM4\ [\mu M]}{BT062\ [\mu M]} \quad \textbf{(VII)}$$

A252	measured absorption at a wavelength of 252 nm
0.344	ratio of absorbance of BT062 antibody at 252 nm and 280 nm
DF	dilution factor
A280	measured absorption at a wavelength of 280 nm
1000000	conversion factor M : µM
24377	molar extinction coefficient of DM4 at 252 nm
5180	molar extinction coefficient of DM4 at 280 nm
216060	molar extinction coefficient of nBT062 at 280 nm

3.5.3 Determination of DM4 distribution in nBT062-DM4 variants by LC-MS analysis

Human IgG4 antibodies carry approx. 30 lysines in each H chain and 12 lysines in each L chain, which are potentially available for the conjugation with SPDB-DM4. Since in ADC development a striven average DAR is much lower than the number of conjugatable lysines, several species containing different DARs are generated. To investigate the distribution range of conjugated DM4 in WT nBT062, stable nBT062, half nBT062 and bispecific nBT062-natalizumab model variants, an intact mass spectrometric analysis with upstream liquid chromatography (LC-MS) was performed at Triskelion B.V. (Netherlands). In a first step, the different molecules in the sample solution were separated by reversed phase LC to concentrate the nBT062 variants and to remove residual buffer. During this procedure hydrophobic molecules are adsorbed by a hydrophobic solid in a polar mobile phase. Decreasing the polarity of the mobile phase reduces the hydrophobic interactions between the analytes of the sample and the solid phase leading to desorption. The more hydrophobic the analytes, the more time they spend on the column. In a second step concentrated nBT062 variants were injected into a mass spectrometer. This analyzer ionizes the injected molecules, which are then passed through a mass analyzer for separation by their mass-to-charge ratio. A detector acquires the signals and the abundance of each ion can be calculated.

Reversed phase LC was performed prior to the MS analysis to enhance the MS signals by direct injection of selected protein peaks. A Zorbax RRHD 300-Diphenyl column (Agilent), Eluens C and Eluens D (see section 3.8.10) were connected to a Dionex Ultimate 3000 HPLC System (Thermo Fisher Scientific). The column was heated to 75°C and the auto sampler was set to 10°C. 10 µl of each nBT062-DM4 model variant (0.2 – 0.5 µg) was injected at a flow rate of 0.5 ml/min running the gradient program as indicated in Table 3-11.

Antibody peaks were detected at 280 nm and peaks between 4.0 and 6.5 minutes were directly injected into the Thermo Q Exactive Orbitrap MS instrument using heated electrospray ionization (HESI). The resolution was set to 17,500, since the average mass determination of the molecular species was accurate and the signal to noise ratio appropriate. Further instrument settings are indicated in Table 3-12. Data evaluation and MS spectra deconvolution was done using OPTON-20159 Protein Deconvolution software (Thermo Scientific).

Table 3-11: Gradient program for reversed phase LC.

Time (min)	% Eluens C	% Eluens D	Divert value
0	80	20	Waste
0.5			MS
6.5	50	50	
8	10	90	Waste
8.5	10	90	
8.6	80	20	
10	80	20	

Table 3-12: Thermo Q Exactive Orbitrap Instrument settings.

Parameter	Value
Spray voltage (kV)	4.0
Capillary temperature (°C)	275
Sheath gas	60
Aux gas	20
Spare gas	0
Probe temperature (°C)	320
S-lens RF level	80
In-source CID (eV)	80
AGC target	1e6
Maximum IT (ms)	100
Microscan	2
Scan range (m/z)	1600-6000

3.5.4 DM4 conjugation site mapping

To investigate and identify the DM4 conjugation sites in the different nBT062 model variants, peptide mapping was performed at Immungen by LC-MS analysis (USA).

In a first step, samples were diluted to approx. 2 mg/mL with water prior to desalting. An illustra NAP-5 column (GE Healthcare) was equilibrated with 5 mL of ultra-pure water and 500 µL ADC sample was loaded onto the resin of the NAP-5 column. Subsequently, 1000 µL of water was added and the eluate containing the antibody was collected. The desalted ADC was dried overnight in a centrifugal vacuum concentrator. The dried conjugate was reconstituted by adding 200 µL of denaturing buffer (see section 3.8.11) and 5 µL of 1 M dithiothreitol (DTT) solution. Under these conditions disulfide bonds were reduced in order to cleave H and L chains and DM4 within the SPDB linker. The sample was incubated at 37°C for 1 hour. Alkylation was carried out following addition of 12 µL of 1 M iodoacetic acid at ambient temperature in the dark for 40 minutes. The alkylation reaction was quenched by adding 7 µL of 1 M DTT solution.

The alkylated sample was loaded onto another NAP-5 column equilibrated with 5 mL of digestion buffer (see section 3.8.11). The column was washed with 500 µL of digestion buffer, and the antibody was eluted with another 500 µL of digestion buffer. The protein concentration in the eluate was determined by UV absorption spectroscopy so that the amount of enzyme needed for digestion can be calculated accordingly. The sample was enzymatically digested with trypsin using a protein-to-enzyme ratio of 1:25 (w/w). The digestion was stopped by adding 2.5 µL of trifluoroacetic acid (TFA) after 2 hours incubation at 37°C.

A 20 µl aliquot of the digested sample was injected onto a reversed phase C18 column connected to a UPLC-QTOF (Waters) LC-MS system. Peptides were separated by applying a gradient of eluent A and B (see section 3.8.11) and eluted proteins detected at absorption at 280 nm were directly injected into the MS instrument. The UV and mass spectrometry data were acquired by MassLynx 4.1 (Waters). The raw LC-MS data were processed using Biopharmalynx1.3.2 (Waters) for peptide peak identification.

3.5.5 *In vitro* cytotoxicity assay

To determine the cytotoxic effect of DM4-conjugated WT nBT062, stable nBT062, half nBT062 and bispecific nBT062-natalizumab model antibodies *in vitro*, NCI-H929 ($CD138^+/CD49d^+$) cells were incubated with different concentrations of these ADC's for 5 days. Jurkat ($CD138^-/CD49d^+$) cells were used as negative control. Viability of the cells was analyzed by WST-1 substrate metabolism. Due to mitochondrial dehydrogenase activity of

the cells, the tetrazolium salt WST-1 (4-[3-(4-Iodophenyl)-2-(4-nitrophenyl)-2H-5-tetrazolio]-1,3-benzene disulfonate) is reduced to formazan, while NADH is oxidized. Thus, the amount of formazan detected by absorbance at 450 nm wavelength correlates with the amount of viable cells.

3.5.5.1 Procedure

NCI-H929 or Jurkat cells were cultured according to section 3.1. On day 0, 18 to 24 h prior seeding the cells into 96-wells they were passaged as described. On day 1, viable cells were counted by mixing 10 µl of cell culture with 10 µl of 0.2% trypan blue solution and subsequent counting in a Neubauer counting chamber. The appropriate amount of cells was diluted with respective growth medium to a cell number of 1.12 x 10^5 cells/ml. To minimize evaporation of samples, boarder wells of a 96-well F-bottom plate (CellStar, Greiner) were filled with 100 µl medium and the inner wells were filled with 90 µl of the NCI-H929 or Jurkat cell solution (10,000 cells/well). Cells were incubated for 18 to 24 h at 37°C and 5% CO_2. On day 2, DM4-conjugated nBT062 model antibodies were added. Antibodies were diluted with assay buffer (see section 3.8.12) to the following concentrations: 40, 10, 4, 2, 1, 0.6, 0.4, 0.2, 0.1 nM. 10 µl of each antibody concentration were mixed with the respective 90 µl of the cell suspension within the plate to results in a 10-times diluted final concentration. As negative control, 90 µl of cells were mixed with 10 µl of assay buffer (0 nM). All samples were measured in triplicates. Cells were incubated for 120 h at 37°C and 5% CO_2.

On experiment day 7, the viability of the cells was determined by adding 10 µl of WST-1 (Roche) to each well. Plates were incubated for 3 h at 37°C and 5% CO_2. The intensity of the WST-1 color reaction was determined by absorbance at 450 nm using a 690 nm reference wavelength.

3.5.5.2 Data evaluation

Microsoft Excel 2007 was used for primary data evaluation. Average and standard deviation of triplicates including the medium samples (blank) were calculated. Grubbs outlier test was performed for each triplicate and single values, which did not satisfy the following formula, were eliminated:

$$\frac{single\ value - average}{standard\ deviation} \leq 1.513 \qquad \textbf{(VIII)}$$

1.513: critical value for n=3 at a confidence interval of 95%

Blank subtracted average OD values were normalized to the positive control (cells incubated with 0 nM antibody) including standard deviations of triplicates. A graph of these normalized values was drawn as shown in Figure 3-3B (example). The antibody concentration killing

50% of the cells, referred to as IC_{50}, was calculated using the next-neighbor method shown in Figure 3-3A.

A

$$m = \frac{y2 - y1}{x2 - x1} \quad \textbf{(IX)}$$

$$IC_{50} = x1 - \frac{y1 - 0.5}{m} \quad \textbf{(X)}$$

B

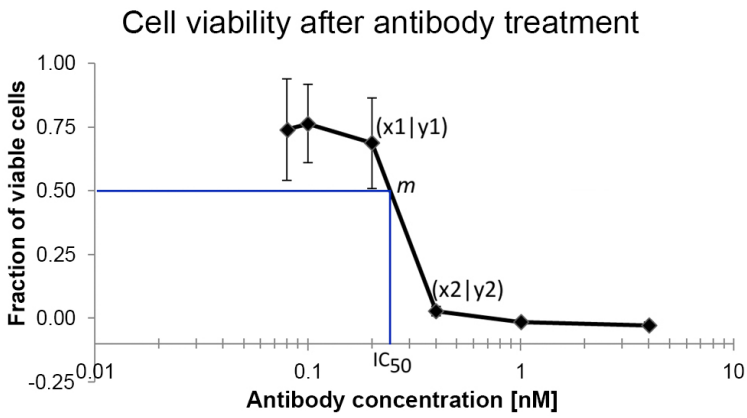

Figure 3-3: Determination of IC_{50} value for cytotoxicity.

A: Equations of next-neighbor method to determine IC_{50}. **B:** Example graph of normalized cell viability. X-axis shows the antibody concentration, while Y-axis indicates the fraction of viable cells. *m* and IC_{50} are marked.

For further data processing, reciprocal IC_{50} (rIC_{50}) values were created (see formula XI) and normalized to one DM4 molecule per antibody (see formula XII). Finaly, normalization to WT nBT062-DM4 was performed.

$$rIC_{50} = \frac{1}{IC_{50}} \quad \textbf{(XI)}$$

$$Normalization\ to\ one\ DM4\ molecule = \frac{rIC_{50}}{DAR\ of\ specific\ nBT062\ variant} \quad \textbf{(XII)}$$

For additional visualization of ADC concentration-dependent cell inhibition curves and statistical analysis using t-tests, GraphPad Prism was used.

3.6 *In vivo* efficacy of nBT062-DM4 variants

3.6.1 Evaluation of nBT062-DM4 variants in a xenograft mouse model

To evaluate the antitumor activity of DM4-conjugated WT nBT062, stable nBT062, half nBT062 and bispecific nBT062-natalizumab *in vivo*, a study using a mammary cancer

xenograft mouse model was performed at Charles River Discovery Research Services GmbH (Freiburg).

3.6.1.1 Xenograft mouse generation

Tumor samples were derived from surgical specimens from cancer patients and implanted subcutaneously into immunodeficient mice. Patient-derived tumor xenografts (PDX) were subcutaneously passaged, until a stable growth pattern developed and master stocks were frozen after early passaging. In this study the MAXF (Mammary cancer xenograft Freiburg) 1322 tumor model was used. This tumor model is derived from a metastasis of a 49 year old female patient suffering from a mammary adenocarcinoma.

Immunodeficient female NMRI nu/nu mice (NMRI-Foxn1^{nu}; NMRI nude) were delivered by Envigo RMS SARL (France) at the age of four to six weeks and were used for experiments after at least one week of acclimatization. Animals were kept under sterile and standardized conditions including a 14/10 h light/dark cycle, 25°C and a relative humidity between 40 and 70%. Feed and water were provided *ad libitum*.

MAXF 1322 tumors were raised in donor mice, extracted, cut into 3-4 mm length pieces and placed in PBS containing 10% penicillin/streptomycin. Recipient female NMRI nude mice were anesthetized by inhalation of isoflurane and were transplanted with tumor implants subcutaneously into one flank. Animals and tumors were monitored daily. When tumors reached a size between 50-250 mm³, preferably 80-200mm³ (see section 3.6.1.4), mice were separated into experimental groups, aiming at comparable median and mean group tumor volumes. The day of randomization was set as day 0.

3.6.1.2 Study design and observation

The four different model variants WT nBT062-DM4, stable nBT062-DM4, half nBT062-DM4 and bispecific nBT062-natalizumab-DM4 were administered intravenously (i.v.) into the tail vein either at a dose of 4 mg/kg or of 2 mg/kg. ADCs were given either as monotherapy or in combination with 10 ml/kg/dose of an intravenous human Ig preparation (IVIg, Intratect 10%, Biotest) to evaluate the influence of endogenous IgG4 on the therapeutic efficacy of nBT062-DM4 variants. As negative controls, animals received the IVIg preparation or DPBS. ADCs were injected using a volume of 5 ml/kg, while the IVIg preparation was given in a volume of 10 ml/kg. When dosed in combination, the IVIg preparation was given one hour before the ADCs. Each drug was injected once weekly for three consecutive weeks and the observation phase lasted up to day 86. The dosing schedule and individual groups are shown in Table 3-13. The mortality was assessed daily, while mouse body weights and absolute tumor volumes were measured twice-weekly during the whole study.

Table 3-13: Study design for MAXF 1322 xenograft model.

Group ID	Therapy	Total Daily Dose	Schedule [Dosing days]	Appl. Route	No. of Animals
1	Vehicle Control	10 ml/kg	1, 8, 15 (h:0)	i.v.	5
2	IVIg	10 ml/kg	1, 8, 15 (h:0)	i.v.	5
3	WT BT062-DM4	4 mg/kg	1, 8, 15 (h:1)	i.v.	5
4	Stable BT062-DM4	4 mg/kg	1, 8, 15 (h:1)	i.v.	5
5	Half BT062-DM4	4 mg/kg	1, 8, 15 (h:1)	i.v.	5
6	Bispecific BT062-natalizumab-DM4	4 mg/kg	1, 8, 15 (h:1)	i.v. // i.v.	5
7	IVIg // WT BT062-DM4	10 ml/kg // 4 mg/kg	1, 8, 15 (h:0) // 1, 8, 15 (h:1)	i.v. // i.v.	5
8	IVIg // Stable BT062-DM4	10 ml/kg // 4 mg/kg	1, 8, 15 (h:0) // 1, 8, 15 (h:1)	i.v. // i.v.	5
9	IVIg // Half BT062-DM4	10 ml/kg // 4 mg/kg	1, 8, 15 (h:0) // 1, 8, 15 (h:1)	i.v. // i.v.	5
10	IVIg // Bispecific BT062-natalizumab-DM4	10 ml/kg // 4 mg/kg	1, 8, 15 (h:0) // 1, 8, 15 (h:1)	i.v. // i.v.	5
11	WT BT062-DM4	2 mg/kg	1, 8, 15 (h:1)	i.v.	5
12	Stable BT062-DM4	2 mg/kg	1, 8, 15 (h:1)	i.v.	5
13	Half BT062-DM4	2 mg/kg	1, 8, 15 (h:1)	i.v.	5
14	Bispecific BT062-natalizumab-DM4	2 mg/kg	1, 8, 15 (h:1)	i.v.	5
15	IVIg // WT BT062-DM4	10 ml/kg // 2 mg/kg	1, 8, 15 (h:0) // 1, 8, 15 (h:1)	i.v. // i.v.	5
16	IVIg // Stable BT062-DM4	10 ml/kg // 2 mg/kg	1, 8, 15 (h:0) // 1, 8, 15 (h:1)	i.v. // i.v.	5
17	IVIg // Half BT062-DM4	10 ml/kg // 2 mg/kg	1, 8, 15 (h:0) // 1, 8, 15 (h:1)	i.v. // i.v.	5
18	IVIg // Bispecific BT062-natalizumab-DM4	10 ml/kg // 2 mg/kg	1, 8, 15 (h:0) // 1, 8, 15 (h:1)	i.v. // i.v.	5

3.6.1.3 Blood sampling

Blood was taken by retro-orbital sinus puncture during isoflurane anesthesia and directly transferred into standard plasma vials containing lithium heparin as anticoagulant. The blood was incubated for 10 min at RT, centrifuged at 2875 x g for 10 min and plasma was collected. Heparin plasma samples were collected from all animals one week before therapy, 24 h after the first and 24 h after the third injection. Plasma samples were stored at -80°C.

3.6.1.4 Data Evaluation

Tumor volumes were calculated using formula (XIII) and normalized relative to study day 0.

$$tumor\ volume = (A * B^2) * 0.5 \quad \textbf{(XIII)}$$

A= largest tumor diameter
B= perpendicular tumor diameter

The test versus control value (T/C in %) was assessed as median relative tumor volume (RTV) of the test group compared to the control group according to formula II. Criteria for efficacy rating are shown in Table 3-14.

$$T/C_x\,[\%] = \frac{median\ RTV_x\ treated\ group}{median\ RTV_x\ control\ group} * 100 \quad \textbf{(XIV)}$$

Table 3-14: Tumor control efficacy criteria.

Classification	T/C*
Inactive	≥65%
Borderline	50% – <65%
Moderate	25% – <50%
High	10% – <25%
Very high	5% – <10%
Complete remission	<5%

*T/C=median tumor volume in test group/median tumor volume in control group

To illustrate tumor growth curves, tumor volumes of animals that were sacrificed due to their tumor load were further included using the Last-Observation-Carried-Forward methodology for as long as this increased the group's median tumor volume.

The non-parametric Kruskal-Wallis test followed by Dunn's method for pairwise comparisons (Kruskal, Wallis 1952; Dunn 1964) was used to determine significance of the anti-tumor activity of applied antibodies. To evaluate the differences in time to tumor progression, the cut off of absolute tumor volume was set to 2000 mm² and Kaplan-Meier survival-style

statistics combined with the log-rank Mantel-Cox test for pairwise comparisons were employed (Kaplan, Meier 1958) using GraphPad Prism.

3.6.2 Determination of bispecific antibody formation in xenografts

Plasma samples obtained as described in section 3.6.1.3 from the MAXF 1322 xenograft mouse study were analyzed by a hybrid ligand binding assay (LBA)/LC-MS method at Triskelion, Netherlands. The aim was to determine the formation of bispecific antibodies in the different nBT062-DM4 model variants administered as monotherapy or in combination therapy with the IVIg preparation containing human IgG4 antibodies.

In brief, DM4-conjugated nBT062 model variants were purified from murine plasma samples using an anti-BT062 idiotypic antibody immobilized to magnetic beads. nBT062-DM4 variants were eluted from beads, denatured, reduced, alkylated, and digested with trypsin. During method development the amino acid sequence TIYNEK was identified as signature peptide unique for nBT062. GLPSSIEK was obtained as a generic peptide for IgG4 antibodies. Prepared samples were analyzed by ultra-performance liquid chromatography - tandem mass spectrometry (UPLC-MS/MS) together with spiked stable isotope labeled internal standard peptides of TIYNEK and GLPSSIEK. Concentrations of nBT062-DM4 variants were calculated including the fraction of bispecific antibodies formed by calculating the ratio of TIYNEK to GLPSSIEK.

3.6.2.1 Purification of nBT062 variants from murine plasma

Prior to antibody loading, 50 µl Streptavidin beads (Merck Millipore) were washed with 200 µl PBS by removing the liquid with a pipette while the tube was placed into a magnetic rack attracting the beads to the tubes wall and subsequent addition of PBS. 10 µl of a 100 µg/ml concentrated biotinylated anti-BT062 antibody (Biotest) was added and immobilized onto the beads for 60 min at 1000 rpm on a shaker. The supernatant was removed and unconjugated binding sites on the beads were blocked with 200 µl of a 5% BSA/PBS solution for 15 min at 1000 rpm. Beads were washed three times with 200 µl PBS and finally resuspended in 200 µl PBS. 10 µl of murine lithium heparin plasma (sample) were added and specific nBT062 variant binding was carried out for 60 min at 1000 rpm on a thermoshaker at 22°C. Beads were washed three times with PBS and nBT062 variants were eluted by addition of 50 µl 100 mM glycine –HCl pH 2.5 buffer followed by subsequent incubation at 95°C for 10 min and 1000 rpm. The liquid containing the purified nBT062 variant was transferred into a new vial and 10 µl of stable isotope labeled internal standard peptides TIYNEK-$^{13}C_6{}^{15}N_2$ and GLPSSIEK-$^{13}C_6{}^{15}N_2$ (50 ng/ml) were added. To denature and reduce the protein samples, 10 µl of 1% Rapigest (in 100 mM ammonium bicarbonate buffer) and 6 µl of 0.2 M

DTT were added into the vial. Incubation was performed for 10 min at 1000 rpm. Samples were alkylated with 35 µl of 0.1 M Iodoacetic acid (IAA, in 100 mM ammonium bicarbonate buffer) incubated for 30 min in the dark. The reaction was quenched by adding 3 µl 0.2 M DTT followed by subsequent incubation for 20 min at 37°C and 1000 rpm shaking. Protein digestion was achieved by adding 70 µl of a 100 µg/ml trypsin solution (in 100 mM ammonium bicarbonate buffer) into the vial and incubation was performed for 150 min at 37°C and 1000 rpm. Trypsin specifically cleaves the protein primary structure C-terminally of each lysine (K) and arginine (R). The digestion reaction was terminated by adding 18 µl of acetonitrile solution containing 5% TFA and 10% formic acid (FA), incubated for 10 min at 37°C and 1000 rpm.

3.6.2.2 UPLC-MS/MS analysis of prepared nBT062 variant samples

Prepared nBT062 variant samples were quantitatively analyzed with respect to the presence of the signature peptide TIYNEK of nBT062 and of the generic GLPSSIEK peptide specific for IgG4 antibodies using a UPLC-MS/MS method. 0.1% FA in milliQ water and 0.1% FA in acetonitrile were applied to an Acquity UPLC system (Micromass Waters) as mobile phase A and B, respectively. The autosampler was set to 10°C. 10 µl of a prepared sample (see section 3.6.2.1) were injected into the system and separated on an Acquity HSS T3, 100 x 2.1 mm, 1.8 µm column (Waters) using the phase gradient as depicted in Table 3-15. The flow rate was set to 500 µl/min and a column temperature of 50°C was applied. Samples were injected into the connected XEVO TQS (Micromass Waters) mass spectrometer using an electrospray ionization (Positive mode) and a capillary of 0.7 kV. The source temperature was set to 150°C, the desolvation temperature to 600°C. A cone gas flow of 150 L/h and desolvation gas flow of 1200 L/h was used.

Table 3-15: UPLC phase gradient for bispecific antibody detection via UPLC-MS/MS.

Time (min)	Mobile phase A (%)	Mobile Phase B (%)	Divert valve
0	95	5	Waste
0.25	95	5	
1			LC
3.9	65	35	
5	0	100	
6	0	100	Waste
6.5	95	5	
8	95	5	

3.6.2.3 Data evaluation

A BT062-DM4 reference standard (50 - 0.1 µg/ml) was added directly into pooled murine heparin plasma and used as calibration within each run. For data evaluation, Masslynx software was used to determine the peak areas and the calibration curve equation was calculated in Microsoft Excel. The resulting calibration curve was used to calculate the concentrations in all samples. Outlying results as determined by the Dixon's Q test were excluded. The ratios of both signature peptides GLPSSIEK and TIYNEK were calculated and processed as follows: ratio GLPSSIEK:TIYNEK≤1 matches 0% of IgG4 shuffling, while a ratio GLPSSIEK:TIYNEK=2 matches 100% half-antibody exchange. Graphical display and statistical t test was performed using GraphPad Prism.

3.6.3 Anti-CD138 antibody detection using an electrochemiluminescence assay

For quantitative detection of anti-CD138 antibodies in supernatants from nBT062 variant expressing cells or IVIg preparations, Meso Scale Discovery's (MSD) electrochemiluminescence (ECL) platform was used. This platform uses a Sulfo-Tag marker molecule, which is a derivate of Tris(2,2-bipyridyl)-ruthenium(II)-chloride ($Ru(bpy)_3$) for detection. When applying a voltage to the graphite electrode at the bottom of a multi-array plate, $Ru(bpy)_3$ is oxidized. Simultaneously, the buffer ingredient tripropylamine (TPA) is oxidized by creating a radical. The reaction of both molecules leads to a complex with an excited energy state. Due to the emission of light at 620 nm, this complex passes back to ground state (see Figure 3-4A).

This detection strategy used for anti-CD138 antibody quantification is shown in Figure 3-4B: Soluble CD138 proteins were coated to a surface and solutions containing potential anti-CD138 antibody variants were added for binding. To detect bound CD138-specific antibodies, biotin-conjugated anti-human antibodies were used (see section 3.8.13). Visualization was achieved by adding a Streptavidin-conjugated marker.

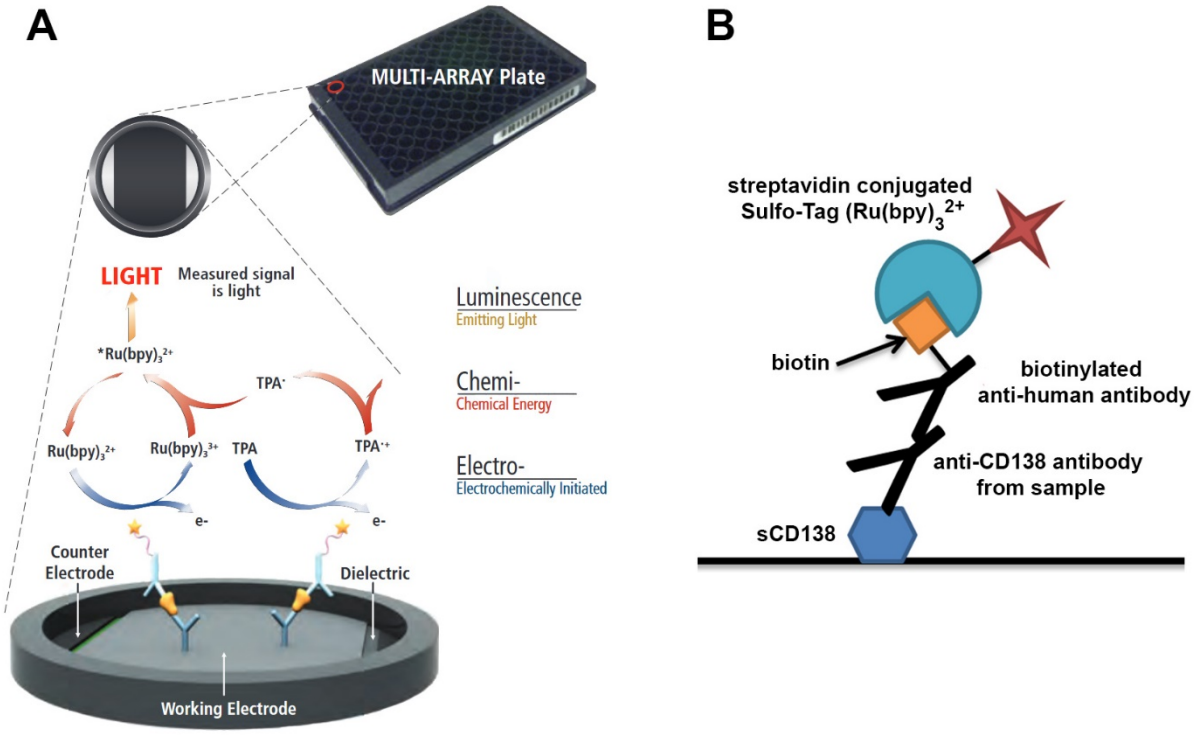

Figure 3-4: Detection of anti-CD138 antibodies by electrochemiluminescence

A: Detection principle of Meso Scale Discovery's electrochemiluminescence plattform. Ru(bpy)3 attached to the protein of interest forms a complex with tripropylamine (TPA) when applying a voltage. A subsequent complex-decay results in the emission of detectable light (adapted from Meso Scale Diagnostics 2013). **B:** Schematic assay design: soluble CD138 is coated onto a Multi-Array plate. Anti-CD138 antibodies within a test solution are captured and subsequently detected by an biotinylated anti-human antibody itself captured by a streptavidin-conjugated Sulfo-Tag ($Ru(bpy)_3$).

3.6.3.1 Procedure

Coating of plates

Freeze-dried soluble CD138 (sCD138, R&D Systems) was reconstituted according to the manufacturer's instructions. A coating solution containing 1 µg/ml sCD138 in PBS was prepared and 50 µl were transferred into each well of a 96-well standard multi array plate (MSD). Soluble CD138 was coated during an incubation of 4 h at RT and 600 rpm shaking conditions. Uncoated proteins were washed away with three cycles of liquid aspiration and subsequent addition of 150 µl washing solution (see section 3.8.13) into each well using the automated Tecan plate washer (Tecan). After the last washing cycle the supernatant was aspirated.

Preparation of test- and standard samples

Natalizumab was used as negative control and nBT062 was used as positive control. Both antibody standards were diluted with PBST-KS blue (Biotest) to an initial concentration of

100 µg/ml and 10-times serial dilutions up to 0.01 ng/ml were prepared. IVIg preparations and cell culture supernatants were also prepared in 10-times serial dilutions. 200 µl of standards and test samples were transferred into respective wells of the sCD138-coated plate. All approaches were measured in triplicates. For homogenization, the plate was shaken for 1 min at 600 rpm and incubated for approx. 16 h stationary.

Detection of anti-CD138 antibodies

The plate was washed as described above. 50 µl of a biotinylated goat anti-human IgG antibody (Jackson ImmunoResearch, 15 ng/ml in PBST-KS blue) were added into each well and the multi array plate was incubated for 60 min at 600 rpm to enable antibody binding. Unbound detection antibodies were removed by applying the washing program. Streptavidin-conjugated SulfoTag (MSD) was diluted with PBST-KS blue to a concentration of 0.5 ng/ml and 50 µl were transferred to each well. After an incubation of 20 min at 600 rpm, the plate was washed. Read buffer T (MSD) was diluted 1:4 with water and each well was filled with 150 µl of the solution. After 2 min of incubation at 600 rpm, the ECL signal was detected using a MSD Sector Imager 6000. Data evaluation was done using GraphPad Prism 6.

3.7 General reagents and kits

Reagent	Manufacturer/ Supplier	Cat.-No.
2-propanol	Merck	1070222511
BT062	Biotest AG	
BT062 formulation buffer	Biotest	
DM4	Immunogen Inc.	
Dulbecco's Balanced Salt Solution (DPBS)	Thermo Fisher Scientific	14190136
Ethanol 100%	Merck	1009831000
Hydrochloric acid (HCl), 5 mol/L	Merck	4807915000
nBT062	Biotest AG	
Sodium hydroxide (NaOH) Solution, 5 mol/L	Merck	1099130001
Tysabri (natalizumab)	Biogen Idec	
Kits		
Dylight 488 Amine-Reactive Labeling Kit	Pierce / Thermo Scientific	53024

3.8 Approach specific reagents, buffers and solutions

3.8.1 Cell cultivation

Cell line	Manufacturer/ Supplier
FreeStyle CHO-S	Thermo Fisher Scientific (R80007)
Jurkat	ATCC (TIB-152)
NCI-H929	ATCC (CRL-9068)
Ba/F3	DSMZ (ACC 300)
Ba/F3-hCD138	Sirion Biotech GmbH / Biotest AG

	Final concentration	Total addition
FreeStyle CHO-S medium		
FreeStyle™ CHO Expression Medium (Thermo Fisher Scientific, 12651014) For Selection: Puromycin (Thermo Fisher Scientific, A1113803) and MTX (Sigma-Aldrich, M8407) as described in Section 3.2.2.2		1000 ml

Jurkat medium

RPMI 1640 with L-glutamine (Lonza, BE12-702F)		500 ml
Fetal Bovine Serum (PAA, A15-105)	10%	55 ml
L-glutamine (100x, Lonza, BE17-605E)	2 mM	5.5 ml
HEPES Puffer (100x, Gibco, 15630-056)	10 mM	5.5 ml
sodium pyruvate (100x, Gibco, 11360-039)	1 mM	5.5 ml

NCI-H929 medium

RPMI 1640 with L-glutamine (Lonza, BE12-702F)		500 ml
Fetal Bovine Serum (PAA, A15-105)	10%	55 ml
L-glutamine (100x, Lonza, BE17-605E)	2 mM	5.5 ml

Ba/F3 medium

RPMI 1640 with L-glutamine (Lonza, BE12-702F)		500 ml
Fetal Bovine Serum (PAA, A15-105)	10%	55 ml
L-glutamine (100x, Lonza, BE17-605E)	2 mM	5.5 ml
Murine Interleukin-3 (R&D Systems, 403-ML-010), directly added to flask	10 ng/ml	20 µl per 20 ml cells

Ba/F3-hCD138

RPMI 1640 with L-glutamine (Lonza, BE12-702F)		500 ml
Fetal Bovine Serum (PAA, A15-105)	10%	55 ml
L-glutamine (100x, Lonza, BE17-605E)	2 mM	5.5 ml
Puromycin (Gibco, A11138-03)	0.375 ng/ml	21 µl
Murine Interleukin-3 (R&D Systems, 403-ML-010), directly added to flask	10 ng/ml	20 µl per 20 ml cells

3.8.2 Expression of Antibodies

Reagent	Manufacturer/ Supplier	Cat.-No.
SG Cell Line 4D-Nucleoctor X Kit	Lonza	V4XC-3024
Complex feed #1	Biotest	n/a
Mini Kleenpak Fluorodyne II 0.2µm filter	Pall	KA02DFLP8G

3.8.3 Antibody affinity purification

Material/Reagent	Manufacturer/ Supplier	Cat.-No.
HiTrap MabSelect 5 ml Protein A column	GE Healthcare	28-4082-55
Slide-A-Lyzer dialysis cassettes, 10kDa MWCO	Thermo Fisher Scientific	66807

	Final concentration	Total addition
0.1 M citrate buffer pH 3.75		
Citric acid (Merck, #100247	0.1 M	19.21 g
Adjust pH to 3.75		
MilliQ-H_2O		Ad 1000 ml
0.1 M citrate buffer pH 2.7		
Citric acid (Merck, #100247)	0.1 M	19.21 g
Adjust pH to 2.7		
MilliQ-H_2O		Ad 1000 ml
1M Tris-base pH 8.0		
Tris-base (Prolabo, #103156X)	1 M	12.11 g
Adjust pH to 8.0		
MilliQ-H_2O		Ad 100 ml

3.8.4 SDS-PAGE

Reagent	Manufacturer/ Supplier	Cat.-No.
Novex 4-12% Tris-Glycine Gel	Thermo Fisher Scientific	NP0335PK2
NuPAGE LDS Sample buffer, 4x	Thermo Fisher Scientific	NP0007
NuPAGE Sample reducing agent, 10x	Thermo Fisher Scientific	NP0009
NuPAGE MOPS SDS Running buffer, 20x	Thermo Fisher Scientific	NP0001
SeeBlue Plus2 Protein Standard	Thermo Fisher Scientific	LC5925

	Final concentration	Total addition
Fixation solution		
Methanol (Merck, 1.06009.2511)	37.2%	372 ml
Acetic acid 100% (VWR, 20102.292)	7%	70 ml
MilliQ-H_2O		Ad 1000 ml
Staining solution		
Reagent 1		
Coomassie Brilliant Blue (Sigma, B0770)	1 g/L (in final solution)	0,5 g
MilliQ-H_2O		Ad 10 ml

Reagent 2		
Orthophosphoric acid 85% (Merck, 1.00552.0250)	20 g/L	10 g
Ammonium sulfate (Merck, 1.01211.1000)	150 g/L	75 g
MilliQ -H_2O		Ad 500 ml
Stock staining solution		
Reagent 1	2%	10 ml
Reagent 2	98%	490 ml
Final staining solution		
Stock staining solution	80%	40 ml
Methanol (Merck, 1.06009.2511)	20%	10 ml
Fast-destaining solution		
Methanol (Merck, 1.06009.2511)	25%	250 ml
Acetic acid 100% (VWR, 20102.292)	10%	100 ml
MilliQ -H_2O		Ad 1000 ml
Slow-destaining solution		
Methanol (Merck, 1.06009.2511)	25%	250 ml
MilliQ -H_2O		Ad 1000 ml
Glycerol solution		
Glycerol (VWR, 444482V)	1%	1 g
MilliQ -H_2O		Ad 100 ml
400 mM NEM solution		
N-Ethylmaleimide (Merck, 34115)	0.4 M	0.05g
MilliQ -H_2O		1 ml

3.8.5 Isoelectric focusing

Reagent	Manufacturer/ Supplier	Cat.-No.
Novex IEF Sample Buffer pH 3-10 (2X)	Thermo Fisher Scientific	LC5311
IEF Marker 3-10	Serva	39212.01
Novex pH 3-10 IEF Protein Gels	Thermo Fisher Scientific	56015
Novex IEF Cathode Buffer pH 3-10 (10X)	Thermo Fisher Scientific	LC5310
Novex IEF Anode Buffer (50X)	Thermo Fisher Scientific	LC5300
PVDF Transfer Membrane, 0.45 µm	Thermo Fisher Scientific	88585
Novex Tris-Glycine Transfer Buffer (25X)	Thermo Fisher Scientific	LC3675
Odyssey Blocking Buffer (PBS)	Licor	927-40000
Anti-natalizumab-HRP, IgG1	Bio-Rad	HCA249P
Biotinylated Anti-BT062 idyotype antibody	Biotest	
Anti-HRP-800CW (Chemi-IR Detection Kit)	Licor	926-32236
Streptavidin-680RD	Licor	926-68079

	Final concentration	Total addition
Fixation solution		
Trichloroacetic acid (Merck, 1.00807.1000)	120 g/l	120 g
Sulfosalicylacid dihydrat (Merck, 8.00691.0250)	35 g/l	35 g
MilliQ -H_2O		Ad 1000 ml

3.8.6 Size exclusion Chromatography

	Final concentration	Total addition
nBT062 SEC buffer		
Reagent A		
Na_2HPO_4 (Merck, 1.06580)	0.2 M	35.6 g
MilliQ -H_2O		Ad 1000 ml
Reagent B		
NaH_2PO_4 (Merck, 1.06345)	0.2 M	31.2 g
MilliQ -H_2O		Ad 1000 ml

Add Reagent B into A until pH 7.0 is obtained

Denaturing SEC buffer		
K_2HPO_4 (Merck, 1.05104)	0.1 M	11.12 g
KH_2PO_4 (Merck, 1.04877)	0.1 M	8.72 g
KCl (Merck, 1.04936)	0.25 M	11.92 g
Adjust pH to 7.0		
MilliQ -H_2O		Ad 800 ml
2-propanol (Merck, 1.00995)	20%	200 ml

3.8.7 *In vitro* half-antibody exchange analysis

	Final concentration	**Total addition**
GSH solution		
Reduced glutathione (Sigma, G6013)	100 mM	30.73 mg
MilliQ -H_2O		1 ml
GSSG solution		
Oxidized glutathione (Sigma, G4376)	100 mM	61.26 mg
MilliQ -H_2O		1 ml

3.8.8 Fluorescence microscopy

Reagent	**Manufacturer/ Supplier**	**Cat.-No.**
Paraformaldehyde, 4% in PBS	Santa Cruz	30525-89-4
Rabbit anti-LAMP1 antibody	Abcam	ab24170
Cy3-labeled goat anti-rabbit H+L	Jackson ImmunoResearch	111-165-003
Prolong Gold Antifade Mountant with DAPI	Thermo Fisher Scientifc	P36935

	Final concentration	**Total addition**
0.02% Saponin		
Saponin (Merck,)	0.02%	20 mg
DPBS		Ad 100 g
1x BMB/PBS		
Reagent A		
Maleic acid (Sigma-Aldrich, M0375-500G)	100 mM	11.6 g
NaCl (Merck, 1064045000)	250 mM	14.61 g
MilliQ -H_2O		Ad 1000 ml

Reagent B (BMB 10x Stock)		
Blocking Reagent (BMB, Roch, 11096176001)	10 %	10 g
Reagent A		Ad 100 g
1xBMB/PBS (final solution)		
Reagent B	10 %	10 ml
DPBS		Ad 100 ml

3.8.9 DM4-conjugation of antibodies

Reagent	**Manufacturer/ Supplier**	**Cat.-No.**
SPDB Linker	Immunogen	n/a
DM4	Immunogen	n/a
Dimethylacetamid (DMA)	Merck	8032351000
	Final concentration	**Total addition**
Buffer A		
KH_2PO_4 (Merck, 1.04877)	50 mM	6.8 g
NaCl (Merck, 1064045000)	50 mM	2.922 g
EDTA (Sigma-Aldrich, 34103-500GM)	2 mM	0.744 g
Adjust pH to 6.5		
MilliQ -H_2O		Ad 1000 ml

3.8.10 DM4 distribution analysis by LC-MS

Reagent	**Manufacturer/ Supplier**	**Cat.-No.**
Zorbax RRHD 300-Diphenyl, 1.8 µm, 2.1x100mm	Agilent	858750-944
	Final concentration	**Total addition**
Eluens C		
Isopropanol (Merck, 1096341011)	2%	20 ml
Trifluoroacetic acid (Merck, 8082600500)	0.1%	1 ml
MilliQ-H_2O		Ad 1000 ml
Eluens D		
Acetonitrile (Merck, 1000032500)	10%	100 ml
Isopropanol (Merck, 1096341011)	20%	200 ml
Trifluoroacetic acid (Merck, 8082600500)	0.1%	1 ml
MilliQ-H_2O		Ad 1000 ml

3.8.11 DM4 conjugation site mapping by LC-MS

Reagent	**Manufacturer/ Supplier**	**Cat.-No.**
1 M DTT	Merck	20-265
Trifluoroacetic acid	Merck	8082601000
	Final concentration	**Total addition**
Denaturing buffer		
Guanidine HCl	6 M	
Tris-HCl	1.2 M	
Adjust pH to 7.74		
MilliQ Water		Ad 1000 ml
Digestion buffer		
Tris-HCl	50 mM	
$CaCl_2$	1 mM	
pH 8.0		
MilliQ water		Ad 1000 ml
Eluent A		
Acetonitrile (Merck,1000032500)	2%	20 ml
Trifluoroacetic acid (Merck, 8082601000)	0.05%	0.5 ml
MilliQ-H_2O		Ad 1000 ml
Eluent B		
Acetonitrile (Merck, 8082601000)	80%	800 ml
Trifluoroacetic acid	0.05%	0.5 ml
MilliQ-H_2O		Ad 1000 ml

3.8.12 Cytotoxcity Assay

Reagent	**Manufacturer/ Supplier**	**Cat.-No.**
WST-1	Roche	11 644 807 001
	Final concentration	**Total addition**
Assay buffer		
Bovin serum albumin	0.1%	0.5 g
DPBS		Ad 500 ml
Adjust pH to 7.74		

3.8.13 Anti-CD138 antibody detection assay

Reagent	Manufacturer/ Supplier	Cat.-No.
sCD138	R&D Systems	2780-SD-050
biotinylated goat anti-human IgG antibody	Jackson ImmunoResearch	109-066-097
Streptavidin SULFO-TAG Labeled	Meso Scale Discovery	R32AD-1
Read Buffer T (4x)	Meso Scale Discovery	R92TC
PBST-KS blue	Biotest	1081

	Final concentration	Total addition
Washing solution		
Bovin serum albumin	0.1%	0.5 g
PBS		Ad 500 ml
Adjust pH to 7.74		

3.9 Laboratory equipment

Equipment	Manufacturer	Type
96-Well plate, U-bottom	Greiner	CellStar , No. 650180
Äkta chromatography system	GE Healthcare	Äkta Avant 150
Illustra NAP-25 columns	GE Healthcare	17-0852-01
Illustra NAP-5 columns	GE Healthcare	17-0853-01
Amicon Ultra 0.5 ml 30 kDa	Merck	UFC503096
Sterile filter 0.2 µm	VWR	514-0064
Peristaltic pump	Watson	Marlow 323
12-Well plate, F-bottom	VWR	No. 734-2778
Blotting Paper	Sigma-Aldich	Whatman 3MM papers
Nucleofector	Lonza	Lonzas 4D-Nucleofector
Cell count chamber	Neubauer; VWR	631-1131
Cell culture flask	Sarstedt	25 cm^3; 75 cm^3
Cell culture cryogenic tubes	Nunc / Thermo Scientific	1.8 ml, No. 377267
Cell culture shaking flask	Corning	125 ml, 250 ml, 500 ml, 1 L
Cell freezing container	Nalgene / Thermo Scientific	Mr. Frosty, No. 5100-0001
Centrifuge	Thermo Scientific	Heraeus Multifuge 3L-R rotor: 75006445
Centrifuge tube	VWR	50 ml, No. 525-0224
CO_2 incubator, static	Thermo Scientific	HeraCell 240i
CO_2 incubator, shaking	Kuhner	Climo-Shaker ISF1-X
Dialysis Devices, 500 µl, 10K MWCO	Pierce / Thermo Scientific	Slide-A-Lyzer MINI Dialysis; No. 88401

Electrophoresis chamber	Thermo Scientific	XCell SureLock Mini-Cell
Flow cytometer	Becton & Dickinson	FACSCanto II Flow Cytometer
Fluorescence imaging system	Licor	Odyssey CLx imager
SEC column	Tosoh Bioscience	TSKgel G3000SW, No. 05789
Nano HPLC System	Dionex	Ultimate 3000
IEF System	GE Healthcare Life Science	Multiphor II
Laminar flow	Thermo Scientific	HeraSafe KS15
Micro centrifuge	Thermo Scientific	Heraeus Biofuge fresco
Microscope	Carl Zeiss	Axiovert 40C
Orbital Shaker	Heidolph	Polymax 1040
pH-Meter	WTW	InoLab pH 730
Plate photometer	BMG Labtech	POLARstar Omega
Cuvette photometer	Amersham Biosciences	Ultrospec 2100 pro
Plate Shaker	IKA	MTS 2/4 digital microtiter shaker
96-Well Plate Washer	Tecan	Power Washer PW96
Pipetboy	IBS Integra Biosciences	Pipetboy comfort
Pipette 0,5-10 µl	Brand	Transferpette
Pipette 100-1000 µl	Brand	Transferpette
Pipette 10-100 µl	Brand	Transferpette
Scanner	Epson	Perfection V700 Photo
SDS-PAGE Power Supply	Life technologies	PowerEase 90W Power Supply
MSD ECL Reader	Meso Scale Discovery	Sector Imager 6000
Thermoshaker	VWR	PHMT-PSC24N
Vortexer	IKA	MS2 Minishaker
Water bath	Grant	SUB Aqua 18

Software

CellSens	Olympus	Version 1.9
Chromeleon	Dionex	Version 6.8
Discovery Workbench 2006	MSD	3.0.18
Excel	Microsoft	Microsoft Office 2007
FACSDiva Software	Becton&Dickinson	Version 6.1.3
Flowjo	Treestar Inc.	Mac Version 9.3
GraphPad Prism	GraphPad Software Inc.	Version 6
Image Studio	Licor	Version 1.0.11
Unicorn	GE Healthcare	Version 6.2

4 Results

4.1 Generation and characterization of nBT062 model variants by SDS-PAGE, IEF and SEC

In 2009 Labrijn and colleagues reported that the therapeutic monoclonal antibody natalizumab undergoes half-antibody exchange with endogenous IgG4 in humans (Labrijn et al. 2009). In this thesis, IgG4-related half-antibody exchange and its potential effect on the antibodies functionality and efficacy was investigated for the anti-CD138 antibody-drug conjugate BT062. Therefore, four model variants as shown in Figure 4-1 were generated: (I) WT nBT062, comprises the backbone of an unmodified human IgG4 antibody. (II) Stable nBT062 was generated by introducing stabilizing mutations within the hinge and CH3 domains into the WT nBT062 sequence to prevent half-antibody exchange. (III) By exchanging the cysteines at position 226 and 229 in the hinge region to serines in WT nBT062, covalent dimerization of the heavy chains was inhibited resulting in nBT062 half-antibodies (half nBT062). (IV) To study effects of bispecific antibodies derived by half-antibody exchange with endogenous IgG4, a stabilized, bispecific nBT062-natalizumab was designed as described in section 3.1. All variants were expressed in FreeStyle CHO-S cells using an 8-day batch cultivation. Supernatants were 0.2 µm filtered and frozen until purification (see section 3.2.2). nBT062 variants were purified by Protein A affinity chromatography as exemplarily demonstrated for WT nBT062 in Figure 4-2 followed by a buffer exchanging step (see section 3.2.3).

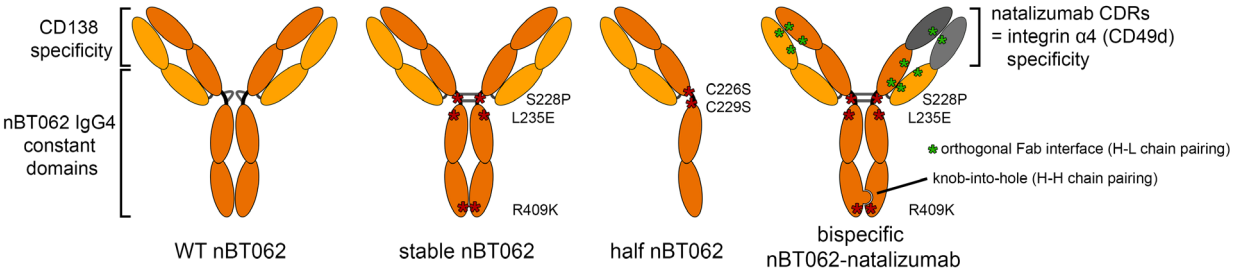

Figure 4-1: Schematic representation of nBT062 model antibodies.

The generated nBT062 model antibodies wild type (WT) nBT062, stable nBT062, half nBT062 and bispecific nBT062-natalizumab are shown. The different variants mimic antibody species produced by *in vivo* IgG4 half-antibody exchange. Different modifications are indicated.

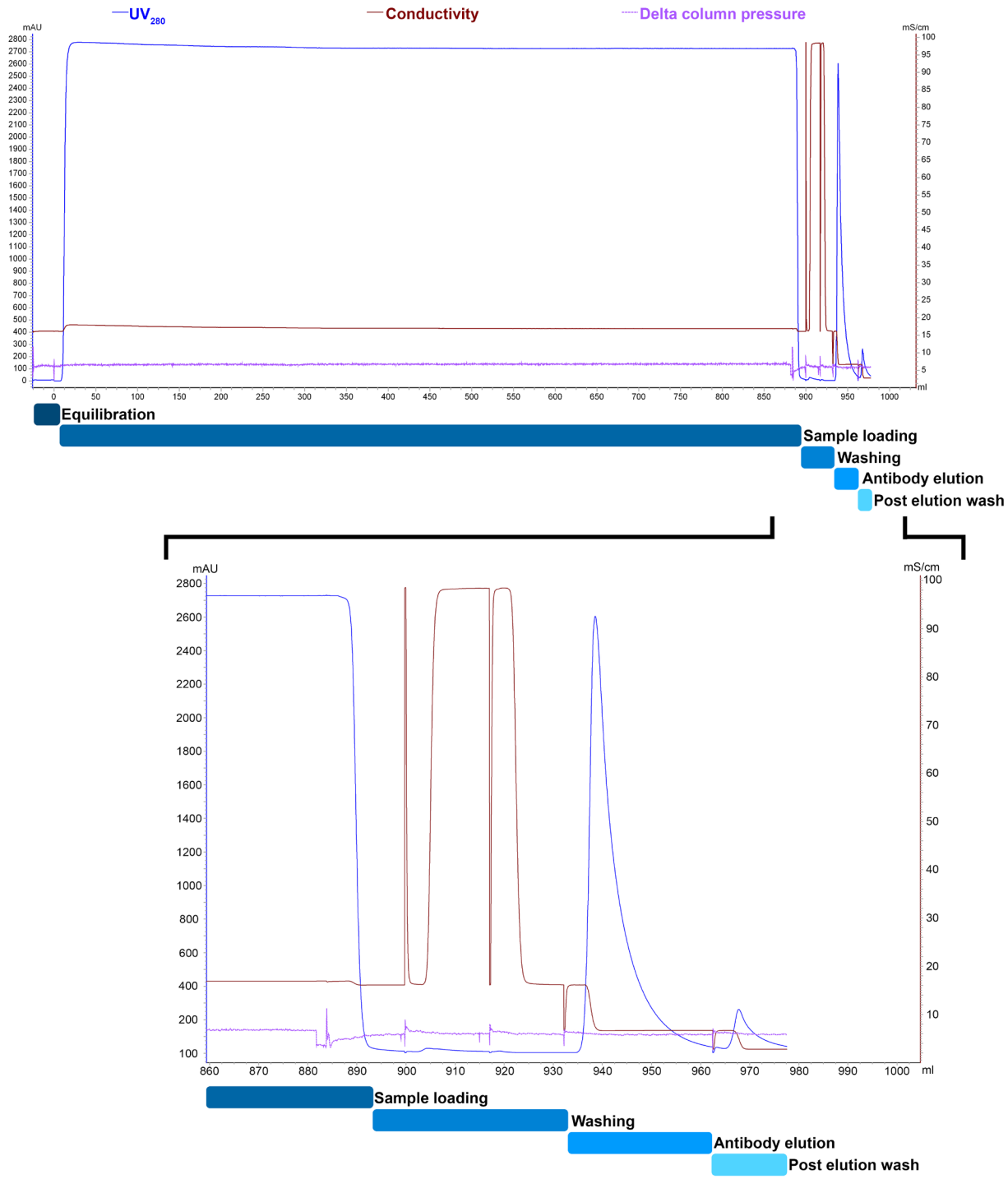

Figure 4-2: Exemplary chromatogram of WT nBT062 affinity chromatography.

Purification of nBT062 variants was performed by affinity chromatography using a mabSelect protein A column connected to an Äkta Avant 150 system. Purification included sample loading, washing steps of column-bound antibodies with DPBS and DPBS + 1M NaCl and elution with glycin-HCl pH 3.5 followed by neutralization and buffer exchange. This chromatogram demonstrates purification of WT nBT062 as example.

To examine correct expression and purification of model antibodies, SDS-PAGE analysis, IEF, and SEC were used for a first characterization. Reducing and non-reducing SDS-PAGE analysis was performed as described in section 3.3.1 and results are shown in Figure 4-3. By applying reducing conditions, all four nBT062 model variants were separated in two bands, one at approx. 25 kDa and one at approx. 50 kDa of molecular weight, representing the antibodies L and H chains, respectively. Within the bispecific nBT062-natalizumab sample, two H chain bands with minimal different molecular weights were obtained, indicating separate nBT062 and natalizumab H chains with calculated weights of 49.7 and 49.3 kDa, respectively (calculated using ProtParam webservice). An additional band at approx. 85 kDa was observed for the stable nBT062 antibody indicating a small fraction of dimerized H chains (H2). By applying non-reducing conditions, WT nBT062, stable nBT062, and bispecific nBT062-natalizumab demonstrated each a high-intensity band at approx. 150 kDa representing full lengh antibodies (H2L2). For WT nBT062 a low-intensity band at approx. 70 kDa was additionally observed, indicating a half antibody fraction which was not detected in stable nBT062 and bispecific nBT062-natalizumab samples. This half antibody fraction at approx. 70 kDa was identified as the only high-intensity band within the half nBT062. Full lenght H2L2 antibodies were lacking in this sample. These SDS-PAGE results indicate that the different nBT062 variants were expressed correctly and each variant demonstrated the specific properties for half antibody occurance as expected. Further, no undefined bands were observed, *e.g.* host cell proteins, demonstrating a high purify of the antibody samples.

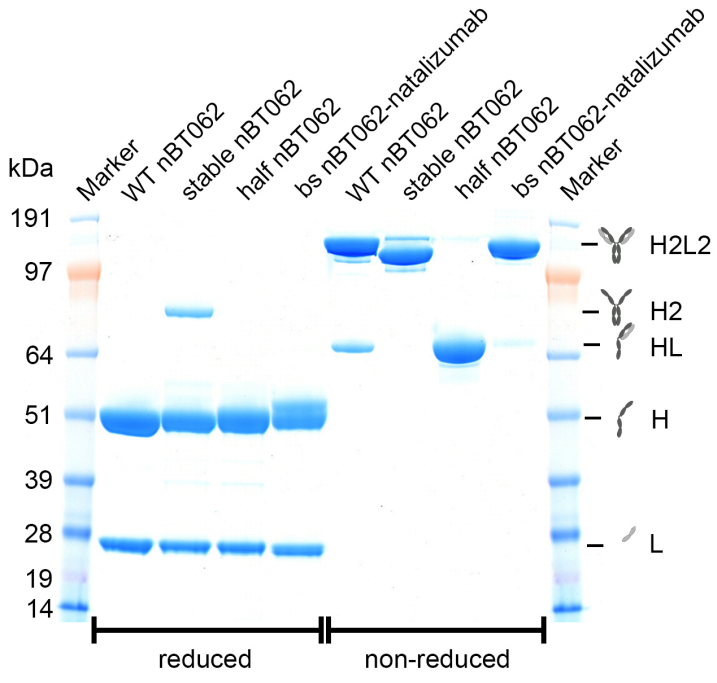

Figure 4-3: Reducing and non-reducing SDS-PAGE of WT, stable, half nBT062 and bispecific nBT062-natalizumab. Non-reduced analyzed antibodies were diluted with NuPAGE LDS sample buffer/100 nM NEM solution and heated 30s at 70°C. Reduced analyzed antibodies were treated with NuPAGE LDS sample buffer/NuPAGE Sample Reducing Agent and heated for 10 min at 70°C. 10 µg of each antibody was loaded onto a NuPAGE Novex 4-12% Bis-Tris Gel. Coomassie staining was used for visualization and SeeBlue Plus 2 Protein Standard for size identification (indicated in kDa). Antibody subunits are marked on the right: H= heavy chain; L= light chain.

IEF was performed to assess the isoelectric points (pIs) of WT nBT062, stable nBT062, half nBT062, and bispecific nBT062-natalizumab and demonstrate differences based on the individually introduced mutations of each variant (see section 3.3.2). Results are shown in Figure 4-4. nBT062 variants were stained by Coomassie blue staining and by immuno-detection after western blotting. The Coomassie stained gel revealed that WT nBT062 was separated in 7 bands ranging from approx. pH 6.5 to 7.3, including one band with the highest intensity nearly at pH 6.8. The pIs of stable nBT062 were ranging from approx. pH 6.4 to 7.0, also separated into 7 bands. The band patterns of WT nBT062 and stable nBT062 were similar with a slightly acidic shift for stable nBT062. For half nBT062 4 bands between pH 6.1 and 6.8 with two high intensity and two low intensity bands were detected. Natalizumab was also divided into 4 bands, two high intensity bands at approx. pH 7.7 and two low intensity bands at approx. pH 7.6 and 7.8. The bispecific nBT062-natalizumab demonstrated 10 bands separated from approx. pH 7.3 to 8.0, including one high intensity band at pH 7.4. This analysis clearly demonstrated a basic pI shift for bispecific nBT062-natalizumab compared to the other nBT062 variants through the introduced mutations. This is most probably based on the introduced natalizumab CDR region rather than the stabilizing and chain-pairing mutations as natalizumab itself has also a basic pI. Multicolor western blotting of an isoelectric focusing gel was performed to identify monospecific antibodies within the bispecific nBT062-natalizumab fraction (Figure 4-4 B). Anti-idiotypic antibodies against nBT062 (green) and natalizumab (red) were used for visualization. The staining revealed that WT nBT062, stable nBT062 and half nBT062 were only detected by the anti-nBT062 idiotypic antibody, while natalizumab was exclusively detected by the anti-natalizumab idiotypic antibody. For bispecific nBT062-natalizumab it was observed that 8 out of 10 bands were stained by both anti-idiotypic antibodies. Two bands were exclusively stained by the anti-natalizumab idiotypic antibody within this fraction. This experiment demonstrated that the bispecific nBT062-natalizumab sample did not contain any monospecific nBT062 antibodies which could interfere with further analysis.

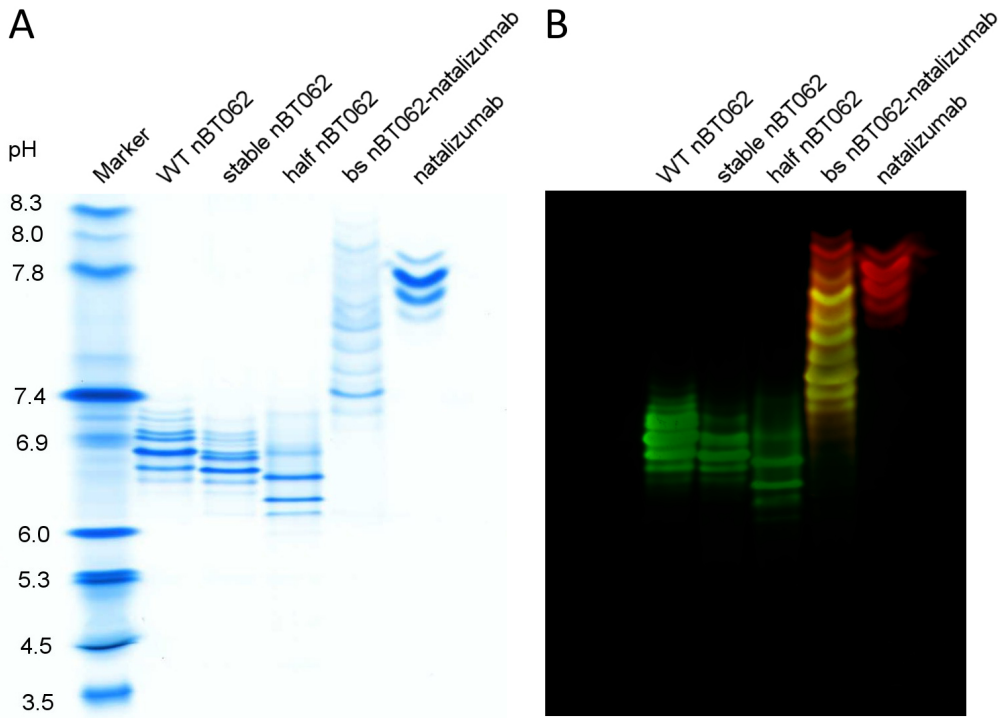

Figure 4-4: Isoelectric focusing of WT, stable, half nBT062 and bispecific nBT062-natalizumab.
10 µg of each untreated antibody was loaded onto an IEF Gel, pH 3- 10 for isoelectric point separation. (A) Serva IEF Marker 3-10 was used for pH identification and Coomassie staining was done for protein visualization. pH values are assigned on the left. (B) After isoelectric focusing, indicated nBT062 model variants were blotted onto a PVDF membrane. Selective nBT062 and natalizumab specificities were detected by anti-idiotypic antibodies visualized in green and red, respectively.

WT nBT062, stable nBT062, half nBT062, and bispecific nBT062-natalizumab were analyzed by SEC using either native running buffer or denaturing running buffer containing 10% 2-propanol (see section 3.3.3). The latter conditions were mainly applied to observe half-antibody formations, while native running buffer was used to focus on aggregates and protein fragments. Detection occurred at 280 nm. Bigger proteins were released earlier from the column than small molecules, which were retained by porous particles of the column material. As demonstrated in Figure 4-5 A, under native conditions main peaks were detected between approx. 29.5 min and 35 min representing the full-length antibodies of all nBT062 variants. Within this time frame, half nBT062 and bispecific nBT062-natalizumab showed a shorter retention time (31.8 min and 32.1 min, respectively). Additionally, the main peak of bispecific nBT062-natalizumab comprises a shoulder at 31.1 min. On the contrary, WT and stable nBT062 demonstrated nearly identical retention times for their peak maxima at 32.5 min. Aggregates were observed for all nBT062 antibody variants, but with different proportions as identified by peak integration: Half nBT062 contained less than 4.5%, WT nBT062 contained 7.4%, and bispecific nBT062-natalizumab showed 7.1%.Suprisingly, most aggregates (25%) were detected in stable nBT062, indicating the BT062 formulation buffer is

not optimal for stable nBT062. However, nearly no antibody-related protein fragments could be observed in the LC spectrum at 280 nm of each nBT062 variant.

Under denaturing conditions, main peaks representing full length antibodies of WT nBT062, stable nBT062, and bispecific nBT062-natalizumab demonstrated comparable retention times at 39.1 min, 39.0 min, and 38.9 min, respectively (Figure 4-5 B). In contrast to that, the main peak of half nBT062 was observed after 42.1 min, indicating a smaller molecule size and, thus, the presence of half-antibodies. Within this sample no full length antibody peak at approx. 39 min was detected. In addition to the main peaks of WT nBT062 and bispecific nBT062-natalizumab, both samples showed small half antibody peaks at 43.1 min and 42.6 min representing 6.1% and 2.3% half-antibodies, respectively. For stable nBT062, no half antibody peak was observed. Even under denaturing conditions in the presence of 10% 2-propanol, aggregate peaks occurred within stable nBT062 with fractions of 7.5%. Interestingly, bispecific nBT062-natalizumab revealed an aggregate fraction of 32.2%.

Taken together, the SEC analysis demonstrated only minor amounts of aggregates for WT nBT062, half nBT062, and bispecific nBT062-natalizumab, while the fraction of aggregates was higher in stable nBT062. The analysis revealed that the presence of half-antibodies seems to depend on the surrounding buffer conditions: Half nBT062 was detected as half-antibodies (HL) only using denaturing running buffer. In native running buffer, half nBT062 molecules seem to dimerize despite the lack of covalent H -H pairing.

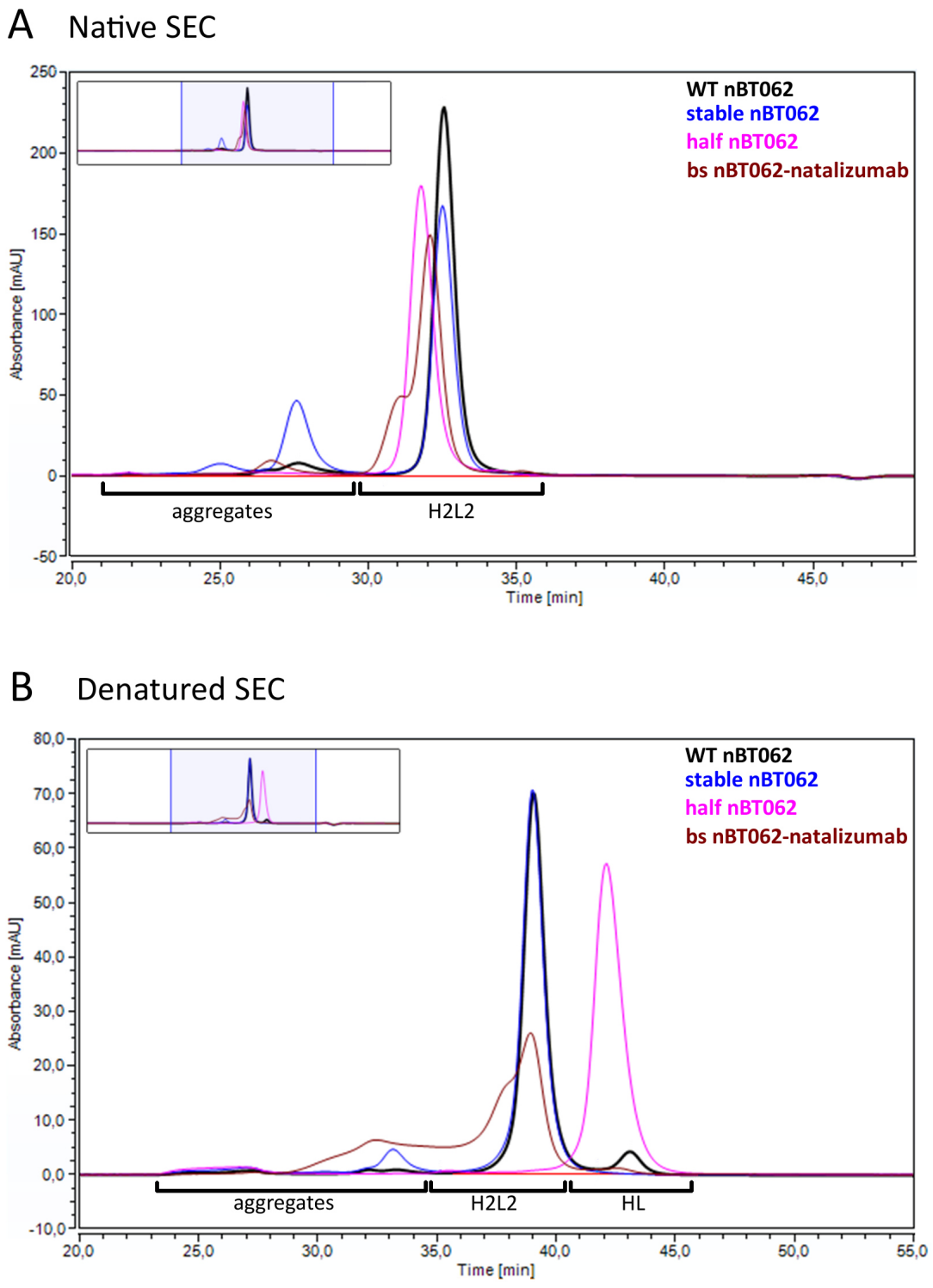

Figure 4-5: Size exclusion chromatography of nBT062 model variants.

WT nBT062, stable nBT062, half nBT062, and bispecific nBT062-natalizumab were separated under native (**A**) or denaturing (**B**) conditions using a TSKgel G3000 column (Tosoh Bioscience) connected to a nano HPLC system. Detection was done at 280 nm and different antibody-related species are indicated. H= Heavy chain, L= light chain.

To investigate if the incorporation of the stabilizing mutations S228P and R409K within stable nBT062 (and bispecific nBT062-natalizumab) can successfully prevent the formation of bispecific antibodies, an *in vitro* assay was performed. WT nBT062 and stable nBT062 were treated in the presence of identical amounts natalizumab with 10 mM GSH to potentially reduce the disulfide bonds of the hinge region for half-antibody formation. GSH was removed and subsequent reoxidation was enabled by GSSG addition (see section 3.3.4). The formation of bispecific antibodies was determined by IEF as shown in Figure 4-6. While untreated control antibodies, WT nBT062 and stable nBT062 separately loaded onto the gel, demonstrated pIs of approx. 6.2 to 6.8, natalizumab bands were more basic in the pH range of approx. 7.5 to 7.7. These bands of all individual antibodies were also observed in the respective mixtures of reoxidized WT nBT062/natalizumab and stable nBT062/natalizumab. However, 4 additional bands in the intermediate pH range of 6.9 to 7.4 were detected in the reoxidized mixture of WT nBT062/natalizumab representing generated bispecific antibodies (red line). Those bispecific antibody bands were lacking in the reoxidized mixture of stable nBT062/natalizumab. Thus, it can be concluded that stabilizing mutations S228P and R409K could successfully prevent the half-antibody exchange under the applied reducing conditions in this experiment.

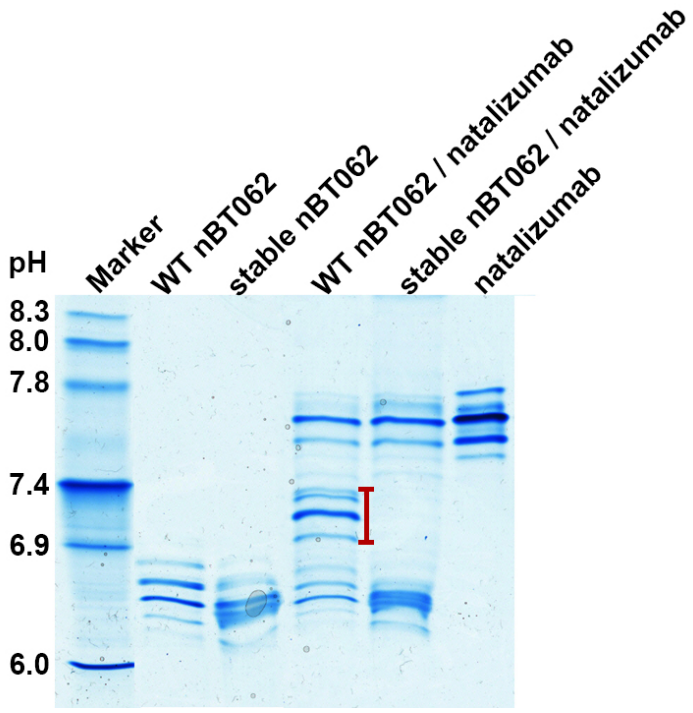

Figure 4-6: Evaluation of *in vitro* half-antibody exchange.

WT nBT062 or stable nBT062 was mixed with natalizumab and treated with 10 mM GSH and after dialysis subsequently with 5 mM GSSG. 10 µg of each treated or untreated control antibody solution was loaded as indicated onto an IEF Gel, pH 3-10 for IEF. Coomassie staining was done for protein visualization. pH values based on the Serva IEF Marker 3-10 are assigned on the left and pH range of bispecific antibodies are indicated in red.

4.2 Antigen-binding of nBT062 model variants

Specific binding of WT nBT062, stable nBT062, half nBT062 and bispecific nBT062-natalizumab to CD138 and CD49d was investigated by flow cytometry according to section 3.4.2. Murine, transgenic Ba/F3-hCD138 cells ($CD138^+$/ $CD49d^-$) and human T lymphocyte Jurkat cells ($CD138^-$/ $CD49d^+$) were incubated with serial dilutions of nBT062 model antibodies and natalizumab ($5x10^{-7}$ - $2.82x10^{-12}$ M). Detection was done using an Alexa Fluor 647 conjugated anti-human secondary antibody. nBT062 and natalizumab were mutually used as isotype controls and cells stained only with the secondary antibody functioned as a further negative control. Cell gating was performed in the forward-sideward scatter (FSC-SSC) of unstained cells. An example for the gating strategy is shown in Figure 4-7 A, including a histogram overlay of cells incubated with different WT nBT062 concentrations demonstrating concentration-dependent staining (see Figure 4-7 B). Median fluorescence intensities (MFIs) were plotted against the corresponding antibody concentrations. As demonstrated in Figure 4-8 A, WT nBT062, stable nBT062 and half nBT062 demonstrated comparable binding to $CD138^+$ Ba/F3-hCD138 cells with avidities of $5.5x10^{-10}$, $7.1x10^{-10}$ and $11.2x10^{-10}$ M, respectively (see Table 4-2). Binding of bispecific nBT062-natalizumab to CD138 was slightly reduced. However, the affinity of nBT062-natalizumab against CD138 was still in the nanomolar range (~$23x10^{-9}$ M, Table 4-2). Natalizumab was not able to bind those $CD138^+$/$CD49d^-$ Ba/F3-hCD138 cells. CD49d-expressing, $CD138^-$ Jurkat cells were bound by natalizumab and bispecific nBT062-natalizumab with binding activities of $4x10^{-10}$ M and $21x10^{-10}$ M, respectively, indicating that both antigens were recognized by the bispecific model variant. The other nBT062 variants did not show any binding to these $CD138^-$ cells. In conclusion, it was demonstrated that all nBT062 variants were able to bind CD138 with low nanomolar avidity, despite the binding of bispecific nBT062-natalizumab was slightly reduced.

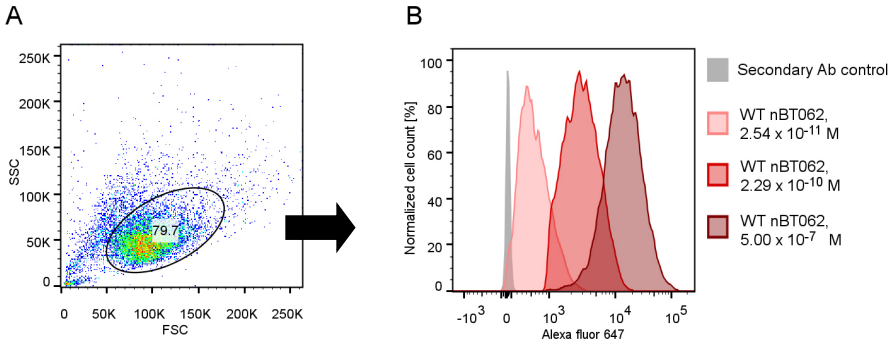

Figure 4-7: Exemplary FACS staining and gating strategy using Ba/F3-hCD138 cells

Ba/F3-hCD138 cells were stained with different concentrations of nBT062 variants and natalizumab. An Alexa Fluor 647-labeled anti-human antibody was used for detection. **A:** Gating of Ba/F3-hCD138 cells in the forward-/sideward scatter. Gating was adjusted for Jurkat cells. **B:** Exemplary overlay histogram of Ba/F3-hCD138 cells incubated with indicated concentrations of WT nBT062 and stained with an Alexa Fluor 647 secondary antibody.

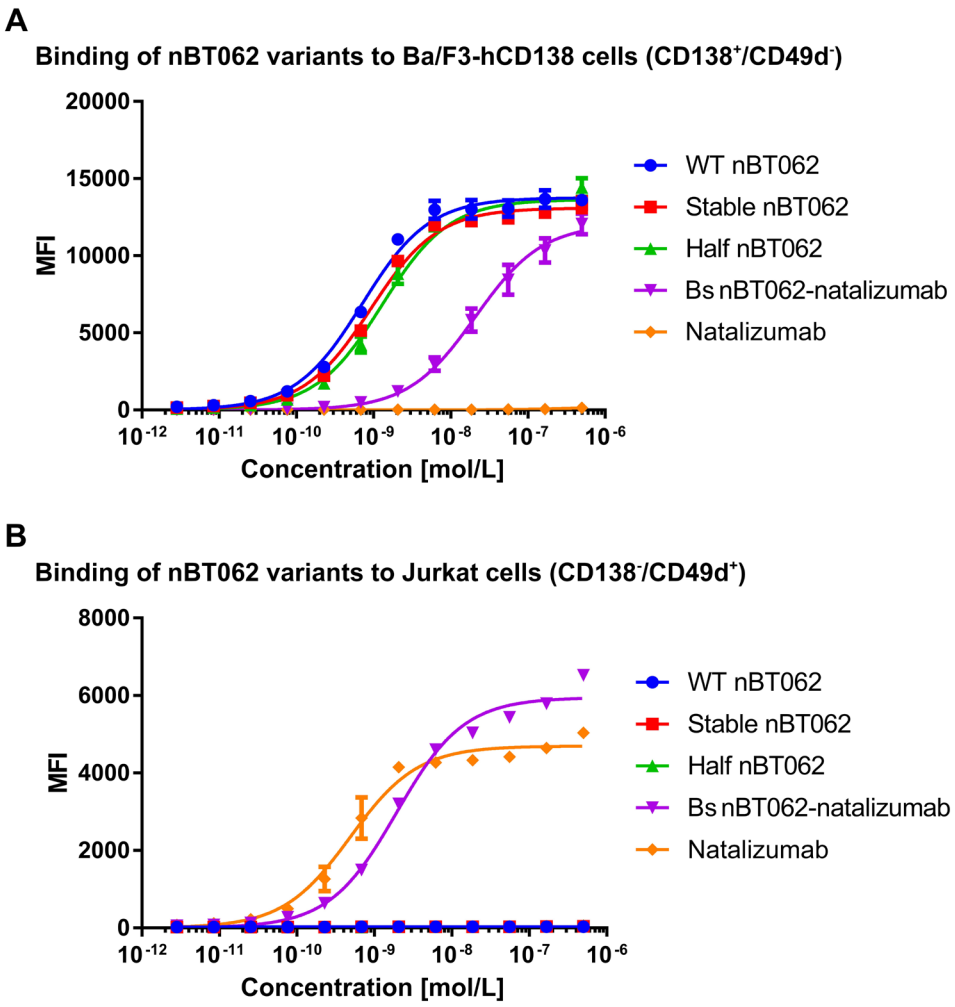

Figure 4-8: nBT062 model variants selectively bind to CD138$^+$ cells in a concentration-dependent manner. Ba/F3-hCD138 cells, positive for nBT062 antigen and negative for natalizumab antigen (**A**), and Jurkat cells, negative for nBT062 antigen and positive for natalizumab antigen (**B**), were incubated with different concentrations ($5x10^{-7}$–$2.82x10^{-12}$ M) of WT nBT062, stable nBT062, half nBT062 and bispecific nBT062-natalizumab antibodies. Data were obtained by flow cytometry using a secondary anti-human antibody for detection. Binding curves demonstrate one representative experiment out of three, each measured in triplicates. MFI= Median Fluorescence Intensity.

4.3 Internalization analysis of nBT062 model antibodies

As cellular antibody internalization is one of the most critical parameters of ADCs, uptake of WT nBT062, stable nBT062, half nBT062 and bispecific nBT062-natalizumab was investigated by flow cytometry and fluorescence microscopy. For both assays, nBT062 model variants directly labeled with Dylight-488 (Dy488) fluorescent dyes according to section 3.4.1 were used.

4.3.1 Internalization by flow cytometry

For flow cytometric analysis, human multiple myeloma derived NCI-H929 ($CD138^+/CD49d^+$) and transgenic Ba/F3-hCD138 ($CD138^+/CD49d^-$) cells were incubated with Dy488-labeled WT nBT062, stable nBT062, half nBT062 or bispecific nBT062-natalizumab for either 0.5 h at 4°C for surface staining or 24 h at 37°C to enable antibody internalization. CD49d expressed on NCI-H929 cells was blocked with an excess of unlabeled natalizumab. To distinguish and verify surface bound or internalized antibodies, CD138 was cleaved of by trypsin. The results of three individual experiments, each measured in triplicates are shown in Figure 4-9 as MFI values. For NCI-H929 cells, highest and similar staining intensities of the different nBT062 variants were observed after 24 h of incubation without trypsin digestion at absolute MFI values of approx. 10,700. Subsequent treatment with trypsin decreased the fluorescence intensities of WT nBT062, stable nBT062 and half nBT062 by approx. 62%, while the intensity of bispecific nBT062-natalizumab was only decreased by 42% (Figure 4-9 A). Thus, the MFI values detected after 24, indicating higher amounts of internalized nBT062-natalizumab compared to the other variants. A shorter incubation period of 0.5 h led to MFIs for WT nBT062, stable nBT062 and half nBT062 which were approx. 67% of the values after 24 h incubation. On the contrary, surface staining of bispecific nBT062-natalizumab reached only 38% of the 24 h incubation, which was significantly different from the monospecific variants. Trypsin treatment after this 0.5 h incubation revealed fluorescence intensities of similar values as unstained cells and negative control staining (natalizumab). Similar findings were observed with Ba/F3-hCD138 cells: The highest MFI values for all nBT062 variants were found after 24 h of antibody incubation without subsequent trypsin digestion. The average MFI was 4460 (Figure 4-9 B). Fluorescence intensities decreased after proteolytic treatment to 73%, 69%, 72% and 77% for WT nBT062, stable nBT062, half nBT062 and bispecific nBT062-natalizumab, respectively. CD138-surface binding (0.5 h incubation) with WT nBT062 led to 24% fluorescence intensity compared to the 24 h incubation without trypsin. Similar to that, stable nBT062 and half nBT062 reached 27%, while only 14% cell surface staining were observed with bispecific nBT062-natalizumab, demonstrating a significant difference between the monospecific variants and the bispecific one. In summary, it was observed that WT nB062, stable nBT062 and half nBT062 demonstrated similar surface binding and internalization on both tested cell lines. In contrast, bispecific nBT062-

natalizumab demonstrated a reduced surface binding in both cell lines, but similar or even higher MFI values for internalization.

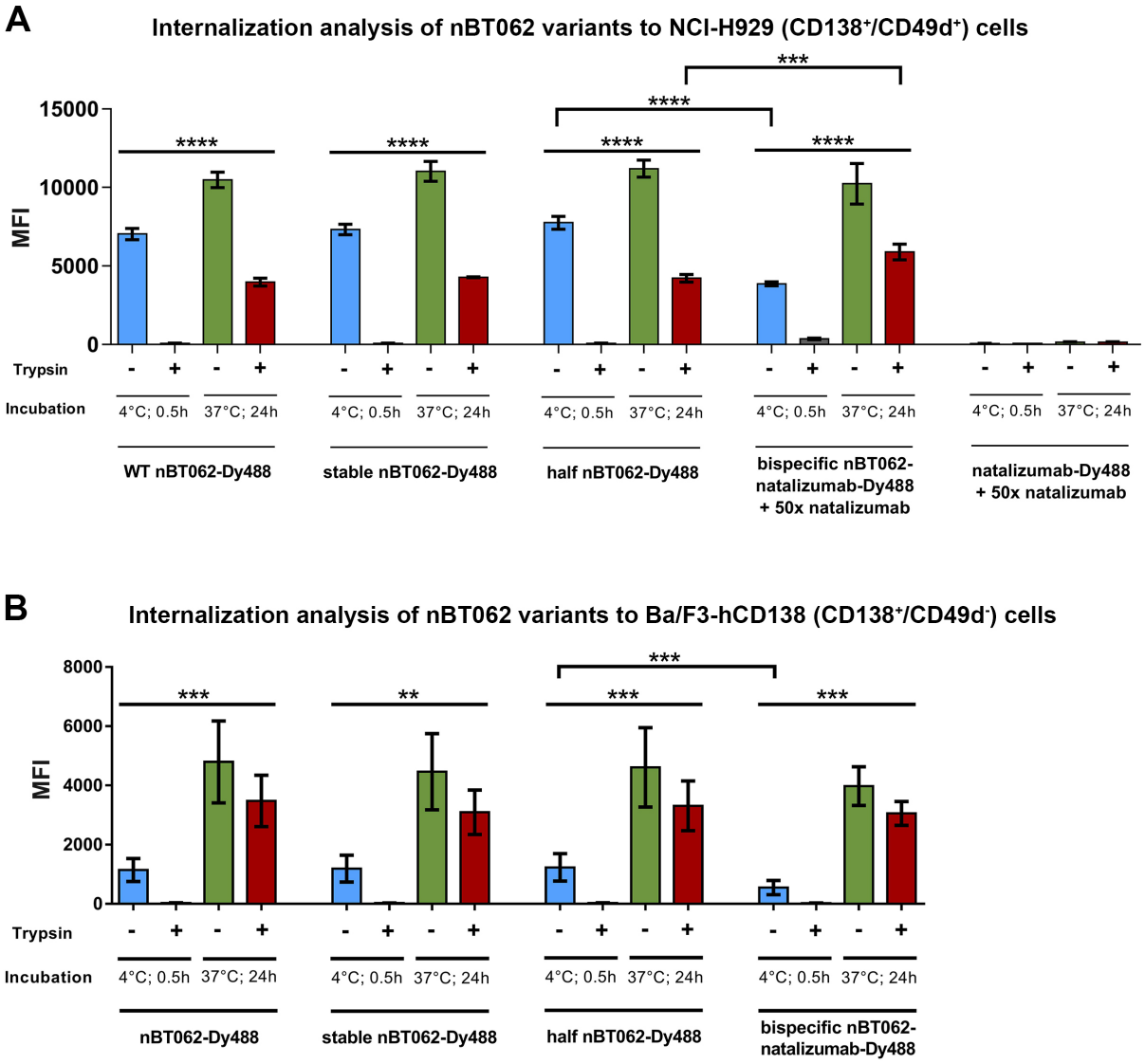

Figure 4-9: Internalization analysis of nBT062 model variants due to CD138 binding.
Dy488 conjugated WT nBT062, stable nBT062, half-nBT062 and bispecific nBT062-natalizumab were incubated for 0.5 h at 4°C or 24 h at 37°C in the presence of an excess of unlabeled natalizumab with NCI-H929 cells (**A**) or without natalizumab on Ba/F3-hCD138 cells (**B**). To distinguish and verify surface bound or internalized antibodies, CD138 was cleaved off by trypsin incubation prior to flow cytometric analyses. The median fluorescence intensity (MFI) for Dylight-488 is shown on the Y-axis. Data are obtained from three individual experiments, each measured in triplicates and statistical analysis was done using t-students test. **p<0.01; ***p<0.001; ****p<0.0001.

4.3.2 Internalization by fluorescence microscopy

To further investigate nBT062 variant internalization and analyze the mechanism of antibody uptake, fluorescence microscopy was used. Dy488-labeled WT nBT062, stable nBT062, half nBT062 or bispecific nBT062-natalizumab was incubated for 0.5h at 4°C with Ba/F3-hCD138 ($CD138^+/CD49d^-$) cells to enable surface binding. Dy488-conjugated natalizumab and Ba/F3 ($CD138^-/CD49d^-$) cells were used as negative controls. After removing unbound antibodies, internalization of surface-bound nBT062 variants was accomplished by a 3 h incubation period at 37°C. Trypsin treated, fixed and permeabilized cells were co-stained with an anti-LAMP1 antibody to mark lysosomes; nuclei were stained with DAPI. Results of fluorescence microscopy are shown in Figure 4-10. For all nBT062 variants, internalization was observed in Ba/F3-hD138 cells. Cells incubated with WT nBT062 and stable nBT062 additionally demonstrated a faint surface staining. This staining was even lower or absent on cells incubated with half nBT062 or bispecific nBT062-natailzumab, respectively. Observations for negative controls were as expected: Neither Ba/F3-hCD138 cells incubated with Dy488-labeled natalizumab (V) showed any green staining, nor $CD138^-$ Ba/F3 cells incubated with WT nBT062-Dy488 (VI). Lysosomes visualized by the anti-LAMP1 antibody were detected as small red dots in each cell (b). Overlay pictures (d) of the three fluorescence channels demonstrated a clear merged staining of each nBT062 variant and anti-LAMP1 antibody indicated by the white arrows.

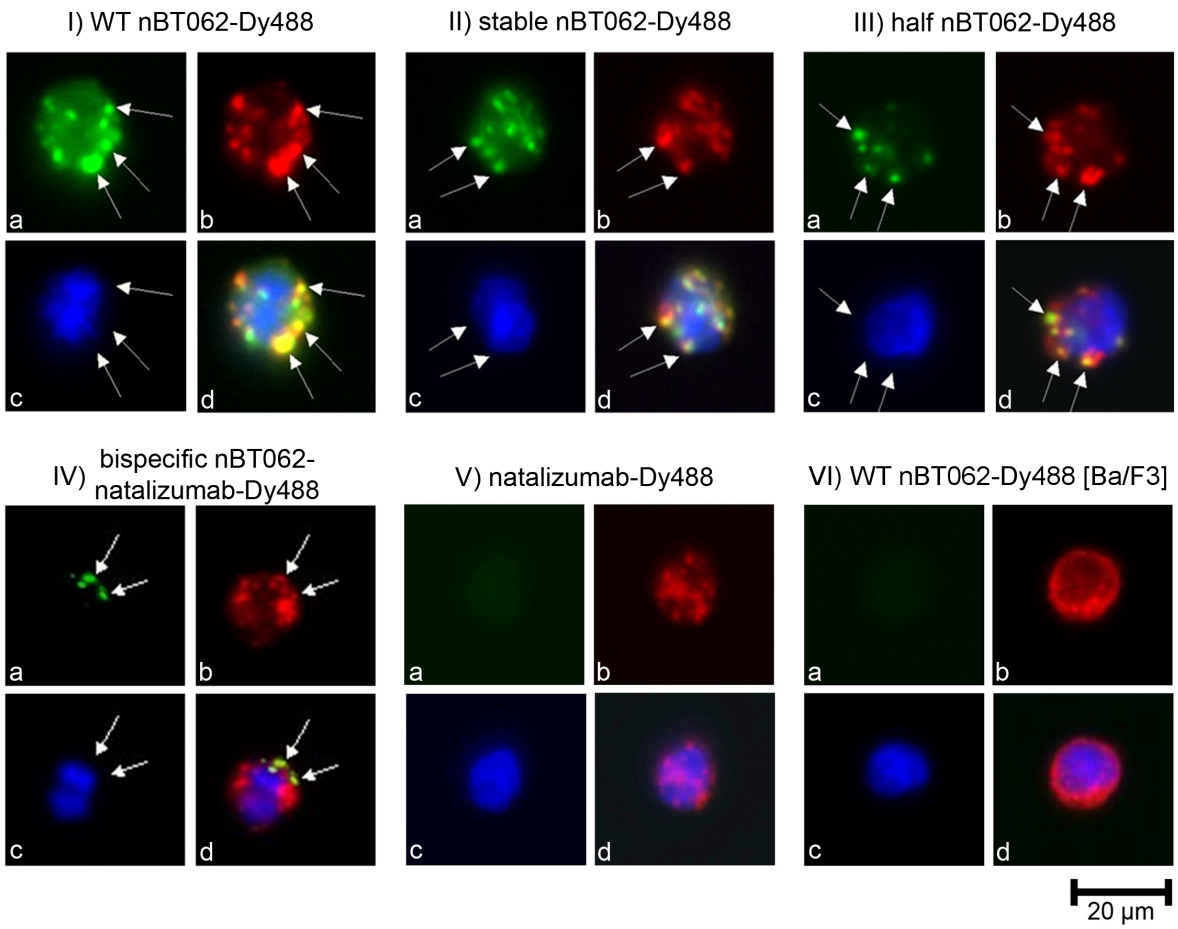

Figure 4-10: Internalization of nBT062 model variants analyzed by fluorescence microscopy.
Ba/F3-hCD138 cells were incubated with Dy488-labeled WT nBT062 (I), stable nBT062 (II), half nBT062 (III), bispecific nBT062-natalizumab (IV) or natalizumab (V, green). As negative control, Ba/F3 cells were incubated with Dy488-labeled WT nBT062 (VI). Lysosomal staining was performed with an anti-LAMP1 antibody (b, red) and cell nuclei were stained with DAPI (c, blue). Pictures of merged channels are shown in the lower right (d). White arrows indicate co-staining of nBT062 antibodies and anti-LAMP1 antibody (yellow). Pictures are taken from one representative experiment out of three individuals.

4.4 DM4-conjugation of nBT062 models and characterization of the derived nBT062 ADC variants

According to section 3.5.1, WT nBT062, stable nBT062, half nBT062 and bispecific nBT062-natalizumab were conjugated with the maytansine DM4, a tubulin inhibiting agent, to generate respective ADCs. The conjugation was performed in two steps: In a first reaction, the SPDB linker was attached to the nBT062 variant and, in a second step, DM4 was added to react with the pyridyldithio group of the SPDB linker. During the conjugation process, antibody and DM4 concentrations were monitored based on OD_{280} and OD_{252} absorptions, respectively. WT nBT062, stable nBT062 and half nBT062 were conjugated with 100% of SPDB linker and DM4 to aim for a DAR of 3.5. As shown in Table 4-1, for WT nBT062-DM4 a DAR of exactly 3.5 was reached and the conjugation of stable nBT062-DM4 led to a DAR of 3.4. Half nBT062 was conjugated identical to full length WT nBT062 and stable nBT062 as it was seen in the SEC analysis that half antibody occurrence seems to depend on surrounding buffer conditions and half nBT062 molecules were dimerized under native conditions (see section 4.1). Therefore, for dimerized half nBT062 molecules a DAR of 3.2 was observed, meaning that in average 1.6 DM4 molecules were attached to each HL fragment of half nBT062-DM4. To mimic potential *in vivo* derived bispecific nBT062-DM4 antibodies with diminished DM4 payload, the molar concentration of SPDB and DM4 to bispecific nBT062-natalizumab was reduced. The use of 70% SPDB and DM4 led to a DAR of 2.6, while 50% SPDB and DM4 result in a final ADC having a DAR of 1.7. The final yield of the conjugation reactions ranged from approx. 8.5 mg (55% of initial amount) for bispecific nBT062-natalizumab-DM4 to approx. 15.9 mg (65% of initial amount) for WT nBT062-DM4. Final ADC concentrations were between approx. 2 mg/ml and 3 mg/ml. For further analysis, the bispecific nBT062-natalizumab-DM4 with a DAR of 1.7 was used as this version reflects better a potentially *in vivo* arisen bispecific nBT062-DM4 species.

Table 4-1: DM4-conjugated nBT062 variant batches. DAR= DM4 to antibody ratio.

Sample	Used SPDB/ DM4 [%]	Final conc. [mg/ml]	Total amount [mg]	DAR	Yield [%]
WT nBT062-DM4	100	2.89	15.87	3.5	65
Stable nBT062-DM4	100	2.48	13.14	3.4	60
Half nBT062-DM4 (H2L2)	100	2.49	12.45	3.2	63
Bs nBT062-natalizumab-DM4	70	2.18	10.45	2.6	63
Bs nBT062-natalizumab-DM4	50	1.96	8.45	1.7	55

4.4.1 DM4 distribution in nBT062-DM4 model antibodies

To characterize the produced nBT062 ADCs, the different DAR species of WT nBT062-DM4, stable nBT062-DM4, half nBT062-DM4 and bispecific nBT062-natalizumab-DM4 were analyzed by LC-MS analysis (see section 3.5.3). Results from deconvoluted MS spectra are shown in Figure 4-11. Among the ADC variants, WT nBT062-DM4, stable nBT062-DM4 and half-nBT062-DM4, a small fraction of unconjugated antibodies was observed (DAR 0). The detected mass of unconjugated WT nBT062 and stable nBT062 was 148674 Da for both variants. For half nBT062-DM4, eight DAR 0 peaks were observed representing different glycosylation species with masses from 74304 Da to 75125 Da. The main glycosylation species had a mass of 74963 Da. No DAR 0 species was detected for nBT062-natalizumab-DM4 as determined by measuring an unconjugated nBT062-natalizumab sample having a main glycosylation species with a mass of 148805 Da (data not shown). Each SPDB-DM4 complex adds approx. 880 Da to each antibody backbone.

Deconvoluted MS spectra of WT nBT062-DM4 and stable nBT062-DM4 were similar as both demonstrate DAR species from DAR 0 to DAR 6 with main species of DAR 2 to DAR 4 as determined by the area under the curve. For each of these DAR species, from one up to five peaks were observed and identified as different antibody glycosylation forms. The half nBT062-DM4 variant comprised fractions having zero to four DM4 molecules per antibody molecule while DAR 0, DAR 1 and DAR 2 species were the most potent ones. Compared to WT nB062-DM4, stable nBT062-DM4 and bispecific nBT062-natalizumab-DM4, the half nBT062-DM4 demonstrated a more complex glycosylation pattern as up to 14 different glycosylation species could be observed. For bispecific nBT062-natalizumab-DM4, DAR 1, DAR 2 and DAR 3 species were detected, separated in two different glycosylation species. Taken together, this analysis demonstrated that there were several DAR species for each nBT062-DM4 variant beside the mean DAR species as calculated by the $OD_{280/252}$ absorption method. However, only marginally amounts of unconjugated antibodies and no more than 6 DM4 molecules per antibody were detected indicating an even conjugation reaction.

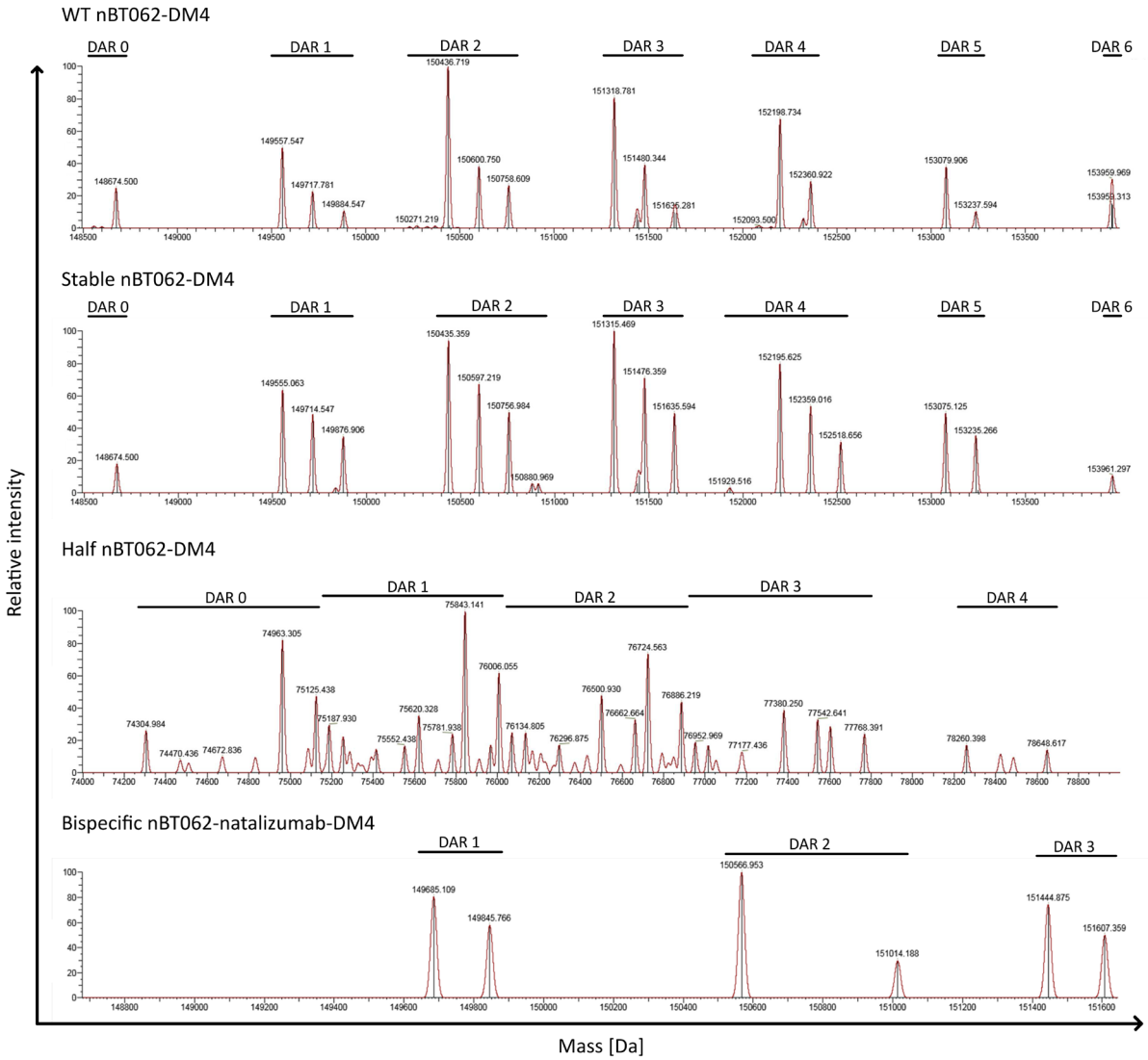

Figure 4-11: Deconvoluted MS spectra of DM4-conjugated nBT062 variants.

WT nBT062-DM4, stable nBT062-DM4, half nBT062-DM4 and bispecific nBT062-natalizumab-DM4 were separated by reversed phase LC and antibody peaks were directly analyzed by mass spectroscopy. The deconvoluted MS spectra are shown. The mass is indicated on the X-axis and relative intensity on the Y-axis. DAR= DM4 to antibody ratio.

4.4.2 Mapping of DM4-conjugation sites

IgG4 H chains contain approx. 30 lysines, while L chains have approx. 12 lysines. Conjugation of SPDB-DM4 is achieved by random acylation of lysine amino groups. To study the effects of the introduced mutations in stable nBT062 (S228P, L235E and R409K) or half nBT062 (C226S and C229S) on the conjugation sites, a LC-MS analysis of denatured, alkylated and digested samples was performed (see section 3.5.4). Based on the low amount of DM4-conjugated material, bispecific nBT062-natalizumab-DM4 could not be analyzed by this method. Figure 4-12 schematically depicts the results of individual H and L chain conjugated sites. It is shown that no differences were observed between the L chains of WT nBT062-DM4, stable nBT062-DM4 and half nBT062-DM4 as the 10 identical lysines were partly found to be SPDB-conjugated in each of those variants. Additionally, for all of the three variants a SPDB-DM4 conjugation was detected on the N-terminal amino group. Within the H chains of WT nBT062-DM4, stable nBT062 and half nBT062-DM4, 14 identical lysines were partly found to be conjugated with SPDB. However, no further conjugation site was obtained in half nBT062-DM4, while K250 was additionally available for conjugation in stable nBT062-DM4 and WT nBT062-DM4. Even further, WT nBT062-DM4 was the only antibody variant which had K223 conjugated with SPDB-DM4. These results indicate that the introduced mutations did only marginally influence the availability of lysines for SPDB-DM4 conjugation.

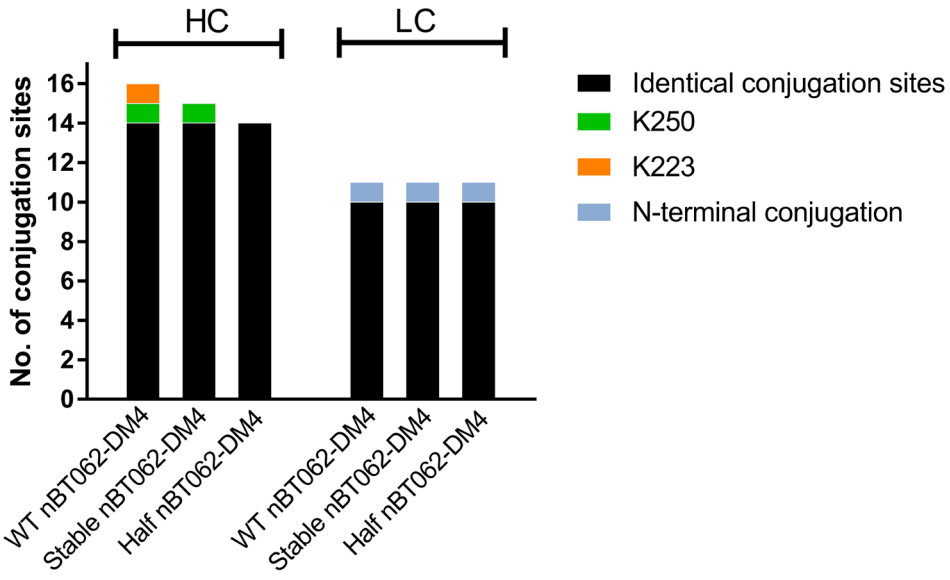

Figure 4-12: SPDB-DM4 conjugation sites of WT nBT062-DM4, stable nBT062-DM4 and half-nBT062-DM4. WT nBT062-DM4, stable nBT062-DM4 and half nBT062-DM4 were denatured, alkylated, digested and analyzed by LC-MS to identify SPDB-DM4 conjugated amino groups. Identical conjugated lysines are shown in black, differences or N-terminal conjugation is shown in color as indicated. HC= heavy chain; LC= light chain.

4.4.3 Influence of DM4 conjugation on CD138-specific binding activity

In line with the CD138-binding analysis shown in section 4.2, the influence of DM4 conjugation on the CD138-binding activity of nBT062-DM4 model variants was investigated. Ba/F3-hCD138 cells ($CD138^+/CD49d^-$) and NCI-H929 cells ($CD138^+/CD49d^+$) were incubated with unconjugated or DM4-conjugated WT nBT062, stable nBT062, half nBT062 and bispecific nBT062-natalizumab. Each variant was tested in a concentration series ranging from $2.82x10^{-12}$ to $5x10^{-7}$ mol/L. Binding of the nBT062 variants to target cells was detected by flow cytometric analysis using an Alexa Fluor 647 conjugated anti-human IgG (see section 3.4.2). Binding curves from three experiments, each measured in triplicates, were merged and are shown in Figure 4-13. Corresponding K_D values were calculated by non-linear fitting using GraphPad Prism and K_D values are listed in Table 4-2 (see Annex 7.3 for individual values). Absolut detection maxima were different in both cell lines: Ba/F3-hCD138 cells reached MFIs of approx. 11,000, while MFI values of approx. 60.000 were obtained on NCI-H929 cells. These findings indicate a higher surface expression of CD138 on the NCI-H929 cells. In accordance with results in section 4.2, WT nBT062, stable nBT062 and half nBT062 demonstrated nearly identical binding curves within each cell line tested, Ba/F3-hCD138 and NCI-H929. Binding of bispecific nBT062-natalizumab was slightly reduced compared to the monospecific variants. The CD138-binding activities of unconjugated and respective DM4-conjugated nBT062 variants were comparable. Based on nonlinear regression fitting of normalized results including best-fit statistical comparison of EC50 values, there was no difference in CD138-binding avidity of unconjugated WT nBT062, stable nBT062, half nBT062 and bispecific nBT062-natalizumab compared to their respective DM4-conjugated variants (see appendix 7.3). Binding of WT nBT062, stable nBT062 and half nBT062 either DM4-conjugated or naked to NCI-H929 cells was between 1- $2x10^{-9}$ M, while bispecific nBT062-natalizumab binds with approx. 8-$9x10^{-9}$ M (combined binding of CD138 and CD49d). Binding avidity to Ba/F3-hCD138 cells was slightly higher with 0.5- $1x10^{-9}$ M for the monospecific nBT062 variants and approx. $20x10^{-9}$ M for bispecific nBT062-natalizumab, either conjugated or not. Taken together, these results indicate that the DM4 conjugation did not influence the binding activity of any nBT062 variant.

Table 4-2: Binding avidities of DM4 conjugated or unconjugated nBT062 model variants.

Cells	DM4-conjugate	WT nBT062 [M]	Stable nBT062 [M]	Half nBT062 [M]	bispecific nBT062-natalizumab [M]
NCI-H929	No	1.16E-09	1.57E-09	1.88E-09	9.25E-09*
NCI-H929	Yes	1.68E-09	1.79E-09	2.02E-09	7.89E-09*
Ba/F3-hCD138	No	5.46E-10	7.05E-10	1.12E-09	2.26E-08
Ba/F3-hCD138	Yes	7.28E-10	7.00E-10	9.00E-10	1.79E-08

*Bispecific nBT062-natalizumab is capable of CD49d binding on NCI-H929 cells.

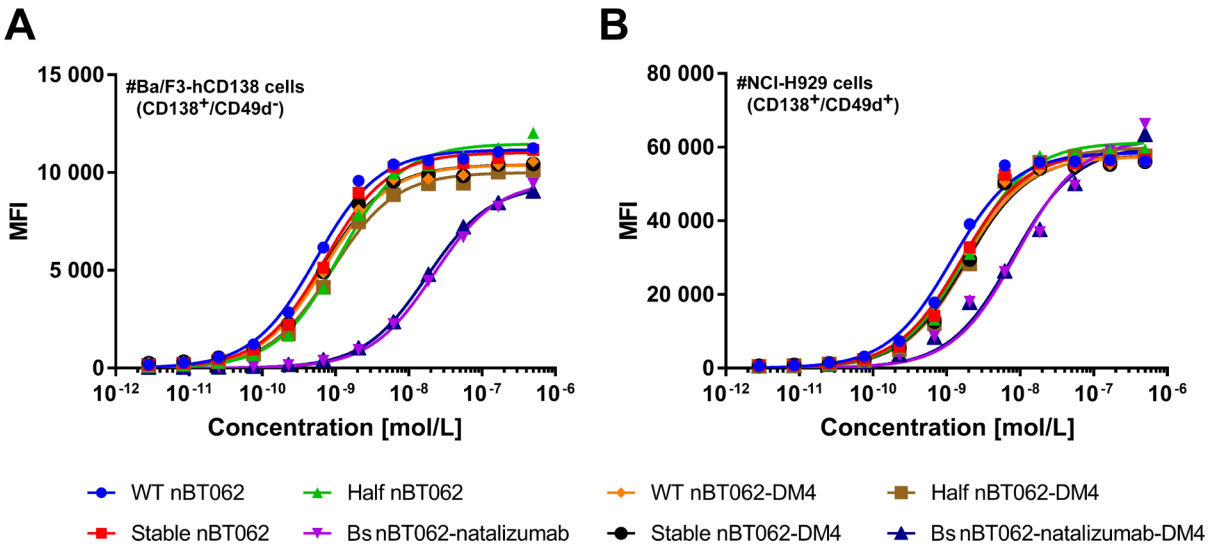

Figure 4-13: Binding of unconjugated and DM4 conjugated nBT062 variants.

Ba/F3-hCD138 cells ($CD138^+/CD49d^-$; **A**) and NCI-H929 cells ($CD138^+/CD49d^+$; **B**) were incubated with different concentrations ($5x10^{-7}$–$2.82x10^{-12}$ M) of unconjugated or DM4-conjugated WT nBT062, stable nBT062, half nBT062 and bispecific nBT062-natalizumab antibodies. Data were obtained via flow cytometry using a secondary anti-human antibody for detection. Binding curves demonstrate mean values of three individual experiments, each measured in triplicates, and non-linear fitting with GraphPad Prism. R^2= 0.91- 0.97. MFI= Median Fluorescence Intensity.

4.5 *In vitro* cytotoxicity of nBT062-DM4 variants on NCI-H929 cells

To investigate the cytotoxic activity of generated nBT062-DM4 variants, NCI-H929 cells ($CD138^+/CD49d^+$) were incubated with different concentrations of either WT nBT062-DM4, stable nBT062-DM4, half nBT062-DM4 or bispecific nBT062-natalizumab-DM4 and the cells' viability was tested after 5 days. To block CD49d binding of bispecific nBT062-natalizumab-DM4, this antibody variant was additionally incubated with a 50x excess of natalizumab. As control, the influence of 50x natalizumab was also tested in combination with WT nBT062-DM4. WST-1 substrate turnover of viable cells was determined and IC_{50} values were calculated as described in section 3.5.1. The IC_{50} value is defined as the drug concentration at which the proliferation rate of the cells is 50% compared to untreated cells. This value is also represented in normalized, non-linear fitted concentration-dependent inhibitory curves as point of inflection. The mean inhibition curves of three experiments, each measured in triplicates, are shown in Figure 4-14 A. It was observed that curves of WT nBT062-DM4, stable nBT062-DM4 and half nBT062-DM4 were similar with points of inflection near 10^{-10} M. In contrast, the point of inflection of bispecific nBT062-natalizumab-DM4 was shifted to approx. 10^{-9} M. Paired t test analysis revealed that this shift was significant against WT and stable nBT062-DM4.

WT nBT062-DM4, stable nBT062-DM4 and half nBT062-DM4 demonstrated mean IC_{50} values of 0.105, 0.085, and 0.137 nM, respectively. These differences were not significant. The IC_{50} of bispecific nBT062-natalizumab-DM4 was significantly reduced to 0.456 nM. IC_{50} results were further processed and are shown as relative cytotoxicity normalized to WT nBT062-DM4 in Figure 4-14 B. Relative to WT nBT062-DM4, stable nBT062-DM4 and half nBT062-DM4 variants demonstrated cytotoxicities of 127% and 85%, respectively. These differences were not significant at all. Bispecific nBT062-natalizumab-DM4 demonstrated a relative cytotoxicity of 52% in the absence of natalizumab. This inhibitory potency was even further reduced to 32% in the presence of natalizumab. Significant differences between the monospecific variants and nBT062-natalizumab-DM4 we only observed to the group with additional natalizumab. Natalizumab itself did not mediate any cytotoxic effect. Nevertheless, there was a trend to decrease the efficacy of bispecific nBT062-natalizumab-DM4 but also slightly influenced the cytotoxicity of WT nBT062-DM4 in terms of variability. No unspecific cytotoxicity of nBT062-DM4 variants was detected on $CD138^-$ Jurkat cells in concentrations ranging from 0.01 - 4 nM (see Appendix 7.4). In conclusion, it was demonstrated that all nBT062-DM4 variants were capable to mediate CD138-specific cytotoxicity in the nanomolar range.

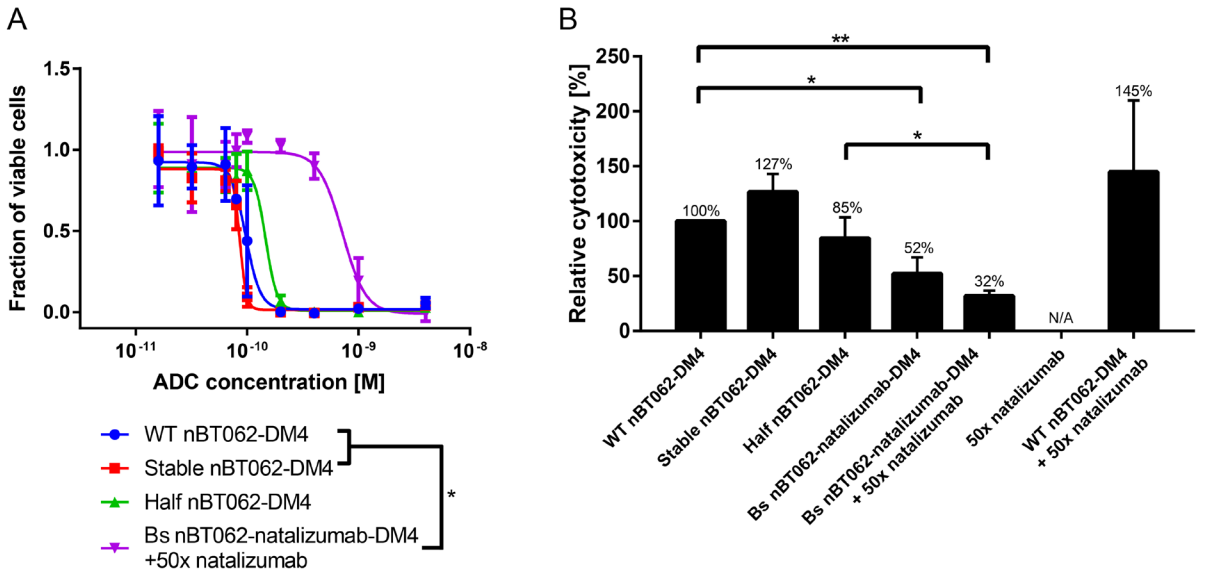

Figure 4-14: Cytotoxic effect of nBT062-DM4 variants on NCI-H929 cells.

NCI-H929 cells ($CD138^+/CD49d^+$) were incubated with different concentrations of WT nBT062-DM4, stable nBT062-DM4, half nBT062-DM4 or bispecific nBT062-natalizumab-DM4, as indicated in the presence or absence of an excess of natalizumab. After 5 days of incubation, a WST-1 assay was used to determine the viability. Exemplary concentration dependent inhibition curves are shown in A. Reciprocal IC50 values of each nBT062-DM4 variant were normalized to WT nBT062-DM4 and one DM4 molecule per antibody. Results are shown in B from three separate experiments each measured in triplicates. N/A= not available; no cytotoxic activity was obtained. *p<0.05, **p<0.01.

4.6 *In vivo* assessment of nBT062-DM4 model variants

4.6.1 Efficacy of nBT062-DM4 variants in a xenograft mouse model

In addition to *in vitro* cytotoxicity assays, the efficacy of WT nBT062-DM4 and generated corresponding model variants, mimicking ADC species potentially arisen *in vivo*, was assessed in a xenograft mouse model. Immunodeficient NMRI nude mice were inoculated with the patient-derived mammary cancer MAXF 1322 known for CD138 expression. Mice were treated three times with either 4 or 2 mg/kg/week of WT nBT062-DM4, stable nBT062-DM4, half nBT062-DM4 or bispecific nBT062-natalizumab-DM4. The influence of endogenous IgG4 on the efficacy of the therapeutic ADCs was investigated by administering the nBT062-DM4 model variants either alone or in combination with 10 ml/kg/week of a 10% IVIg preparation containing also the IgG4 subtype.

Results are summarized in Table 4-3 and tumor growth curves are shown in Figure 4-15. WT nBT062-DM4, stable nBT062-DM4 and half nBT062-DM4 monotherapy at both dose levels of 4 mg/kg/week and 2 mg/kg/week all induced complete remission of tumors with a minimum T/C value (see section 3.6.1.4) of 0.0% in all groups. Additionally, no tumor

regrowth was detected in the treatment-free observation period up to day 86. For bispecific nBT062-natalizumab-DM4 monotherapy a borderline efficacy was observed at 4 mg/kg/week (min. T/C: 62.1%) while one treated animal out of five within this group showed a very good response (opt. T/C: 8.2). However, the treatment was inactive at 2 mg/kg/week (min. T/C: 97.5%). In addition, no tumor inhibition was detected by co-administration of the human IVIg preparation at both dose levels (min. T/C values ≥ 98.5%). In the presence of IgG antibodies, WT nBT062-DM4, stable nBT062-DM4 and half nBT062-DM4 also led to complete tumor remissions at dosing of 4 mg/kg/week (all min. T/C 0.0%). At a dosage of 2 mg/kg/week, a decrease in efficacy by the co-administration of the IVIg preparation was observed: Half nBT062-DM4 demonstrated a moderate efficacy (min. T/C 45.3%) and WT nBT062-DM4 reached a borderline effect (min. T/C 58.9%). This decrease was significant in both cases. Compared to that, stable nBT062-DM4 was only minor influenced by the human IgG antibodies as complete remission of tumors and survival was seen in 3 of 5 mice (min. T/C: 0.0%).

Kaplan-Meier survival curves are shown in Figure 4-16. As mice with tumors larger than 2000 mm³ were excluded from the experiment, this analysis is also an indicator of a delay in tumor growth. It was observed that WT nBT062-DM4, stable nBT062-DM4 and half nBT062-DM4 at 4 mg/kg/week both alone and in the presence of human IgG antibodies demonstrated a significant delayed tumor growth and extended survival compared to the control group. In combination with the IVIg preparation, survival was not significantly different to the corresponding nBT062-DM4 variant monotherapies but was significantly extended compared to the IVIg alone for all three variants at 4 mg/kg/day. Tumor growth compared to the vehicle control was also significantly delayed by monotherapy with 2 mg/kg/week of WT nBT062, stable nBT062-DM4 and half nBT062-DM4 ($p \leq 0.013$). When given with the IVIg preparation, tumor growth was only significantly delayed compared to the vehicle control for stable nBT062-DM4 treatment ($p=0.0277$) but not for WT nBT062-DM4 and half nBT062-DM4. Indeed, based on the Mantel-Cox test the IVIg preparation had a significant negative effect on the 2 mg/kg/week treatment with half nBT062-DM4 ($p=0.0018$) but a lower effect on treatment with WT nBT062-DM4 ($p=0.0251$). Direct comparison of stable nBT062-DM4 at 2 mg/kg/week with and without the IVIg did not lead to a significant difference in tumor growth delay. Treatment with bispecific nBT062-natalizumab-DM4 did not significantly prolong survival compared to the vehicle control in any of tested dosage and combinations.

In summary, these data demonstrate that nBT062-DM4 and the models mimicking potentially related IgG4 species are all capable of $CD138^+$ tumor cell killing *in vivo*. Indeed, the bispecific nBT062-natalizumab-DM4 was the least potent variant. However, at low doses WT nBT062-DM4 and half nBT062-DM4 were reduced in their efficacy in the presence of human

IgGs, which was hardly seen for the stable nBT062-DM4. This indicates that the stabilizing mutations S228P and R409K might be able to prevent IgG4-based ADCs from a half-antibody exchange mediated loss in efficacy.

Table 4-3: Overview of the antitumor efficacy in the different treatment groups.

Group ID	Therapy[1]	Dose Level	Minimum T/C* [%] (Day)[2]	Efficacy Rating	Td** [Days]
1	Vehicle Control	10 ml/kg/week	n/a	n/a	3.0
2	IVIg	10 ml/kg/week	100.0 (0)	-	2.1
3	WT nBT062-DM4	4 mg/kg/week	0.0 (27)	++++	n.r.
4	Stable nBT062-DM4	4 mg/kg/week	0.0 (27)	++++	n.r.
5	Half nBT062-DM4	4 mg/kg/week	0.0 (27)	++++	n.r.
6	Bispecific nBT062-natalizumab-DM4	4 mg/kg/week	62.1 (27)	+/-	2.4
7	IVIg // WT nBT062-DM4	10 ml/kg/week // 4 mg/kg/week	0.0 (27)	++++	1.8
8	IVIg // Stable nBT062-DM4	10 ml/kg/week // 4 mg/kg/week	0.0 (27)	++++	n.r.
9	IVIg // Half nBT062-DM4	10 ml/kg/week // 4 mg/kg/week	0.0 (27)	++++	n.r.
10	IVIg // Bispecific nBT062-natalizumab-DM4	10 ml/kg/week // 4 mg/kg/week	100.0 (0)	-	1.9
11	WT nBT062-DM4	2 mg/kg/week	0.0 (23)	++++	n.r.
12	Stable nBT062-DM4	2 mg/kg/week	0.0 (27)	++++	2.0
13	Half nBT062-DM4	2 mg/kg/week	0.0 (27)	++++	n.r.
14	Bispecific nBT062-natalizumab-DM4	2 mg/kg/week	97.5 (6)	-	2.8
15	IVIg // WT nBT062-DM4	10 ml/kg/week // 2 mg/kg/week	58.9 (27)	+/-	1.7
16	IVIg // Stable nBT062-DM4	10 ml/kg/week // 2 mg/kg/week	0.0 (23)	++++	1.5
17	IVIg // Half nBT062-DM4	10 ml/kg/week // 2 mg/kg/week	45.3 (27)	+	1.7
18	IVIg // Bispecific nBT062-natalizumab-DM4	10 ml/kg/week // 2 mg/kg/week	98.5 (9)	-	1.7

*T/C= median tumor volume in test group/median tumor volume in control group
**Td: Tumor volume doubling time;
Efficacy rating: ++++, T/C <5%; +++, T/C 5 - <10%; ++, T/C 10 - <25%; +, T/C 25 - <50%; +/-, T/C 50-65%; -, T/C ≥ 65%

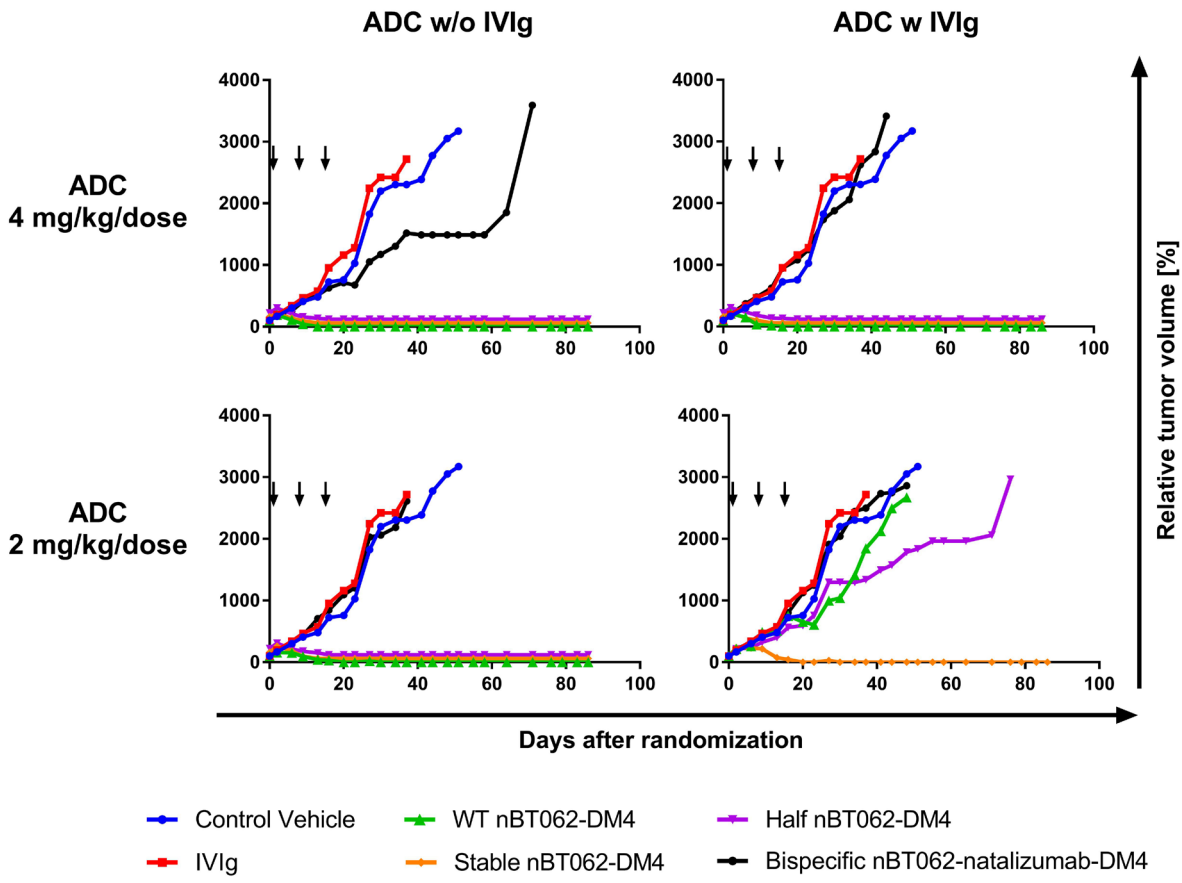

Figure 4-15: Relative tumor growth curves demonstrating *in vivo* efficacy of nBT062-DM4 variants

Immunodeficient NMRI nude mice bearing MAXF 1322 mammary cancer xenografts were treated with 2 or 4 mg/kg/week of WT nBT062-DM4, stable nBT062-DM4, half nBT062-DM4 or bispecific nBT062-natalizumab-DM4 as indicated. ADCs were administered either alone or in combination with 10 ml/kg/week of a 10% human IVIg preparation containing endogenous IgG4 antibodies. Three intravenous injections were administered as specified by the arrows. PBS was used as control vehicle and the IVIg preparation was also tested as monotherapy. Curves demonstrate median of relative tumor volumes over time.

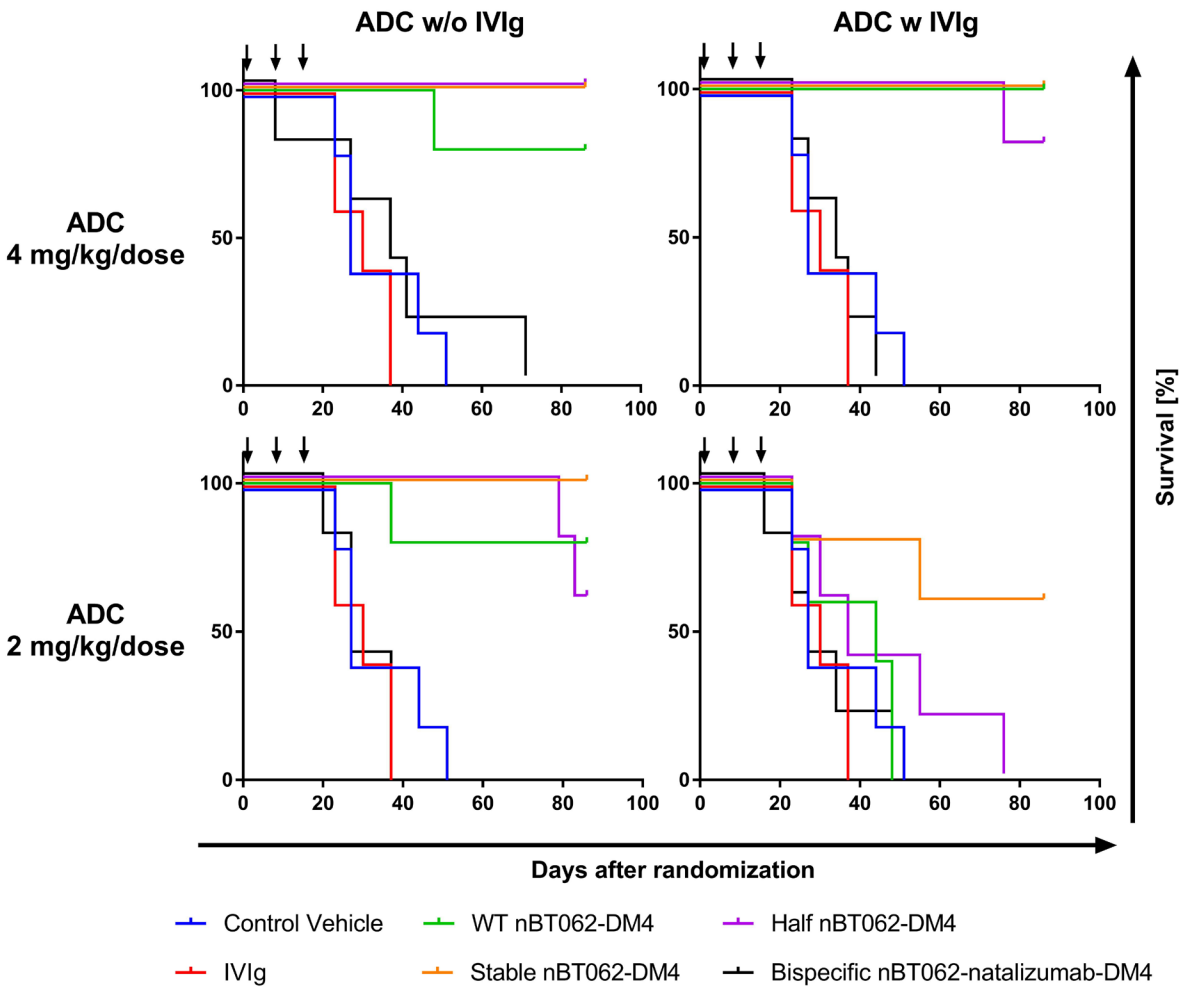

Figure 4-16: Kaplan-Meier survival plots from MAXF 1322 xenograft mouse model testing nBT062 variants.

Immunodeficient NMRI nude mice bearing MAXF 1322 mammary cancer xenografts were treated with 2 or 4 mg/kg/week of WT nBT062-DM4, stable nBT062-DM4, half nBT062-DM4 or bispecific nBT062-natalizumab-DM4 as indicated. ADCs were administered either alone or in combination with 10 ml/kg/week of a 10% human IVIg preparation containing endogenous IgG4 antibodies. Intravenous injections were administered on day 1, 8 and 15 as specified by the arrows. PBS was used as control vehicle and the IVIg preparation was also tested as monotherapy. Curves demonstrate survival of individual treated groups over time until day 86 after randomization of mice.

4.6.2 Body weight changes of nBT062-DM4 variant treated mice

During preclinical mouse studies, body weight changes of the treaded mice are used as indicator for drug tolerability. Median of relative body weights from mice of this study are presented in Figure 4-17. Group median body weight loss (BWL) was not observed in seven groups (Group IDs 5, 6, 9, 11, 12, 13, 14 according Table 4-3). All other groups demonstrated BWL of less than 1.9%. In the group that received 2 mg/kg/day half nBT062-DM4 with the IVIg preparation BWL was 9.4% on day 41, since one of the two remaining animals showed weight loss below 20%. There was a second drop in group median BWL within this group on day 58 when one of the two remaining mice was excluded from the experiment for tumor burden. However, the mice treated with half nBT062-DM4 in combination with the IVIg preparation and which had once a BWL of more than 20% was the one survived the longest in this group. Taken together, these data demonstrate that all nBT062-DM4 variants and also the IVIg preparation were tolerated at the dosages administered.

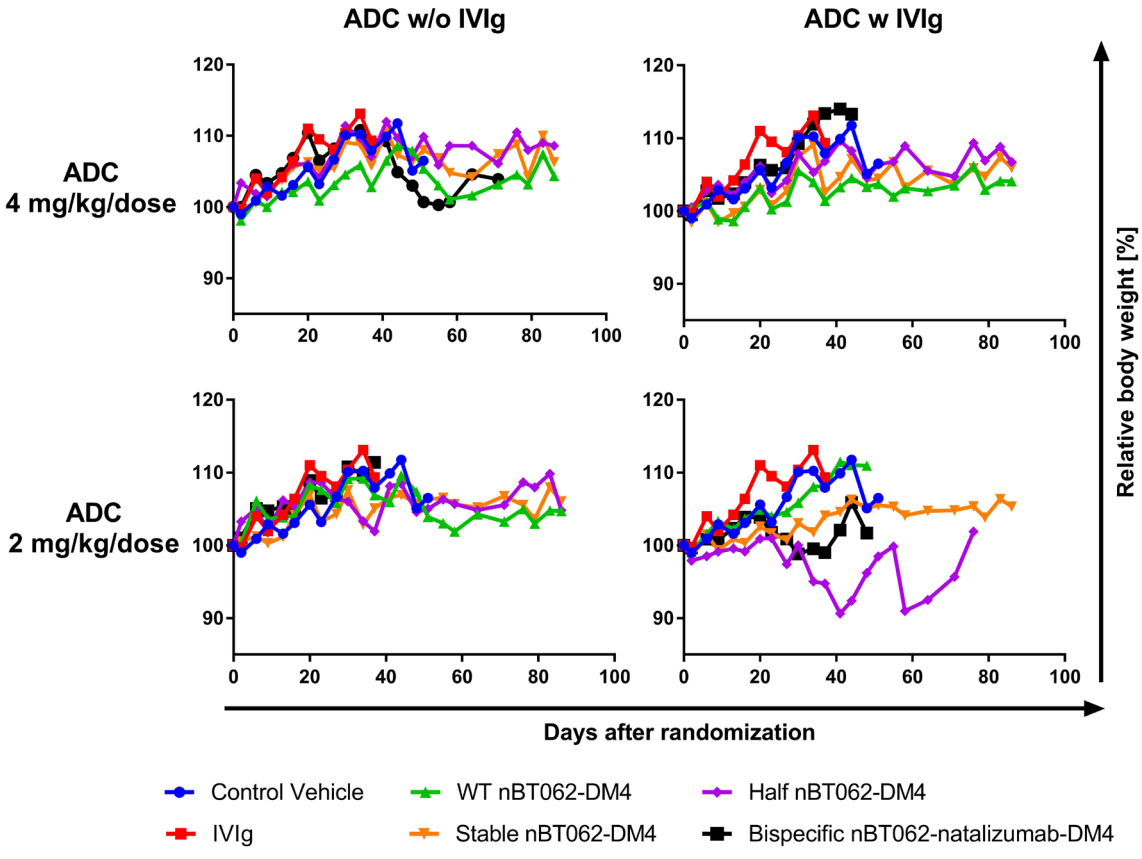

Figure 4-17: Impact of nBT062-DM4 variant treatments on body weights of mice.

Immunodeficient NMRI nude mice bearing MAXF 1322 mammary cancer xenografts were treated with 2 or 4 mg/kg/week of WT nBT062-DM4, stable nBT062-DM4, half nBT062-DM4 or bispecific nBT062-natalizumab-DM4 as indicated. ADCs were administered either alone or in combination with 10 ml/kg/week of a 10% human IVIg preparation containing IgG4 antibodies. PBS was used as control vehicle and the IVIg preparation was also tested as monotherapy. Median of relative body weights are mapped by the curves.

4.6.3 Detection of bispecific antibodies in plasma of mice treated with nBT062-DM4 variants

It was observed in the MAXF 1322 xenograft model that the antitumor efficacy of nBT062-DM4 variants was decreased when coadministered with an IVIg preparation. This loss of efficacy was more pronounced for WT nBT062-DM4 and half nBT062-DM4. To investigate if this attenuated anti-tumor effect was based on an IgG4 shuffling related phenomenon, heparin plasma samples from mice of the *in vivo* study described in section 4.6.1 were analyzed. Blood samples were taken one week prior treatment (predose samples) and 24 h after the first and third treatment with nBT062-DM4 variants either with or without administration of the IVIg preparation and analyzed by LBA/LC-MS (see section 3.6.2). This method uses a magnetic CD138-bead pull down assay to isolate CD138-specific antibodies. Those antibodies were trypsinated and analyzed by LC-MS regarding a specific nBT062 signature peptide sequence and a generic human IgG4 peptide sequence. The amount of shuffled antibodies was then calculated by the ratio of the specific nBT062 signature peptide to the IgG4 generic peptide. The predose samples were taken as negative controls and, indeed, none of both signature peptides neither specific for nBT062 nor human IgG4 in general were found. As a second negative control, plasma from mice treated with the IVIg preparation alone was also tested. Within these samples nearly no amounts of signature peptides were detected demonstrating that the upstream CD138 pull down assay worked well. Results of the half-antibody exchange analysis on WT nBT062-DM4, stable nBT062-DM4 and half nBT062-DM4 are shown in Figure 4-18. Without the co-administration of the IVIg preparation the three nBT062-DM4 variants did not display any nBT062-related IgG4 shuffled fraction. Samples from the IVIg combination therapy exhibited IgG4 shuffling of 53% and 67% for WT nBT062-DM4 at dosages of 4 and 2 mg/kg/week, respectively while half nBT062-DM4 combination treatment led to half-antibody exchange fractions of 7% and 10% at identical dosing. Compared to each respective monotherapy, these increases in IgG4 shuffling were significant. No half-antibody exchange was observed in samples containing stable nBT062-DM4 in combination with human IgGs. However, the extent of shuffling was significantly higher in WT nBT062-DM4 combination treatment compart to IVIg combinations with either stable nBT062-DM4 or half nBT062-DM4. These results indicate that the stabilizing mutations S228P and R409K incorporated into stable nBT062 were successfully able to prevent monoclonal antibodies from undergoing the IgG4 half-antibody exchange *in vivo*.

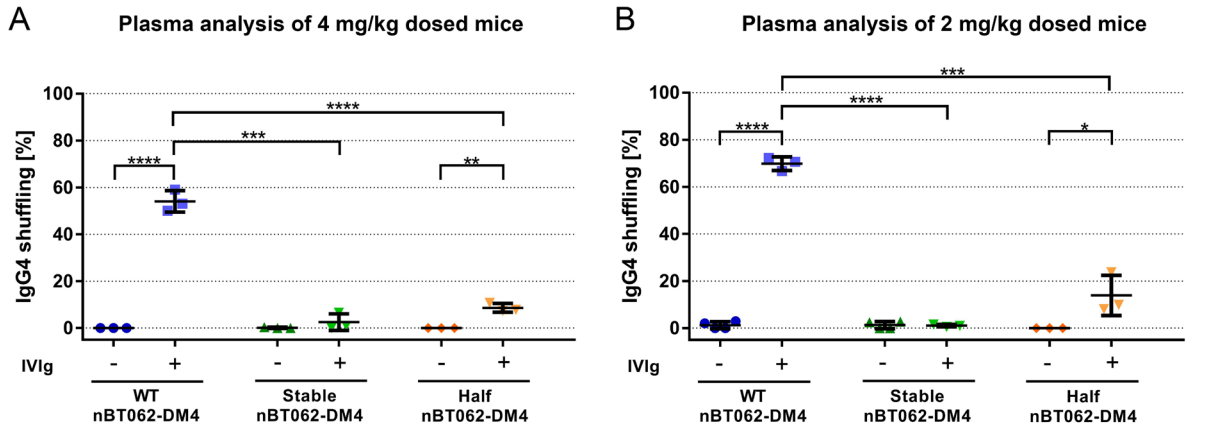

Figure 4-18: *In vivo* half-antibody exchange in MAXF 1322 xenografts treated with nBT062 variants.
Heparin plasma samples from MAXF 1322 xenograft mice treated with WT nBT062-DM4, stable nBT062-DM4 or half nBT062-DM4 alone or in combination with an IVIg preparation were analyzed by LC-MS analysis after excluding non-CD138-binding antibodies using a magnetic bead pull down assay. Signature peptides specific for nBT062 and human IgG4 antibodies were used to identify the frequency of half-antibody exchange. Three mice from each treatment were analyzed, while each mouse provided a predose sample (negative control) and samples 24 h after the first and third drug injection (combined). T test was used for statistical analysis. *p<0.05; **p<0.01; ***= p<0.001; ****p<0.0001.

4.6.4 Analysis of the IVIg preparation

The 10% human IVIg preparation used in this xenograft mouse study was analyzed for endogenous anti-CD138 antibodies to exclude potential competing effects with nBT062-DM4 variants binding tumor-expressed CD138. An ECL binding assay was performed as described in section 3.6.3. As demonstrated in Figure 4-19, WT nBT062 was used as positive control resulting in a concentration-related saturation curve with a maximum signal intensity of approx. 500,000. The linear detection range for this assay was determined from 0.0001 µg/ml to 0.1 µg/ml. The use of antibody concentrations above 1 µg/ml led to a decrease in signal intensity, indicating a hook effect. Natalizumab, used as negative control, was not capable to induce specific CD138 binding. However, concentrations higher than 1 µg/ml induced false positive detections. The IVIg preparation was tested in triplicates as 10-times serial dilutions of total antibody concentrations between 10,000 µg/ml and 0.001 µg/ml. No CD138-specific, concentration-dependent signal was detected for the IVIg preparation. Those signals obtained were already in the false positive detection range of natalizumab. Thus, it was ascertained that the administered IVIg preparation did not contain any endogenous anti-CD138 antibodies which could have been competed with the nBT062 variants for tumor-expressed CD138 binding in xenograft mice to diminish the efficacies of the ADCs.

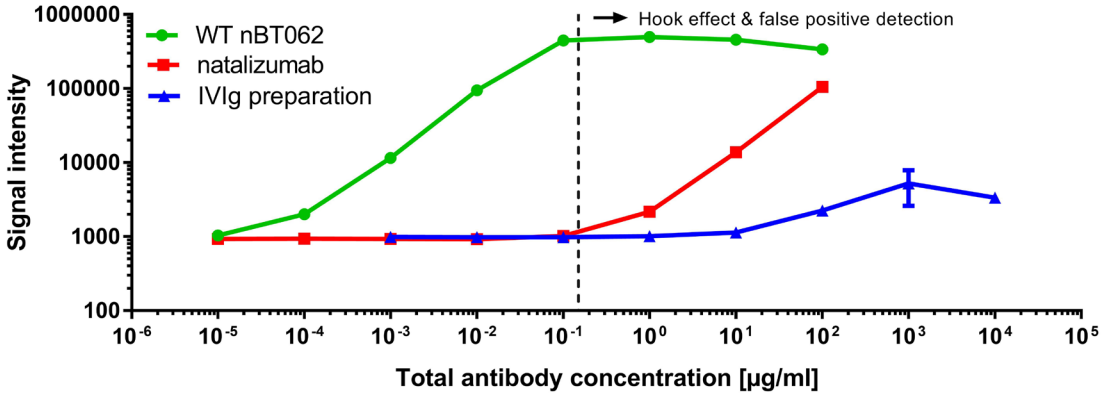

Figure 4-19: Analysis of the IVIg preparation to anti-CD138 antibodies.

CD138-coated plates were incubated with the IVIg preparation and detection of anti-CD138 antibodies was done by electrochemiluminescence measurement after applying a biotinylated anti-human secondary antibody and streptavidin-conjugated sulfo-TAG. WT nBT062 was used as positive and natalizumab as negative control. Measurements were performed in triplicates and concentrations were tested as indicated on the X-axis.

5 Discussion

Human IgG4 antibodies are known to be the only class of antibodies able to exchange randomly half-antibodies *in vivo* leading to bispecific, monovalent antibodies. This phenomenon was shown for endogenous IgG4 antibodies but also for monoclonal, therapeutic ones (Schuurman et al. 1999; Labrijn et al. 2009; Young et al. 2014). Aalberse and Schuurman published that the mechanism of this half-antibody exchange is mainly based on a reduced distance between the two disulfide bonds in the CH2 of the IgG4 backbone, leading to a more instable hinge compared to the IgG1 subclass (Aalberse, Schuurman 2002). Today it is known, that both amino acid substitutions S228P and R409K can individually prevent this half-antibody exchange (Labrijn et al. 2011). Based on this knowledge the influence of half-antibody exchange on the functionality and efficacy of IgG4 ADCs was investigated in this thesis using BT062. Therefore, nBT062 model variants mimicking potential *in vivo* derived BT062 species were generated and characterized beside WT nBT062 according to their function of CD138 binding and subsequent internalization. As the core function of therapeutic BT062 is tumor cell killing, WT nBT062 and respective model variants were conjugated to DM4 and tested for *in vitro* cytotoxicity. The direct impact of IgG4 shuffling was investigated *in vivo* using a breast cancer xenograft mouse model.

5.1 Successful generation of nBT062 model variants

nBT062 model antibodies, mimicking relevant stable or transition species of the half-antibody exchange were first designed *in silico* and respective DNA plasmids were expressed in FreeStyle CHO-S cells and purified by protein A affinity chromatography. Beside WT nBT062 comprising an unchanged human IgG4 backbone able to undergo half-antibody exchange, a stable nBT062 was generated containing the stabilizing mutations S228P and R409K to prevent any exchange of half-antibodies. By amino acid substitutions C226S and C229S covalent interactions of the heavy chains were inhibited resulting in the half nBT062 model variant. A bispecific nBT062 mimicking a final product of performed half-antibody exchange *in vivo* was created by incorporation of several mutations and co-expression of two different H and two different L chains bearing the CDRs of nBT062 or natalizumab (see section 3.2).

The four produced nBT062 variants, WT nBT062, stable nBT062, half nBT062 and bispecific nBT062-natalizumab were analyzed by SDS-PAGE, IEF combined with western blotting, and size exclusion chromatography for correct protein expression (see section 4.1). Under reducing conditions, Coomassie stained SDS-PAGE analysis obtained for all nBT062 variants H and L chains of approx. 50 and 25 kDa, respectively (see section 4.1). This is in line with molecular masses expected for IgG molecules (Murphy, Weaver 2017). An

additional band at approx. 85 kDa was detected for stable nBT062. This fraction seemed to be a result of incomplete reduction of disulfide bonds using 50 mM DTT as reducing agent. It is possible that two H chains bound together run coiled below their actual molecular weight of approx. 100 kDa. SDS-PAGE using non-reducing conditions demonstrated bands of 150 kDa within the WT nBT062, stable nBT062 and bispecific nBT062-natalizumab samples, but a band of this size was not present in the half nBT062 sample. Additionally, a band at approx. 70 kDa occurred in the WT nBT062 and as the only species within the half nBT062. These molecular weights of 150 kDa and 70 kDa are in accordance with the literature for full length and half-antibodies, respectively (Rispens et al. 2010). The SDS PAGE results gave a first hint that the introduced amino acid substitutions led to desired structural modifications as WT nBT062 formed half-antibodies, whereas the stable nBT062 and bispecific nBT062-natalizumab did not contain any half-antibodies. Further, the amino acid substitutions C226S and C229S within half nBT062 seemed to inhibit covalent heavy chain pairing. In addition, this analysis demonstrated successful purification by protein A as no further host cell protein bands occurred.

Isoelectric focusing of the nBT062 model variants revealed that WT nBT062, stable nBT062 and half nBT062 had slightly acidic to neutral pIs of pH 6.5 to 7.3, pH 6.4 to 7.0 and pH 6.1 to 6.8, respectively. On the contrary, the pI of natalizumab was slightly basic (pH of 7.6 to 7.8) and bispecific nBT062-natalizumab demonstrated a neutral to basic pI between pH 7.3 to 8.0. These differences in the pIs between the distinct monoclonal antibodies can be based on the one hand on the individual amino acid substitutions, but on the other hand on several additional modifications. Such modifications may include glycosylation, carboxyl or amino terminal processing at the post-translational level or chemical alterations like oxidation and amidation/deamidation which can occur at the downstream processing level or during storage (Gaza-Bulseco et al. 2008; Harris 1995; Zheng et al. 2011; Vanam et al. 2015). Since the nBT062 variants were produced by stable cell pools but not by single cell clones, post-translational modifications might be highly variable for each model antibody resulting in a more heterogenous band pattern and a broader pI range. However, the incorporation of the natalizumab CDRs and pairing mutations within the bispecific nBT062-natalizumab led to a more basic pI. Western blotting of these samples using anti-nBT062 and anti-natalizumab antibodies for immunodetection demonstrated that all bands observed in the Coomassie gel were specific for either nBT062 and/or natalizumab. In line with the SDS-PAGE results, this method further demonstrated the purity of the recombinantly expressed antibody variants. Further, this analysis was mainly used as a quality control to identify any monospecific antibody fractions within the bispecific nBT062-natalizumab sample. Since 8 out of 10 bands were bound by both anti-idiotypic antibodies and thus found to be bispecific, there were 2 bands exclusively detected by the anti-natalizumab antibody. The extended knob-into-hole

technology for H chain - H chain pairing used for the generation of bispecific antibodies is one of the most efficient strategies with approx. 95% heterogenic pairing (Carter 2001). Nevertheless, it is known that hole-hole homodimeric pairing is possible, while knob-knob homodimers do generally not occur (Klein et al. 2014). To prevent interferences of a monospecific nBT062 antibody fraction within the bispecific nBT062-natalizumab sample on further binding, internalization and cytotoxicity analysis, the natalizumab part of the bispecific antibody was chosen as “hole” backbone. The results of this IEF analysis are in accordance with those described by Klein et al., 2014 and confirm the absence of a monospecific nBT062 fraction within the bispecific nBT062-natalizumab.

In addition to SDS-PAGE analysis, the nBT062 variants were further characterized by SEC to investigate the presence of fragments, aggregates or half-antibodies (see section 4.1). While nearly no small antibody fragments were found using native running buffer conditions, bigger aggregates were detected in amounts of 4.5%, 7.4%, 7.1% and 25% in half nBT062, WT nBT062, bispecific nBT062-natalizumab and stable nBT062, respectively. Protein aggregation is a well-known phenomenon in monoclonal antibody drug development, although the underlying reasons are only poorly understood (Wang 2005). Aggregation can occur during the different antibody production steps including fermentation, purification, final formulation, and storage (Vázquez-Rey, Lang 2011). Kiese et al. postulate that full or partial protein unfolding exposes hydrophobic regions, which in turn promote intermolecular interactions resulting in aggregation or precipitation of sub-visible or visible particles (Kiese et al. 2008). These aggregates might finally influence the activity, solubility and immunogenicity of the produced drug (Vázquez-Rey, Lang 2011). Individually developed affinity chromatography, ion exchange chromatography, SEC and tangential flow filtration are used in combination with an optimized formulation buffer to prevent or diminish aggregate formation (Ansaldi, Lester 1999; Wan, Wang 1998; Phillips et al. 2001; Wang et al. 2006). However, during the nBT062 variant production for this preclinical study no separate aggregate-diminishing steps were included besides protein A affinity chromatography. The detected higher amounts of aggregates within the stable nBT062 compared to the other nBT062 variants might be based on the individual structure in combination with an un-optimized formulation buffer for storage. Interestingly, when 10% 2-propanol denaturing running buffer was applied, the bispecific nBT062-natalizumab tended to form aggregates which were not seen with native running buffer. Aggregates of stable nBT062 did also not fully resolve under denaturing conditions. This is in line with aggregate categories from Cromwell et al. separating them into soluble/insoluble, covalent/non-covalent, reversible/non-reversible and native/denatured ones (Cromwell et al. 2006). Besides that, the denaturing SEC analysis confirms the results of the non-reducing SDS-PAGE analysis: While stable nBT062 and bispecific nBT062-natalizumab did hardly contain half-antibodies, WT nBT062

samples provided a small fraction of those product related fragments and the half nBT062 variant was present only as half-antibodies. Since half nBT062 demonstrated under native conditions a similar or even slightly higher retention time which is accompanied with a slightly bigger protein size compared to WT nBT062 and stable nBT062, this SEC analysis provides evidence that dimerization of half-antibodies does occur based on non-covalent interactions dependent on surrounding conditions. Such non-covalent interactions are described between the CH3 domains of two H chains (Labrijn et al. 2011).

The capability to prevent half-antibody exchange of nBT062 antibodies due to the incorporation of the stabilizing S228P and R409K mutations was investigated by exposing mild reducing conditions to WT nBT062 and stable nBT062, each in the presence of natalizumab. The *in vitro* formation of bispecific antibodies was obtained in a mixture of WT nBT062 and natalizumab, but they could not be detected in samples of stable nBT062 and natalizumab. Thus, as expected and in line with the results from Labrijn it can be concluded that S228P and R409K mutations could successfully prevent half-antibody exchange under reducing conditions *in vitro* (Labrijn et al. 2011).

In summary, it was shown that WT nBT062, stable nBT062, half nBT062 and bispecific nBT062-natalizumab were produced in a sufficient quality and incorporation of mutations lead to the expected analytical characteristics.

5.2 All nBT062 variants bind CD138 and are internalized

Specific antigen binding of nBT062 model variants was analyzed by flow cytometry. All model variants, WT nBT062, stable nBT062, half nBT062 and bispecific nBT062, were capable of specific CD138 binding in the low nanomolar range as observed by concentration dependent incubation of Ba/F3-hCD138 ($CD138^+/CD49d^-$) cells. On the contrary, bispecific nBT062-natalizumab was the only variant able to bind Jurkat ($CD138^-/CD49^+$) cells with a 5x times reduced avidity compared to natalizumab. While WT nBT062, stable nBT062 and half nBT062 showed comparable binding activities towards CD138 on Ba/F3-hCD138 cells, binding of bispecific nBT062-natalizumab was significantly reduced. This reduced binding might be based on two major aspects: First, it is known that clustering of CD138 on the cells surface is mediated by heparin binding domains of heparinase (Ramani et al. 2013). As nBT062-natalizumab is monovalent for each antigen this variant is not capable to crosslink clustered antigens potentially leading to a weaker interaction. With respect to the SEC analysis, half nBT062 antibodies might be present as dimers under the conditions used in this experiment and thus act as bivalent antibodies. In 1972, Hornick and Karush already described the increasing effect of multivalency on the antibody-antigen binding strength supporting this assumption (Hornick, Karush 1972). Second, several mutations for correct H

and L chain pairing were incorporated into the framework regions next to the CDRs of the nBT062-natalizumab variant which might affect the non-covalent interactions between the antibody and its epitope. Taken together, these data on the binding activity provide evidence that the generated nBT062 variants can function as model antibodies mimicking *in vivo* derived antibodies species as they all demonstrated binding in the nanomolar range and act as expected.

The mode of action of BT062 and other ADCs is based on the tumor cell specific delivery of toxins. Beside ADC binding, this process further includes internalization as an indispensable step. Thus, it was important to analyze if all potential BT062 derived species are capable to induce such antigen-mediated antibody uptake. Fluorescently labeled WT nBT062, stable nBT062, half nBT062 and bispecific nBT062-natalizumab were therefore incubated on Ba/F3-hCD138 ($C138^+/CD49d^-$) and NCI-H929 ($C138^+/CD49d^+$) cells and internalization was assessed by flow cytometry as well as fluorescence microscopy. It is known that CD138 can be cleaved off from cell surfaces using proteolytic enzymes such as trypsin or chymopapain (Beckman Coulter 2011; Sun et al. 1997). Cells were incubated with nBT062 variants for either 0.5 h at 4°C or 24 h at 37°C and analyzed by flow cytometry after trypsin incubation or not. Both cell lines tested showed significantly higher staining intensities after 24 h than after 0.5 h. Digestion with trypsin after 0.5 h of incubation decreased the staining intensity of treated cells to that of unstained ones, while cells incubated for 24 h still demonstrated high staining intensities. Thus, it can be concluded that the increase in fluorescence intensity between 0.5 h and 24 h is not based on unbound CD138 molecules on the surface at the earlier time point, but on internalization of nBT062 variants. In general, the results demonstrated that all nBT062 variants WT nBT062, stable nBT062, half nBT062 and bispecific nBT062-natalizumab were internalized within 24 h into both cell lines. However, there were slight differences between the monospecific and the bispecific nBT062 variants and between the cell lines NCI-H929 and Ba/F3-hCD138. WT nBT062, stable nBT062 and half nBT062 demonstrated similar fluorescence intensities for each incubation test set. On the contrary, bispecific nBT062-natalizumab had approx. 2-fold lower initial surface staining at 4°C but interestingly the detected fluorescence from internalized antibodies was even higher for NCI-H929 cells and similar for Ba/F3-hCD138 cells. Thus, it might be assumed that bispecific nBT062-natalizumab had a higher internalization rate. It was further recognized that within each antibody panel and for both cell lines, the sum of fluorescence intensity of surface staining and internalized staining was approx. the total fluorescence observed after 24h of incubation. This demonstrates that the amount of surface staining was similar after 0.5 h and 24 h and gives a hint that CD138 molecules are expressed to a constant level on the surface. In addition, there was a major difference between both tested cell lines: As internalization was much higher as the initial surface staining on Ba/F3-hCD138

cells for all nBT062 variants, monospecific nBT062 models demonstrated higher surface staining as internalization on NCI-H929 cells. However, on those cells bispecific nBT062-natalizumab was the only variant having a higher internalization fluorescence compared surface staining. Thus, this observation might be a further hint showing that the internalization rate was increased for the bispecific nBT062-natalizumab. A potential molecular explanation could be the lack of CD138 crosslinking leading to an independent and thus faster internalization of the receptors.

Results of fluorescence microscopy qualitatively confirmed the internalization of WT nBT062, stable nBT062, half nBT062 and bispecific nBT062-natalizumab into Ba/F3-hCD138 cells as green fluorescent spots were detected for each molecular variant, but not for non-binding fluorescence labeled natalizumab (see section 4.3.2). Co-localization of all nBT062 variants with LAMP-1 demonstrated their transport into lysosomes where DM4 would be released by proteolysis. In general, two different mechanisms for CD138 internalization are reported depending on the type of ligand: While internalization of atherogenic lipoproteins enriched in lipoprotein lipase (LpL) is mediated via lipid rafts, heparinase for example seems to be internalized by clathrin coated pits (Fuki et al. 1997; Fuki et al. 2000; Chen, Williams 2013). With respect to kinetics the latter type of uptake occurs quite fast within 15 min, whereas $t_{1/2}$ is approx. 1 h for lipid raft internalization (Goldstein et al. 1985; Nadav et al. 2002; Fux et al. 2009; Shteingauz et al. 2014). Based on observations during fluorescence microscopy method development, first signs of cellular nBT062 antibody uptake were seen after 1-2 h of incubation at 37°C, which would be in line with an antibody uptake based on lipid rafts. Endocytosis of bispecific nBT062-natalizumab antibodies indicated that CD138 crosslinking which could only be mediated by monospecific, bivalent nBT062 antibodies is not a compulsory requirement for the uptake. Efficient lysosomal trafficking is important for ADCs to evolve the full potential of the cytotoxic agent. In a recent study de Goeij and colleagues generated a bispecific IgG1 antibody targeting the tumor specific antigen HER2 and CD63, a protein known to shuttle between the plasma membrane and intracellular compartments. Conjugated to duostatin-3, this bispecificity led to an improved cytotoxic potential compared to the respective monospecific antibodies (Goeij et al. 2016).

In summary, these data demonstrate that all nBT062 model variants were capable of sufficient CD138 binding followed by internalization and processing due to endosomal and lysosomal pathway and thereby provide the potential to specifically transport cytotoxic agents into CD138-expressing tumor cells *in vivo*.

5.3 Conjugation of nBT062 variants to DM4

The different nBT062 model variants, WT nBT062, stable nBT062, half nBT062 and bispecific nBT062-natalizumab were fused to the cytotoxic agent DM4. This was done by a two stage conjugation process attaching the SPDB linker to the respective nBT062 variant first, followed by conjugating DM4 to the thiol-reactive group of the SPDB linker. Since drug substance material of BT062 used in clinic trials has approx. 3.5 DM4 molecules per antibody, this DAR was also aimed for when monospecific, bivalent WT nBT062 and stable nBT062 were conjugated. Half-antibodies and bispecific antibodies evolved by the *in vivo* IgG4 half-antibody exchange mechanism would result in 50% of the initial payload. Thus, for DM4 conjugation of one half nBT062 molecule (HC+LC) and one bispecific nBT062-natalizumab, it was also aimed for 50% payload, respectively 1.75 DM4 molecules per antibody. The DM4 conjugation was successfully performed resulting in ADCs with DARs of 3.5, 3.4, 1.6, and 1.7 for WT nBT062-DM4, stable nBT062-DM4, half nBT062-DM4 and bispecific nBT062-natalizumab-DM4, respectively. The DAR is one of the major critical factors in ADC development as attaching less payload will decrease the efficacy. On the contrary, fusion of too many toxic agents will destabilize the ADC resulting in altered PK, increased plasma clearance, reduced half-life and increased systemic toxicity (Perez et al. 2014; Diamantis, Banerji 2016). For example, it was shown that ADCs with a DAR of approx. 2 to 4 demonstrated comparable PK to unconjugated antibodies, but ADCs with a DAR of 8 cleared more rapidly resulting in a reduced antitumor efficacy *in vivo*. This was potentially due to an increased exposure of the latter ADC leading to faster clearance and, consequently, to a smaller PK area under the curve (Hamblett et al. 2004; Kim, Kim 2015). Thus, most of current ADCs approved or in clinical development utilizing a lysine conjugation approach provide an average of 3-4 cytotoxic payloads per antibody (Lambert 2013). For example, trastuzumab emtansine, a DM1 conjugated anti-Her2 antibody approved for the treatment of breast cancer, also utilizes a DAR of 3.5, which is exactly in line with the amount of payload used for BT062 (Kim et al. 2014; Jain et al. 2015). Compared to the WT nBT062 conjugation reaction, 70% and also 50% of each, SPDB linker and DM4 were tested for bispecific nBT062-natalizumab ADC generation. This resulted in DARs of 2.6 (74% SPDB/DM4) and 1.7 (49% SPDB/DM4), respectively. Therefore, it can be concluded that the SPDB linker and DM4 conjugation reactions seem to be proportional and potentially easy to adjust for aiming at a specific DAR.

The DM4 distribution in each nBT062-DM4 variant was determined ranging from 0 to 6, 0 to 6, 0 to 4, and 1 to 3 drugs per antibody molecule for WT nBT062-DM4, stable nBT062-DM4, half nBT062-DM4 and bispecific nBT062-natalizumab-DM4, respectively. Compared to the three bivalent nBT062-DM4 variants (~150 kDa), half nBT062-DM4 was measured with masses of approx. 75 kDa (HC+LC). Thus, when assuming non-covalent interactions leading

to half nBT062-DM4 dimerization, this model demonstrated the broadest drug distribution range of zero to eight DM4 molecules per full length antibody. For bispecific nBT062-natalizumab, the DM4 distribution range was reduced by 50%, proportionally in line with the reduced amount of SPDB linker and DM4 during conjugation. In contrast to WT nBT062-DM4 and stable nBT062-DM4, bispecific nBT062-natalizumab did not comprise any fraction of unconjugated antibodies. However, those observations suggest that SPDB-DM4 conjugation follows a binomial distribution. This theory is further supported by Goldmacher et al., who published an algorithm for identification of an acceptable statistical model for experimental drug load distributions in ADCs (Goldmacher et al. 2015). Furthermore, the results observed in this thesis are in accordance with other lysine-based ADCs: Trastuzumab emtansine is known to contain a distribution of zero to eight DM1 molecules per antibody (Kim et al. 2014), while the DM1 conjugated anti-CD56 ADC, HuN901-DM1, displays a drug distribution profile of one to six cytotoxic molecules (Wang et al. 2005). Interestingly, gemtuzumab ozogamicin, an anti-CD33 mAb conjugated to calicheamicin, seems to be the only current ADC, wherein up to 50% of the antibodies are unconjugated, while the other fractions comprise a payload of four to six cytotoxic molecules per antibody leading to an overall DAR of approx. 2-3 (Kim, Kim 2015). The MS spectrum further revealed, that half nBT062-DM4 had much more different glycosylation species than any of the other three nBT062-DM4 variants. Glycosylation of IgGs is *e.g.* known to modulate effector functions and half-life (B. Wong 2012). The major glycosylation site of the IgG4 subtype is found between the two CH2/CH3 domains forming the Fc, namely the N-linked glycosylation at position 297 (Vidarsson et al. 2014). While half nBT062 antibodies lack covalent dimerization, it is conceivable that the accessibility during glycosylation taking place in the endoplasmic reticulum and the Golgi is increased leading thereby to a higher glycosylation level. nBT062 variants were produced from stable CHO cell pools but not from single cell clones, which might result in a higher variation in the glycosylation pattern. Nevertheless, these minor differences in glycosylation should not influence the efficacy of the different nBT062-DM4 variants.

Full length IgG comprises approx. 80-100 lysines allocated on the two H and two L chains, carrying each an ε-amino group potentially available for random conjugation (Goldmacher et al. 2015). This random lysine conjugation results in ADC subpopulations with different numbers of cytotoxic moieties attached, but also in different locations of their linkage. MS analysis of WT nBT062-DM4, stable nBT062-DM4 and half nBT062-DM4 obtained eleven identical conjugation sites in the LCs of each variant. Since no modifications were incorporated in the LCs of those variants, this was not surprising. In contrast and compared to WT nBT062-DM4, the conjugation site K223 was lacking in stable nBT062 and half nBT062-DM4 and additionally for half nBT062-DM4 the K250 was not found to be conjugated. K223 is located next to the S228P substitution in stable nBT062-DM4 and

C226S and C229S mutations in half nBT062. Known that these amino acid substitutions have an influence on the protein structure, the resulting conformational alterations might have prevented lysine conjugation of K223 and K250 by steric hindrance. The approved ADC trastuzumab emtansine contains in total 88 lysines and 4 N-terminally amino groups, of which 82 sites (13 LC conjugation sites, 28 HC conjugation sites) were found to be partially conjugated (Chen et al. 2016). Wang et al. have previously reported 36 conjugations sites for huN901-DM1, namely six within each L chain and twelve within each H chain, while none of those modifications were found in the CDR regions. In conclusion, these results for trastuzumab emtansine, huN901-DM1 and the nBT062-DM4 variants demonstrate that lysines are conjugated quite differently, probably due to the individual specificities of each antibody and the conditions used for ADC conjugation.

As efficient payload delivery is based on the ADCs' antibody binding, flow cytometric analysis was used in this study to examine the influence of DM4 conjugation on the binding avidity of each nBT062 variant. No significant difference in CD138 binding between unconjugated and the respective DM4-conjugated variant was observed for WT nBT062-DM4, stable nBT062-DM4, half nBT062-DM4 and bispecific nBT062-natalizumab-DM4 in two cell lines tested. Again, similar observations were made for trastuzumab emtansine where neither an influence of DM1 linkage on the binding affinity to Her2 was detected, nor a reduction of trastuzumab’s anti-tumor effects itself were identified (Junttila et al. 2011; Barok et al. 2011b, 2011a; Barok et al. 2014). In contrast, Bondza and colleagues investigated the influence of biotin or fluorescence conjugation on the binding activity of the anti-EGFR antibody cetuximab using the LigandTracer method. Their results demonstrate that minor modifications could already lead to a reduced affinity to EGFR, while an anti-CD44v6 antibody was not influence on its antigen binding (Bondza et al. 2014). Thus, conjugation of small molecules to antibodies seems to be individual for each antibody, linker, payload and the conjugation technology used. Therefore, the in-depth characterization of the resulting ADCs is an important aspect during their development.

Taken together, it can be concluded that WT nBT062, stable nBT062, half nBT062 and bispecific nBT062-natalizumab were successfully conjugated to the cytotoxic agent DM4. In addition, each model variant resulted in DARs of the respective antibody species evolved by an IgG4 half-antibody exchange. The analytical characterization obtained similar properties compared to other ADCs, especially to trastuzumab emtansine. Thus, the generated nBT062-DM4 variants provide a suitable model on the different IgG4 shuffling related antibody species for comparing the cytotoxic potential.

5.4 All nBT062-DM4 variants mediate CD138-specific cytotoxicity *in vitro*

The cytotoxicity of all nBT062-DM4 variants was assessed in WST-1 viability assays to compare the anti-tumor activity and draw conclusions on the influence of the *in vivo* IgG4 half-antibody exchange on the efficacy. No significant difference in the potencies of WT nBT062-DM4, stable nBT062-DM4 and half nBT062-DM4 were observed (IC_{50}: ~0.08-0.14 nM). Since one half nBT062-DM4 molecule carried only 50% payload, there are two explanations for the similar potency of WT nBT062-DM4 and stable nBT062-DM4 compared to half nBT062: As tumor cell killing is only associated with the amount of DM4 molecules brought into the cell, half nBT062-DM4 molecules (75 kDa) had either (I) a higher internalization rate or (II) had to be dimerized by non-covalent interactions during this testing. In flow cytometric internalization experiments, higher internalization of half nBT062 was not seen: Initial surface binding and level of internalized antibodies was similar to the WT nBT062 and stable nBT062 models. Additionally, non-denatured SEC analysis provided information, that dimerization of half nBT062 took place. Thus, it can be concluded that half-nBT062-DM4 variants dimerized without hinge-stabilizing disulfide bonds in this experiment. However, in comparison to the monospecific WT nBT062-DM4, a decrease in the cytotoxicity of bispecific nBT062-natalizumab-DM4 was observed by approx. 50% in the absence or by 70% in the presence of a CD49d blocking antibody, respectively. This limited cytotoxic potency can be related to the reduced DM-4 payload per antibody leading to a lower cellular accumulation of the maytansine derivate. Internalization analyses have shown that natalizumab-epitope specific binding to CD49d did not lead to any antibody internalization (see section 4.3) and no cytotoxic activity was mediated by natalizumab itself. Despite this lack of bispecific nBT062-natalizumab-DM4 internalization via CD49d, it can thus be assumed that further ADC accumulation on the cell's surface by CD49d followed by potential crosslinking to CD138 might induce additional internalization of the ADC via the latter receptor increasing the cytotoxicity. Interestingly, there are some approaches trying to generate bispecific ADCs with one specificity against a tumor-specific antigen while the second epitope is located on a receptor known for fast internalization. Bridging those receptors shall lead to a more efficient internalization and prevent ADCs from cellular recycling mechanisms without the release of the cytotoxic agent. For example, Andreev and coworkers have generated a bispecific antibody targeting both, Her2 and prolactin. Besides Her2, the prolactin receptor is also a potential breast cancer target known for rapid internalization and efficient lysosomal trafficking. Crosslinking of both receptors enhanced the cytotoxicity of a respective ADC compared to the monospecific Her2-binding ADC (Andreev et al. 2017). Similar results were obtained by DeVay et al. when targeting Her2 in combination with the Amyloid Precursor Like Protein 2 (APLP2) (DeVay et al. 2017).

However, to draw conclusions from these experiments for the influence of *in vivo* IgG4 half-antibody exchange on the ADC's efficacy, it is important to mention that endogenous IgG4 antibodies are generally not directed against naturally human surface receptors. As *in vivo* shuffling of an IgG4-based ADC would result in a random exchange, the second specificity apart from the tumor-antigen is undefined and thus not available for tumor-specific binding. Hence, the approach blocking CD49d should reflect better the *in vivo* situation. Nevertheless, the IC_{50} of bispecific nBT062-natalizumab-DM4 was still in the picomolar range (456 pM). This reflects a similar cytotoxicity as trastuzumab emtansine when killing SK-BR-3 breast cancer cells (~323 pM) (Beerli et al. 2015). In addition, this further demonstrates the high cytotoxic potential of the monospecific, bivalent nBT06-DM4 variants.

5.5 Human IgG4 reduces the efficacy of unstabilzed nBT062 variants *in vivo*

The influence of *in vivo* IgG4-related half-antibody exchange on the efficacy of an unstabilized therapeutic IgG4 antibody is related to its mode of action. Blocking antibodies such as the approved natalizumab known to undergo half-antibody exchange with endogenous IgG4 might still perform in a sufficient manner (Hutchinson 2007; Labrijn et al. 2009; Broug et al. 2010). Other mode of actions where bivalent binding to certain epitopes is required, *e.g.* antigen crosslinking of identical or distinct proteins, the therapeutics might become inactive after exchanging half-antibodies. For example, wild type IgG4-based 1D09C3 was not able to crosslink human leukocyte antigen-DR (HLA-DR) after this process anymore. Thus, the development of 1D09C3 was discontinued in early clinical trials for advanced B cell malignancies (Hansen et al. 2009; Broug et al. 2010; Schweighofer et al. 2012). In the present work, the influence of IgG4 half-antibody exchange on the efficacy of the ADC BT062 was evaluated in a breast cancer xenograft mouse model using the generated model variants, WT nBT062-DM4, stable nBT062-DM4, half nBT062-DM4 and bispecific nBT062-natalizumab-DM4. Therefore, all nBT062-DM4 variants were tested in doses of 4 or 2 mg/kg/week either as monotherapy or in combination with an IVIg preparation containing human IgG4 antibodies. Administration of IVIgs resulted in serum levels comparable to human IgG4 serum concentrations of 10 µg/ml to >2 mg/ml (Aucouturier et al. 1984). All treatments were well tolerated as nearly no changes in body weights were observed (see section 4.6.2). In the absence of human IgG4, WT nBT062-DM4, stable nBT062-DM4 and half nBT062-DM4 were highly effective, leading to tumor remissions at both dose levels tested. The prescence of IgG4 did not influence the efficacy of the monospecific variants at the high dose, but it reduced the efficacy of WT nBT062-DM4 and half nBT062-DM4 when administered at low dose in terms of both, median tumor growth and

tumor growth delay based on animal survival. The efficacy of stable nBT062-DM4 was not significally influenced by the presence of human IgG4 at low dose, but only 3 of 5 mice demonstrated complete remissions. Compared to that, stable nBT062-DM4 led to 100% survival in the other groups tested (see section 4.6.1). This observation on IgG-mediated loss of anti-tumor activity can be correlated to the *in vivo* half-antibody exchange: Antibody shuffling was shown in plasma samples by LBA/LC-MS for WT nBT062-DM4 and half nBT062-DM4, but was not detected for stable nBT062-DM4 (see section 4.6.3). Interestingly, shuffling of WT nBT062-DM4 tended to be higher at 2 mg/kg/week dosing compared to 4 mg/kg/week dosing, when measuring plasma samples 24 h post injection. As the human IVIg preparation was adminstered at constant levels of 10 ml/kg/week, an increased ratio of ADC to IgG4 within the IVIg preparation occured at the lower dose (ratio ADC:IgG4 = ~1:5 for 4 mg/kg/week or ~1:10 for 2 mg/kg/week dosing). As IgG4 shuffling seems to follow an equilibrium reaction, this might explain such observations since increasing the ratio towards endogenious IgG4 shifts the reaction towards bispecific antibodies. As described, WT nBT062-DM4 and half nBT062-DM4 acted similarly *in vivo* in the presence or absence of endogenous IgG, indicating that half nBT062-DM4 antibodies were able to undergo non-covalent dimerization under physiological conditions. In contrast, detected shuffling levels for half nBT062-DM4 in murine plasma were much lower compared to WT nBT062-DM4. This might be based on the conditions of the CD138 pull down assay before sample digestion and injection into the LC-MS/MS system. Harsh conditions during antibody-bead binding and washing might potentially terminate non-covalent dimerizations, the final eluate would result in a deminished fraction of bispecific antibodies and thus result in an underestimation of shuffling by this method.

Bispecific nBT062-natalizumab-DM4 reached only boarderline efficacy when dosed at 4 mg/kg/week in monotherapy and was ineffective in any other dosing. Thus, it can be assumed that bispecific ADCs as a product of *in vivo* half-antibody exchange were much less effective. A possible explanation might be that the cytotoxic agents were not able to accumulate to a sufficient threshold for *in vivo* tumor cell killing. As WT nBT062-DM4 and half nBT062-DM4 ADCs demonstrated a significantly higher efficacy, even though half-antibody exchange occured, it can be concluded that the process of shuffling takes some time until an equilibrium is adapted. This hypothesis is in line with results from Rispens et al. investigating the IgG4 half-antibody exchange kinects *in vitro* after either DTT reduction of differently labeled IgG4 antibodies or permanently in the presence of 1 mM GSH via Förster resonance energy transfer (FRET). They demonstrated that once the disulfe bonds in the hinge region were reduced by the strong reducing agent DTT, shuffling took place within minutes. In contrast, using the mild reducing conditions by GSH this process took much more time (Rispens et al. 2011). Such a time window until IgG4 shuffling occurs *in vivo* might be

used by WT nBT062-DM4 and half nBT062-DM4 to saturate CD138 receptors on the tumor cells' surfaces resulting in transport of higher DM4 amounts into the cells. This hypothesis further rises the question if IgG4 shuffling can occure once an antibody has already bound to its antigen. An answer might be given by a cellular assay based on two different labeled antibodies using FRET. Furthermore, it would be interesting to study the *in vivo* PK of half-antibody exchange and comparing them with the PK profiles of the ADC and the antibody itself. However, dispite this mouse study demonstrated an improved efficacy of the stable nBT062 in the presence of endogenous IgG4, those benefits were only observered at the low dose treatment. Hence, it can also be assumed from this experiment that an IgG4 shuffling related loss of efficacy might be compensated by an adjusted dosing schedule.

Interestingly, the IVIg preparation reduced the efficacy of the hinge-stabilized bispecific nBT062-natalizumab and also, based on an unsignificant trend at the low dose treatment, the efficacy of stable nBT062-DM4. Blocking of CD138 by antibodies within the IVIg preparation was excluded as no CD138-antibodies were detected in the ECL assay (see section 4.6.4). A possible explanation for these findings might be given by the results of Bleeker et al.: They were able to demonstrate in mice that co-administered IVIg decreased the plasma concentration of a monoclonal IgG1 by ~40% after 3 days (Bleeker et al. 2001). This is based on the competition for FcRn binding, the major receptor responsible for half-life prolongation of IgG. Thus, the half-life of nBT062-DM4 variants might be extendet at low total IgG concentrations in immunodeficient NMRI nude mice, because FcRn competition is lacking. Adding IVIgs then might decrease the ADCs half-life by saturating FcRn molecules. This hypothesis can be proven by measuring the PK as already suggested.

5.6 Safety related aspects of half-antibody exchange

Addressing the influence of IgG4 shuffling on the efficacy of a given ADC is one major issue while the patients' safty is another. In general, side effects due to the exchange of half-antibodies in patients can not be fully excluded, but seem to be unlikely based on the following facts: The self/non-self discrimination of the immune system ensures in people, who do not suffer from auto-immune diseases, that antibodies produced by B cells are not directed against intact, endogenous molecules. This also applies for IgG4: It is mainly known to be associated with allergies and might downregulate inflammatory responses. IgG4 lacks proinflammatory effector functions and reacts with the inhibitory FcγRIIb present on macrophages, monocytes and DCs leading to the production of anti-inflamatory Interleukin-10 (Scott-Taylor et al. 2017; Murphy, Weaver 2017; Nirula et al. 2011). Further, the endogenous IgG4 antibodies circulating in the human blood system are directed against a broad repertoire of antigens. Hence, half-antibody exchange of ADCs would result in

bispecific antibodies having one specificity against the tumor-antigen and another one against any unknown second target out of a variety of many distinct antigens, *e.g.* an allergen, small molecule or maybe although unlikely an endogenous antigen. The propability that a bispecific antibody species against a cellular target different from the specific tumor-antigen arises and is still internalized in amounts necessary to overcome the cytotoxic threshold, seems to be extremely low. In addition, ADCs carrying maytansines, *e.g.* DM4, are only able to affect dividing cells as they inhibit microtubule de-polymerization. These assumptions are further supported by intermediate results from a phase I/IIa clinical trial investigating BT062's safety and efficacy in combination with the standard of care drugs lenalidomide or pomalidomide and dexamethasone for the treatment of multiple myeloma including patients resistant to a prior therapy. The interim analysis has shown that BT062 is well tolerated in doses up to 120 mg/m² in above mentioned combinations with encouraging activities (Kelly et al. 2016).

5.7 Conclusion and outlook

In this thesis, the influence of *in vivo* IgG4 half-antibody exchange on the functionality and efficacy of unstabilized ADCs was investigated using BT062, an anti-CD138 IgG4 antibody conjugated to the cytotoxic agent DM4. Beside WT nBT062 comprising the natural IgG4 hinge available for half-antibody exchange, three model antibodies were successfully generated: Stable nBT062 incorporates amino acid mutations S228P and R409K to prevent IgG4 shuffling, while half nBT062 was used as a model for the transition state as this version is lacking the cysteines in the hinge region responsible for covalent heavy chain dimerization. Bispecific nBT062-natalizumab was used to simulate a potential product of the *in vivo* half-antibody exchange. All nBT062 variants were produced in FreeStyle CHO-S cells, purification worked well and all molecules demonstrated their expected analytical properties as identified by SDS-PAGE and IEF. SEC analysis suggested that half nBT062 was non-covalently dimerized under non-denaturing conditions. Flow cytometric analyses revealed that all nBT062 variants were capable to bind CD138 with nanomolar affinity/avidity, even though the binding activity of bispecific nBT062-natalizumab was slightly reduced compared to the monospecific antibodies. All molecular variants were internalized by the endosomal/lysosomal pathway after binding to CD138 on NCI-H929 ($CD138^+/CD49d^+$) and Ba/F3-hCD138 ($CD138^+/CD49d^-$) cells. Conjugation with SPDB linker and DM4 was succesfully performed aiming at 3.5 DM4 molecules per WT nBT062 and stable nBT062 and, respectively, 50% for half nBT062 (HL, 75 kDa) and bispecific nBT062-natalizumab. The DM4 distribution patterns were in line with their respective DARs and potential conjugation sites were similar for the monospecific variants. Further, the DM4 conjugation did not

influence the CD138 binding activity of any nBT062-DM4 variant. Assessing the *in vitro* cytotoxicity on NCI-H929 cells obtained that each ADC model mediated CD138-specific inhibition in the picomolar range, but monospecific variants were approx. 4 to 5 times more potent (IC_{50}: ~80 to 140 pM) in comparison to bispecific nBT062-natalizumab (~456 pM). Investigation of the nBT062-DM4 models in tumor-bearing xenograft mice demonstrated that hinge-stabilization prevented *in vivo* half-antibody exchange and thereby improved the efficacy at low ADC dosage (2 mg/kg/week) in the presence of human IgG4. Nevertheless, in high dosed mice (4 mg/kg/week) there were no significant differences observed between WT nBT062-DM4, stable nBT062-DM4 and half nBT062-DM-4 in the presence or absence of IgG4 while bispecific nBT062-natalizumab was only able to demonstrate a borderline efficacy in the absence of human IgG4. Based on this observation it was assumed that the *in vivo* half-antibody exchange is time-dependent providing unstabilized ADCs a time window for efficient tumor-specific cytotoxic transport. This potential time window could be investigated by a PK study in mice or even better in patients from clinical studies using the LBA/LC-MS method. A comparision with the PK profiles of the ADC and the unconjugated antibody, detectable *e.g.* by a panel of ELISA assays specific for free DM4, DM4-conjugated to the antibody and the antibody itself, could be used to optimize the dosing schedule. To further investigate the tumor-specific cytotoxicity, it would be interesting to address differences in the tumor-penetration of the nBT062-DM4 variants. For example, this could be done by immunohistochemistry using tumor sections from treated mice stained against both, nBT062 and DM4. The assessment of the systemic antibody distribution and accumulation of nBT062-DM4 variants in the presence or absence of human IgG4 would add important information to the pool of knowlege. By *in vivo* imaging in tumor-bearing nude mice, it would be possible to study if half-antibody exchanged WT nBT062-DM4 labeled with an IR dye can accumulate in any other tissues beside the tumor. As nBT062 only targets human CD138, the generation of a human CD138-transgenic mouse model could be considered to study off-target cytotoxic effects. However, this thesis clearly demonstrated the additional benefits of stabilizing mutations preventing the *in vivo* IgG4 half-antibody exchange and thus their incorporation should be considered when designing new IgG4-based ADCs or biobetters.

6 References

Aalberse, R. C.; van der Gaag, R; van Leeuwen, J. (1983): Serologic aspects of IgG4 antibodies. I. Prolonged immunization results in an IgG4-restricted response. In *J. Immunol.* 130 (2), pp. 722–726.

Aalberse, Rob C.; Schuurman, Janine (2002): IgG4 breaking the rules. In *Immunology* 105 (1), pp. 9–19.

Andreev, Julian; Thambi, Nithya; Perez Bay, Andres E.; Delfino, Frank; Martin, Joel; Kelly, Marcus P. et al. (2017): Bispecific Antibodies and Antibody-Drug Conjugates (ADCs) Bridging HER2 and Prolactin Receptor Improve Efficacy of HER2 ADCs. In *Mol. Cancer Ther.* 16 (4), pp. 681–693. DOI: 10.1158/1535-7163.MCT-16-0658.

Ansaldi, Deborah Ann; Lester, Philip (1999): SEPARATION OF POLYPEPTIDE MONOMERS. Applied for by GENENTECH INC [US] on 5/26/1999. App. no. US19990320100 19990526. Patent no. US2002010319 (A1). G01N30/26;B01J20/285;C07K1/18;C07K14/765;C07K16/06;C07K16/42;G01N30/34;G01N30/74;G01N30/88;C07K16/00. Priority no. US19990320100 19990526;US19980087602P 19980601.

Atwell, S.; Ridgway, J. B.; Wells, J. A.; Carter, P. (1997): Stable heterodimers from remodeling the domain interface of a homodimer using a phage display library. In *Journal of Molecular Biology* 270 (1), pp. 26–35. DOI: 10.1006/jmbi.1997.1116.

Aucouturier, P.; Danon, F.; Daveau, M.; Guillou, B.; Sabbah, A.; Besson, J.; Preud'homme, J. L. (1984): Measurement of serum IgG4 levels by a competitive immunoenzymatic assay with monoclonal antibodies. In *J. Immunol. Methods* 74 (1), pp. 151–162.

B. Wong, Rosie (2012): Functional Role of Glycosylation in a Human IgG4 Antibody Assessed by Surface Plasmon Resonance Technology. In *TOPHARMJ* 6 (1), pp. 27–33. DOI: 10.2174/1874143601206010027.

Bachmann, Martin F.; Jennings, Gary T. (2010): Vaccine delivery: a matter of size, geometry, kinetics and molecular patterns. In *Nat Rev Immunol* 10 (11), pp. 787–796. DOI: 10.1038/nri2868.

Baldo, Brian A. (2016): Safety of Biologics Therapy. Monoclonal Antibodies, Cytokines, Fusion Proteins, Hormones, Enzymes, Coagulation Proteins, Vaccines, Botulinum Toxins. Cham: Springer International Publishing; Imprint; Springer.

Barok, Mark; Joensuu, Heikki; Isola, Jorma (2014): Trastuzumab emtansine. Mechanisms of action and drug resistance. In *Breast cancer research : BCR* 16 (2), p. 209. DOI: 10.1186/bcr3621.

Barok, Mark; Tanner, Minna; Köninki, Katri; Isola, Jorma (2011a): Trastuzumab-DM1 causes tumour growth inhibition by mitotic catastrophe in trastuzumab-resistant breast cancer cells in vivo. In *Breast cancer research : BCR* 13 (2), R46. DOI: 10.1186/bcr2868.

Barok, Mark; Tanner, Minna; Köninki, Katri; Isola, Jorma (2011b): Trastuzumab-DM1 is highly effective in preclinical models of HER2-positive gastric cancer. In *Cancer letters* 306 (2), pp. 171–179. DOI: 10.1016/j.canlet.2011.03.002.

Baumgart, Daniel C.; Sandborn, William J. (2012): Crohn's disease. In *Lancet* 380 (9853), pp. 1590–1605. DOI: 10.1016/S0140-6736(12)60026-9.

Bayer-Garner, I. B.; Sanderson, R. D.; Dhodapkar, M. V.; Owens, R. B.; Wilson, C. S. (2001): Syndecan-1 (CD138) immunoreactivity in bone marrow biopsies of multiple myeloma: shed syndecan-1 accumulates in fibrotic regions. In *Mod. Pathol.* 14 (10), pp. 1052–1058. DOI: 10.1038/modpathol.3880435.

Bayry, Jagadeesh; Lacroix-Desmazes, Sébastien; Kazatchkine, Michel D.; Kaveri, Srini V. (2007): Monoclonal antibody and intravenous immunoglobulin therapy for rheumatic diseases: rationale and mechanisms of action. In *Nat Clin Pract Rheumatol* 3 (5), pp. 262–272. DOI: 10.1038/ncprheum0481.

Beckman Coulter (2011): CD138-PC5 manual. Edited by Beckman Coulter. Available online at http://www.bc-cytometry.com/PDF/DataSheet/A54191D.S.pdf.

Beerli, Roger R.; Hell, Tamara; Merkel, Anna S.; Grawunder, Ulf (2015): Sortase Enzyme-Mediated Generation of Site-Specifically Conjugated Antibody Drug Conjugates with High In Vitro and In Vivo Potency. In *PLoS ONE* 10 (7), e0131177. DOI: 10.1371/journal.pone.0131177.

Bendig, Mary M.; Leger, Olivier J.; Saldanha, Jose; Jones, S. Tarran; Yednock, Ted A. (1995): Humanized antibodies against leukocyte adhesion molecule VLA-4. Applied for by ATHENA NEUROSCIENCES INC [US] on 11/21/1995. App. no. US19950561521 19951121. Patent no. US5840299 (A). C07K;C12N15/09;A61K31/00;A61K39/395;A61P1/00;A61P1/04;A61P3/00;A61P3/10;A61P7/00;A61P9/00;A61P9/10;A61P11/00;A61P11/06;A61P13/00;A61P13/12;A61P17/00;A61P17/06;A61P25/28;A61P29/00;A61P35/00;A61P35/04;A61P37/00;C07H21/04;C07K16/18;C07K16/28;C07K16/46;C12N5/00;C12N5/10;C12N15/13;C12P21/08;G01N33/53;A61K38/00;C12R1/91;A61K39/395;C07K16/28;C12N15/13;C12P21/08. Priority no. US19940186269 19940125;US19950561521 19951121.

Berlot, Giorgio; Rossini, Perla; Turchet, Federica (2015): Biology of immunoglobulins. In *Translational medicine @ UniSa* 11, pp. 24–27.

Bernfield, M.; Götte, M.; Park, P. W.; Reizes, O.; Fitzgerald, M. L.; Lincecum, J.; Zako, M. (1999): Functions of cell surface heparan sulfate proteoglycans. In *Annu. Rev. Biochem.* 68, pp. 729–777. DOI: 10.1146/annurev.biochem.68.1.729.

Bernfield, M.; Kokenyesi, R.; Kato, M.; Hinkes, M. T.; Spring, J.; Gallo, R. L.; Lose, E. J. (1992): Biology of the syndecans: a family of transmembrane heparan sulfate proteoglycans. In *Annu. Rev. Cell Biol.* 8, pp. 365–393. DOI: 10.1146/annurev.cb.08.110192.002053.

Bleeker, W. K.; Teeling, J. L.; Hack, C. E. (2001): Accelerated autoantibody clearance by intravenous immunoglobulin therapy. Studies in experimental models to determine the magnitude and time course of the effect. In *Blood* 98 (10), pp. 3136–3142.

Bondza, Sina; Stenberg, Jonas; Nestor, Marika; Andersson, Karl; Björkelund, Hanna (2014): Conjugation effects on antibody-drug conjugates. Evaluation of interaction kinetics in real time on living cells. In *Molecular pharmaceutics* 11 (11), pp. 4154–4163. DOI: 10.1021/mp500379d.

Bouchard, Hervé; Viskov, Christian; Garcia-Echeverria, Carlos (2014): Antibody-drug conjugates—a new wave of cancer drugs. In *Bioorganic & medicinal chemistry letters* 24 (23), pp. 5357–5363. DOI: 10.1016/j.bmcl.2014.10.021.

Brinkmann, Ulrich; Kontermann, Roland E. (2017): The making of bispecific antibodies. In *MAbs* 9 (2), pp. 182–212. DOI: 10.1080/19420862.2016.1268307.

Broug, Ellen; Bland-Ward, Philip A.; Powell, John; Johnson, Kevin S. (2010): Fab-arm exchange. In *Nature biotechnology* 28 (2), 123-5; author reply 125-6. DOI: 10.1038/nbt0210-123.

Cai, Henry Hongrong (2016): Monoclonal Antibodies for Cancer Therapy Approved by FDA. In *MOJI* 4 (2). DOI: 10.15406/moji.2016.04.00120.

Capra, J. Donald (1997): Antibody engineering. Basel, New York: Karger (Chemical immunology, vol. 65).

Carter, Paul (2001): Bispecific human IgG by design. In *Journal of Immunological Methods* 248 (1-2), pp. 7–15. DOI: 10.1016/S0022-1759(00)00339-2.

Cavaliere, Francesca; Montanari, Enrico; Emerson, Andrew; Buschini, Annamaria; Cozzini, Pietro (2017): In silico pharmacogenetic approach. The natalizumab case study. In *Toxicology and applied pharmacology* 330, pp. 93–99. DOI: 10.1016/j.taap.2017.07.011.

Chen, Keyang; Williams, Kevin Jon (2013): Molecular mediators for raft-dependent endocytosis of syndecan-1, a highly conserved, multifunctional receptor. In *J. Biol. Chem.* 288 (20), pp. 13988–13999. DOI: 10.1074/jbc.M112.444737.

Chen, Liuxi; Wang, Lan; Shion, Henry; Yu, Chuanfei; Yu, Ying Qing; Zhu, Lei et al. (2016): In-depth structural characterization of Kadcyla® (ado-trastuzumab emtansine) and its biosimilar candidate. In *MAbs* 8 (7), pp. 1210–1223. DOI: 10.1080/19420862.2016.1204502.

Chng, Jake; Wang, Tianhua; Nian, Rui; Lau, Ally; Hoi, Kong Meng; Ho, Steven C. L. et al. (2015): Cleavage efficient 2A peptides for high level monoclonal antibody expression in CHO cells. In *mAbs* 7 (2), pp. 403–412. DOI: 10.1080/19420862.2015.1008351.

Compston, Alastair; Coles, Alasdair (2002): Multiple sclerosis. In *Lancet* 359 (9313), pp. 1221–1231. DOI: 10.1016/S0140-6736(02)08220-X.

Compston, Alastair; Coles, Alasdair (2008): Multiple sclerosis. In *Lancet* 372 (9648), pp. 1502–1517. DOI: 10.1016/S0140-6736(08)61620-7.

Cretney, E.; Degli-Esposti, M. A.; Densley, E. H.; Farrell, H. E.; Davis-Poynter, N. J.; Smyth, M. J. (1999): m144, a murine cytomegalovirus (MCMV)-encoded major histocompatibility complex class I homologue, confers tumor resistance to natural killer cell-mediated rejection. In *J. Exp. Med.* 190 (3), pp. 435–444.

Croce, Carlo M. (2008): Oncogenes and cancer. In *N. Engl. J. Med.* 358 (5), pp. 502–511. DOI: 10.1056/NEJMra072367.

Cromwell, Mary E. M.; Hilario, Eric; Jacobson, Fred (2006): Protein aggregation and bioprocessing. In *The AAPS journal* 8 (3), E572-9. DOI: 10.1208/aapsj080366.

Davies, Anna M.; Rispens, Theo; Ooijevaar-de Heer, Pleuni; Gould, Hannah J.; Jefferis, Roy; Aalberse, Rob C.; Sutton, Brian J. (2014): Structural Determinants of Unique Properties of Human IgG4-Fc. In *Journal of Molecular Biology* 426 (3), pp. 630–644. DOI: 10.1016/j.jmb.2013.10.039.

Derksen, P. W. B.; Gorter, D. J. J. de; Meijer, H. P.; Bende, R. J.; van Dijk, M.; Lokhorst, H. M. et al. (2003): The hepatocyte growth factor/Met pathway controls proliferation and apoptosis in multiple myeloma. In *Leukemia* 17 (4), pp. 764–774. DOI: 10.1038/sj.leu.2402875.

DeVay, Rachel M.; Delaria, Kathy; Zhu, Guoyun; Holz, Charles; Foletti, Davide; Sutton, Janette et al. (2017): Improved Lysosomal Trafficking Can Modulate the Potency of

Antibody Drug Conjugates. In *Bioconjugate chemistry* 28 (4), pp. 1102–1114. DOI: 10.1021/acs.bioconjchem.7b00013.

Di Carlo, E.; Forni, G.; Lollini, P.; Colombo, M. P.; Modesti, A.; Musiani, P. (2001): The intriguing role of polymorphonuclear neutrophils in antitumor reactions. In *Blood* 97 (2), pp. 339–345.

Diamantis, Nikolaos; Banerji, Udai (2016): Antibody-drug conjugates--an emerging class of cancer treatment. In *British journal of cancer* 114 (4), pp. 362–367. DOI: 10.1038/bjc.2015.435.

Donnelly, M. L.; Hughes, L. E.; Luke, G.; Mendoza, H.; Dam, E. ten; Gani, D.; Ryan, M. D. (2001a): The 'cleavage' activities of foot-and-mouth disease virus 2A site-directed mutants and naturally occurring '2A-like' sequences. In *The Journal of general virology* 82 (Pt 5), pp. 1027–1041. DOI: 10.1099/0022-1317-82-5-1027.

Donnelly, M. L.; Luke, G.; Mehrotra, A.; Li, X.; Hughes, L. E.; Gani, D.; Ryan, M. D. (2001b): Analysis of the aphthovirus 2A/2B polyprotein 'cleavage' mechanism indicates not a proteolytic reaction, but a novel translational effect. A putative ribosomal 'skip'. In *The Journal of general virology* 82 (Pt 5), pp. 1013–1025. DOI: 10.1099/0022-1317-82-5-1013.

Dore, Jean-Michel; Morard, Florence; Vita, Natalio; Wijdenes, John (1998): Identification and location on syndecan-1 core protein of the epitopes of B-B2 and B-B4 monoclonal antibodies. In *FEBS Letters* 426 (1), pp. 67–70. DOI: 10.1016/S0014-5793(98)00310-X.

Dunn, Olive Jean (1964): Multiple Comparisons Using Rank Sums. In *Technometrics* 6 (3), pp. 241–252. DOI: 10.1080/00401706.1964.10490181.

Elgert, K. D.; Alleva, D. G.; Mullins, D. W. (1998): Tumor-induced immune dysfunction: the macrophage connection. In *J. Leukoc. Biol.* 64 (3), pp. 275–290.

Farrell, H. E.; Vally, H.; Lynch, D. M.; Fleming, P.; Shellam, G. R.; Scalzo, A. A.; Davis-Poynter, N. J. (1997): Inhibition of natural killer cells by a cytomegalovirus MHC class I homologue in vivo. In *Nature* 386 (6624), pp. 510–514. DOI: 10.1038/386510a0.

Fell, H. P.; Yarnold, S.; Hellström, I.; Hellström, K. E.; Folger, K. R. (1989): Homologous recombination in hybridoma cells: heavy chain chimeric antibody produced by gene targeting. In *Proc. Natl. Acad. Sci. U.S.A.* 86 (21), pp. 8507–8511.

Fuki, I. V.; Kuhn, K. M.; Lomazov, I. R.; Rothman, V. L.; Tuszynski, G. P.; Iozzo, R. V. et al. (1997): The syndecan family of proteoglycans. Novel receptors mediating internalization of atherogenic lipoproteins in vitro. In *The Journal of clinical investigation* 100 (6), pp. 1611–1622. DOI: 10.1172/JCI119685.

Fuki, I. V.; Meyer, M. E.; Williams, K. J. (2000): Transmembrane and cytoplasmic domains of syndecan mediate a multi-step endocytic pathway involving detergent-insoluble membrane rafts. In *Biochem. J.* 351 Pt 3, pp. 607–612.

Fux, Liat; Ilan, Neta; Sanderson, Ralph D.; Vlodavsky, Israel (2009): Heparanase. Busy at the cell surface. In *Trends in biochemical sciences* 34 (10), pp. 511–519. DOI: 10.1016/j.tibs.2009.06.005.

Gaza-Bulseco, Georgeen; Faldu, Sagar; Hurkmans, Karen; Chumsae, Chris; Liu, Hongcheng (2008): Effect of methionine oxidation of a recombinant monoclonal antibody on the binding affinity to protein A and protein G. In *Journal of chromatography. B, Analytical*

technologies in the biomedical and life sciences 870 (1), pp. 55–62. DOI: 10.1016/j.jchromb.2008.05.045.

Goeij, Bart E. C. G. de; Vink, Tom; Napel, Hendrik ten; Breij, Esther C. W.; Satijn, David; Wubbolts, Richard et al. (2016): Efficient Payload Delivery by a Bispecific Antibody-Drug Conjugate Targeting HER2 and CD63. In *Molecular cancer therapeutics* 15 (11), pp. 2688–2697. DOI: 10.1158/1535-7163.MCT-16-0364.

Goldmacher, Victor S.; Amphlett, Godfrey; Wang, Lintao; Lazar, Alexandru C. (2015): Statistics of the distribution of the abundance of molecules with various drug loads in maytansinoid antibody-drug conjugates. In *Molecular pharmaceutics* 12 (6), pp. 1738–1744. DOI: 10.1021/mp5007536.

Goldstein, J. L.; Brown, M. S.; Anderson, R. G.; Russell, D. W.; Schneider, W. J. (1985): Receptor-mediated endocytosis. Concepts emerging from the LDL receptor system. In *Annu. Rev. Cell Biol.* 1, pp. 1–39. DOI: 10.1146/annurev.cb.01.110185.000245.

Green, L. L.; Hardy, M. C.; Maynard-Currie, C. E.; Tsuda, H.; Louie, D. M.; Mendez, M. J. et al. (1994): Antigen-specific human monoclonal antibodies from mice engineered with human Ig heavy and light chain YACs. In *Nat. Genet.* 7 (1), pp. 13–21. DOI: 10.1038/ng0594-13.

Grillo-López, Antonio J.; Hedrick, Eric; Rashford, Michelle; Benyunes, Mark (2002): Rituximab: ongoing and future clinical development. In *Semin. Oncol.* 29 (1 Suppl 2), pp. 105–112.

Hamblett, Kevin J.; Senter, Peter D.; Chace, Dana F.; Sun, Michael M. C.; Lenox, Joel; Cerveny, Charles G. et al. (2004): Effects of drug loading on the antitumor activity of a monoclonal antibody drug conjugate. In *Clinical cancer research : an official journal of the American Association for Cancer Research* 10 (20), pp. 7063–7070. DOI: 10.1158/1078-0432.CCR-04-0789.

Hanahan, Douglas; Weinberg, Robert A. (2011): Hallmarks of cancer. The next generation. In *Cell* 144 (5), pp. 646–674. DOI: 10.1016/j.cell.2011.02.013.

Hansen, Kerrin; Ruttekolk, Ivo R.; Glauner, Heike; Becker, Frank; Brock, Roland; Hannus, Stefan (2009): The in vitro biological activity of the HLA-DR-binding clinical IgG4 antibody 1D09C3 is a consequence of the disruption of cell aggregates and can be abrogated by Fab arm exchange. In *Molecular Immunology* 46 (16), pp. 3269–3277. DOI: 10.1016/j.molimm.2009.07.031.

Harding, Fiona A.; Stickler, Marcia M.; Razo, Jennifer; DuBridge, Robert B. (2010): The immunogenicity of humanized and fully human antibodies. Residual immunogenicity resides in the CDR regions. In *MAbs* 2 (3), pp. 256–265.

Harousseau, Jean-Luc; Moreau, Philippe (2009): Autologous hematopoietic stem-cell transplantation for multiple myeloma. In *N. Engl. J. Med.* 360 (25), pp. 2645–2654. DOI: 10.1056/NEJMct0805626.

Harris, R. J. (1995): Processing of C-terminal lysine and arginine residues of proteins isolated from mammalian cell culture. In *Journal of chromatography. A* 705 (1), pp. 129–134.

Honjo, T. (1983): Immunoglobulin genes. In *Annu. Rev. Immunol.* 1, pp. 499–528. DOI: 10.1146/annurev.iy.01.040183.002435.

Hornick, Carole L.; Karush, Fred (1972): Antibody affinity—III the role of multivalence. In *Immunochemistry* 9 (3), pp. 325–340. DOI: 10.1016/0019-2791(72)90096-1.

Hudis, Clifford A. (2007): Trastuzumab--mechanism of action and use in clinical practice. In *N. Engl. J. Med.* 357 (1), pp. 39–51. DOI: 10.1056/NEJMra043186.

Hutchinson, Michael (2007): Natalizumab: A new treatment for relapsing remitting multiple sclerosis. In *Therapeutics and clinical risk management* 3 (2), pp. 259–268.

Igney, Frederik H.; Krammer, Peter H. (2002): Immune escape of tumors: apoptosis resistance and tumor counterattack. In *J. Leukoc. Biol.* 71 (6), pp. 907–920.

Ikeda, Hiroshi; Hideshima, Teru; Fulciniti, Mariateresa; Lutz, Robert J.; Yasui, Hiroshi; Okawa, Yutaka et al. (2009): The monoclonal antibody nBT062 conjugated to cytotoxic Maytansinoids has selective cytotoxicity against CD138-positive multiple myeloma cells in vitro and in vivo. In *Clinical cancer research : an official journal of the American Association for Cancer Research* 15 (12), pp. 4028–4037. DOI: 10.1158/1078-0432.CCR-08-2867.

Inbar, D.; Hochman, J.; Givol, D. (1972): Localization of antibody-combining sites within the variable portions of heavy and light chains. In *Proc. Natl. Acad. Sci. U.S.A.* 69 (9), pp. 2659–2662.

Irani, Vashti; Guy, Andrew J.; Andrew, Dean; Beeson, James G.; Ramsland, Paul A.; Richards, Jack S. (2015): Molecular properties of human IgG subclasses and their implications for designing therapeutic monoclonal antibodies against infectious diseases. In *Mol. Immunol.* 67 (2 Pt A), pp. 171–182. DOI: 10.1016/j.molimm.2015.03.255.

Jain, Nareshkumar; Smith, Sean W.; Ghone, Sanjeevani; Tomczuk, Bruce (2015): Current ADC Linker Chemistry. In *Pharmaceutical research* 32 (11), pp. 3526–3540. DOI: 10.1007/s11095-015-1657-7.

Jakobovits, A. (1995): Production of fully human antibodies by transgenic mice. In *Curr. Opin. Biotechnol.* 6 (5), pp. 561–566.

Jefferis, Roy (2005): Glycosylation of natural and recombinant antibody molecules. In *Adv. Exp. Med. Biol.* 564, pp. 143–148. DOI: 10.1007/0-387-25515-X_26.

Jefferis, Roy (2007): Antibody therapeutics. In *Expert Opin. Biol. Ther.* 7 (9), pp. 1401–1413. DOI: 10.1517/14712598.7.9.1401.

Jefferis, Roy (2012): Isotype and glycoform selection for antibody therapeutics. In *Archives of biochemistry and biophysics* 526 (2), pp. 159–166. DOI: 10.1016/j.abb.2012.03.021.

Junttila, Teemu T.; Li, Guangmin; Parsons, Kathryn; Phillips, Gail Lewis; Sliwkowski, Mark X. (2011): Trastuzumab-DM1 (T-DM1) retains all the mechanisms of action of trastuzumab and efficiently inhibits growth of lapatinib insensitive breast cancer. In *Breast cancer research and treatment* 128 (2), pp. 347–356. DOI: 10.1007/s10549-010-1090-x.

Kaplan, E. L.; Meier, Paul (1958): Nonparametric Estimation from Incomplete Observations. In *Journal of the American Statistical Association* 53 (282), p. 457. DOI: 10.2307/2281868.

Kärre, Klas (2008): Natural killer cell recognition of missing self. In *Nat Immunol* 9 (5), pp. 477–480. DOI: 10.1038/ni0508-477.Define:

Kelly, Kevin R.; Siegel, David S.; Chanan-Khan, Asher A.; Somlo, George; Heffner, Leonard T.; Jagannath, Sundar et al. (2016): Indatuximab Ravtansine (BT062) in Combination with Low-Dose Dexamethasone and Lenalidomide or Pomalidomide. Clinical

Activity in Patients with Relapsed / Refractory Multiple Myeloma. In *Blood* 128 (22), p. 4486. Available online at http://www.bloodjournal.org/content/128/22/4486.

Kiese, Sylvia; Papppenberger, Astrid; Friess, Wolfgang; Mahler, Hanns-Christian (2008): Shaken, not stirred: mechanical stress testing of an IgG1 antibody. In *Journal of pharmaceutical sciences* 97 (10), pp. 4347–4366. DOI: 10.1002/jps.21328.

Kim, Eunhee G.; Kim, Kristine M. (2015): Strategies and Advancement in Antibody-Drug Conjugate Optimization for Targeted Cancer Therapeutics. In *Biomolecules & therapeutics* 23 (6), pp. 493–509. DOI: 10.4062/biomolther.2015.116.

Kim, Michael T.; Chen, Yan; Marhoul, Joseph; Jacobson, Fred (2014): Statistical modeling of the drug load distribution on trastuzumab emtansine (Kadcyla), a lysine-linked antibody drug conjugate. In *Bioconjugate chemistry* 25 (7), pp. 1223–1232. DOI: 10.1021/bc5000109.

Kim, U.; Baumler, A.; Carruthers, C.; Bielat, K. (1975): Immunological escape mechanism in spontaneously metastasizing mammary tumors. In *Proc. Natl. Acad. Sci. U.S.A.* 72 (3), pp. 1012–1016.

Klein, Christian; Sustmann, Claudio; Thomas, Markus; Stubenrauch, Kay; Croasdale, Rebecca; Schanzer, Jürgen et al. (2014): Progress in overcoming the chain association issue in bispecific heterodimeric IgG antibodies. In *mAbs* 4 (6), pp. 653–663. DOI: 10.4161/mabs.21379.

Köhler, G.; Milstein, C. (1975): Continuous cultures of fused cells secreting antibody of predefined specificity. In *Nature* 256 (5517), pp. 495–497.

Kontermann, Roland E. (2012): Dual targeting strategies with bispecific antibodies. In *MAbs* 4 (2), pp. 182–197. DOI: 10.4161/mabs.4.2.19000.

Kontermann, Roland E.; Brinkmann, Ulrich (2015): Bispecific antibodies. In *Drug discovery today* 20 (7), pp. 838–847. DOI: 10.1016/j.drudis.2015.02.008.

Kraus, Elmar; Bruecher, Christoph; Daelken, Benjamin; Germer, Matthias; Zeng, Steffen; Osterroth, Frank et al. (2008): AGENTS TARGETING CD138 AND USES THEREOF. Applied for by BIOTEST AG [DE]; KRAUS ELMAR [DE]; BRUECHER CHRISTOPH [DE]; DAELKEN BENJAMIN [DE]; GERMER MATTHIAS [DE]; ZENG STEFFEN [DE]; OSTERROTH FRANK [DE]; UHEREK CHRISTOPH [DE]; AIGNER SILKE [DE] on 12/23/2008. App. no. WO2008EP68266 20081223. Patent no. WO2009080829 (A1). C07K16/28;A61P35/00;C07K16/30. Priority no. US20070016630P 20071226.

Kruskal, William H.; Wallis, W. Allen (1952): Use of Ranks in One-Criterion Variance Analysis. In *Journal of the American Statistical Association* 47 (260), p. 583. DOI: 10.2307/2280779.

Kuo, Timothy T.; Aveson, Victoria G. (2011): Neonatal Fc receptor and IgG-based therapeutics. In *MAbs* 3 (5), pp. 422–430. DOI: 10.4161/mabs.3.5.16983.

Kupchan, S. Morris; Komoda, Y.; Court, W. A.; Thomas, G. J.; Smith, R. M.; Karim, A. et al. (1972): Tumor inhibitors. LXXIII. Maytansine, a novel antileukemic ansa macrolide from Maytenus ovatus. In *J. Am. Chem. Soc.* 94 (4), pp. 1354–1356. DOI: 10.1021/ja00759a054.

Kyle, Robert A.; Rajkumar, S. Vincent (2004): Multiple myeloma. In *N. Engl. J. Med.* 351 (18), pp. 1860–1873. DOI: 10.1056/NEJMra041875.

Labrijn, A. F.; Rispens, T.; Meesters, J.; Rose, R. J.; den Bleker, T. H.; Loverix, S. et al. (2011): Species-Specific Determinants in the IgG CH3 Domain Enable Fab-Arm Exchange by Affecting the Noncovalent CH3-CH3 Interaction Strength. In *The Journal of Immunology* 187 (6), pp. 3238–3246. DOI: 10.4049/jimmunol.1003336.

Labrijn, Aran F.; Buijsse, Antonio Ortiz; van den Bremer, Ewald T J; Verwilligen, Annemiek Y W; Bleeker, Wim K.; Thorpe, Susan J. et al. (2009): Therapeutic IgG4 antibodies engage in Fab-arm exchange with endogenous human IgG4 in vivo. In *Nat Biotechnol* 27 (8), pp. 767–771. DOI: 10.1038/nbt.1553.

Lambert, John M. (2013): Drug-conjugated antibodies for the treatment of cancer. In *British journal of clinical pharmacology* 76 (2), pp. 248–262. DOI: 10.1111/bcp.12044.

Lander, E. S.; Linton, L. M.; Birren, B.; Nusbaum, C.; Zody, M. C.; Baldwin, J. et al. (2001): Initial sequencing and analysis of the human genome. In *Nature* 409 (6822), pp. 860–921. DOI: 10.1038/35057062.

Lee, Jae-Ghi; Moon, Hana; Park, Chanho; Shin, Sang Hyuck; Kang, KyeongJin; Kim, Tae Jin (2013): Reversible expression of CD138 on mature follicular B cells is downregulated by IL-4. In *Immunol. Lett.* 156 (1-2), pp. 38–45. DOI: 10.1016/j.imlet.2013.09.004.

Lewis, Steven M.; Wu, Xiufeng; Pustilnik, Anna; Sereno, Arlene; Huang, Flora; Rick, Heather L. et al. (2014): Generation of bispecific IgG antibodies by structure-based design of an orthogonal Fab interface. In *Nat Biotechnol* 32 (2), pp. 191–198. DOI: 10.1038/nbt.2797.

Lipson, Evan J.; Drake, Charles G. (2011): Ipilimumab: an anti-CTLA-4 antibody for metastatic melanoma. In *Clinical cancer research : an official journal of the American Association for Cancer Research* 17 (22), pp. 6958–6962. DOI: 10.1158/1078-0432.CCR-11-1595.

Longo, Vito; Brunetti, Oronzo; D'Oronzo, Stella; Dammacco, Franco; Silvestris, Franco (2012): Therapeutic approaches to myeloma bone disease. An evolving story. In *Cancer treatment reviews* 38 (6), pp. 787–797. DOI: 10.1016/j.ctrv.2012.03.004.

Lopus, Manu; Oroudjev, Emin; Wilson, Leslie; Wilhelm, Sharon; Widdison, Wayne; Chari, Ravi; Jordan, Mary Ann (2010): Maytansine and cellular metabolites of antibody-maytansinoid conjugates strongly suppress microtubule dynamics by binding to microtubules. In *Mol. Cancer Ther.* 9 (10), pp. 2689–2699. DOI: 10.1158/1535-7163.MCT-10-0644.

Mack, Fiona; Ritchie, Michael; Sapra, Puja (2014): The next generation of antibody drug conjugates. In *Seminars in oncology* 41 (5), pp. 637–652. DOI: 10.1053/j.seminoncol.2014.08.001.

Mak, Tak W.; Saunders, Mary E. (2006): The immune response. Basic and clinical principles. Amsterdam, Boston: Elsevier/Academic. Available online at http://site.ebrary.com/lib/alltitles/docDetail.action?docID=10188220.

Male, David; Brostoff, Jonathan; Roth, David B.; Roitt, Ivan (2007): Immunology. [online access + interactive extras ; studentconsult.com]. 7. ed., reprint. Philadelphia, Pa: Mosby Elsevier.

Matsuda, M.; Salazar, F.; Petersson, M.; Masucci, G.; Hansson, J.; Pisa, P. et al. (1994): Interleukin 10 pretreatment protects target cells from tumor- and allo-specific cytotoxic T cells and downregulates HLA class I expression. In *J. Exp. Med.* 180 (6), pp. 2371–2376.

Medema, J. P.; Jong, J. de; van Hall, T.; Melief, C. J.; Offringa, R. (1999): Immune escape of tumors in vivo by expression of cellular FLICE-inhibitory protein. In *J. Exp. Med.* 190 (7), pp. 1033–1038.

Merchant, A. M.; Zhu, Z.; Yuan, J. Q.; Goddard, A.; Adams, C. W.; Presta, L. G.; Carter, P. (1998): An efficient route to human bispecific IgG. In *Nat Biotechnol* 16 (7), pp. 677–681. DOI: 10.1038/nbt0798-677.

Meso Scale Diagnostics (2013): MSD Technology Platform. Edited by MSD (19504-v3-2013Jun). Available online at https://www.mesoscale.com/~/media/files/brochures/techbrochure.pdf, checked on 3/4/2018.

Milstein, C.; Cuello, A. C. (1983): Hybrid hybridomas and their use in immunohistochemistry. In *Nature* 305 (5934), pp. 537–540.

Morea, V.; Lesk, A. M.; Tramontano, A. (2000): Antibody modeling: implications for engineering and design. In *Methods* 20 (3), pp. 267–279. DOI: 10.1006/meth.1999.0921.

Murphy, Kenneth M.; Weaver, Casey (2017): Janeway's immunobiology. With assistance of Allan Mowat, Leslie Berg, David Chaplin, Charles A. Janeway, Paul Travers, Mark Walport. 9th edition. New York, London: GS Garland Science Taylor & Francis Group.

Nadav, Liat; Eldor, Amiram; Yacoby-Zeevi, Oron; Zamir, Eli; Pecker, Iris; Ilan, Neta et al. (2002): Activation, processing and trafficking of extracellular heparanase by primary human fibroblasts. In *Journal of cell science* 115 (Pt 10), pp. 2179–2187.

Navolotskaya, E. V. (2014): The second life of antibodies. In *Biochemistry Moscow* 79 (1), pp. 1–7. DOI: 10.1134/S0006297914010015.

Nimmerjahn, Falk; Ravetch, Jeffrey V. (2008): Fcγ receptors as regulators of immune responses. In *Nat Rev Immunol* 8 (1), pp. 34–47. DOI: 10.1038/nri2206.

Nirula, Ajay; Glaser, Scott M.; Kalled, Susan L.; Taylor, Frederick R.; Taylora, Frederick R. (2011): What is IgG4? A review of the biology of a unique immunoglobulin subtype. In *Curr Opin Rheumatol* 23 (1), pp. 119–124. DOI: 10.1097/BOR.0b013e3283412fd4.

O'Connell, Fionnuala P.; Pinkus, Jack L.; Pinkus, Geraldine S. (2004): CD138 (Syndecan-1), a Plasma Cell Marker Immunohistochemical Profile in Hematopoietic and Nonhematopoietic Neoplasms. In *American Journal of Clinical Pathology* 121 (2), pp. 254–263. DOI: 10.1309/617DWB5GNFWXHW4L.

Pardoll, Drew M. (2012): The blockade of immune checkpoints in cancer immunotherapy. In *Nat. Rev. Cancer* 12 (4), pp. 252–264. DOI: 10.1038/nrc3239.

Perez, Heidi L.; Cardarelli, Pina M.; Deshpande, Shrikant; Gangwar, Sanjeev; Schroeder, Gretchen M.; Vite, Gregory D.; Borzilleri, Robert M. (2014): Antibody-drug conjugates. Current status and future directions. In *Drug discovery today* 19 (7), pp. 869–881. DOI: 10.1016/j.drudis.2013.11.004.

Peters, Christina; Brown, Stuart (2015): Antibody-drug conjugates as novel anti-cancer chemotherapeutics. In *Bioscience reports* 35 (4). DOI: 10.1042/BSR20150089.

Phillips, J.; Drumm, A.; Harrison, P.; Bird, P.; Bhamra, K.; Berrie, E.; Hale, G. (2001): Manufacture and quality control of CAMPATH-1 antibodies for clinical trials. In *Cytotherapy* 3 (3), pp. 233–242. DOI: 10.1080/146532401753174061.

Ramani, Vishnu C.; Purushothaman, Anurag; Stewart, Mark D.; Thompson, Camilla A.; Vlodavsky, Israel; Au, Jessie L-S; Sanderson, Ralph D. (2013): The heparanase/syndecan-1 axis in cancer: mechanisms and therapies. In *The FEBS journal* 280 (10), pp. 2294–2306. DOI: 10.1111/febs.12168.

Ridgway, J. B.; Presta, L. G.; Carter, P. (1996): 'Knobs-into-holes' engineering of antibody CH3 domains for heavy chain heterodimerization. In *Protein engineering* 9 (7), pp. 617–621.

Rispens, Theo; den Bleker, Tamara H.; Aalberse, Rob C. (2010): Hybrid IgG4/IgG4 Fc antibodies form upon 'Fab-arm' exchange as demonstrated by SDS-PAGE or size-exclusion chromatography. In *Mol. Immunol.* 47 (7-8), pp. 1592–1594. DOI: 10.1016/j.molimm.2010.02.021.

Rispens, Theo; Ooijevaar-de Heer, Pleuni; Bende, Onno; Aalberse, Rob C. (2011): Mechanism of Immunoglobulin G4 Fab-arm Exchange. In *J. Am. Chem. Soc.* 133 (26), pp. 10302–10311. DOI: 10.1021/ja203638y.

Rojas, Raul; Apodaca, Gerard (2002): Immunoglobulin transport across polarized epithelial cells. In *Nat. Rev. Mol. Cell Biol.* 3 (12), pp. 944–955. DOI: 10.1038/nrm972.

Rowe, J. M.; Lowenberg, B. (2013): Gemtuzumab ozogamicin in acute myeloid leukemia: a remarkable saga about an active drug. In *Blood* 121 (24), pp. 4838–4841. DOI: 10.1182/blood-2013-03-490482.

Ruiz-Velasco, N.; Guerrero-Esteo, M.; Briskin, M. J.; Teixidó, J. (2000): The alpha(4) integrin subunit Tyr(187) has a key role in alpha(4)beta(7)-dependent cell adhesion. In *J. Biol. Chem.* 275 (10), pp. 7052–7059.

Salfeld, Jochen G. (2007): Isotype selection in antibody engineering. In *Nat. Biotechnol.* 25 (12), pp. 1369–1372. DOI: 10.1038/nbt1207-1369.

Sanderson, R. D.; Lalor, P.; Bernfield, M. (1989): B lymphocytes express and lose syndecan at specific stages of differentiation. In *Cell Regul.* 1 (1), pp. 27–35.

Sapra, Puja; Hooper, Andrea T.; O'Donnell, Christopher J.; Gerber, Hans-Peter (2011): Investigational antibody drug conjugates for solid tumors. In *Expert opinion on investigational drugs* 20 (8), pp. 1131–1149. DOI: 10.1517/13543784.2011.582866.

Sapra, Puja; Shor, Boris (2013): Monoclonal antibody-based therapies in cancer: advances and challenges. In *Pharmacology & therapeutics* 138 (3), pp. 452–469. DOI: 10.1016/j.pharmthera.2013.03.004.

Schaefer, Wolfgang; Regula, Jörg T.; Bähner, Monika; Schanzer, Jürgen; Croasdale, Rebecca; Dürr, Harald et al. (2011): Immunoglobulin domain crossover as a generic approach for the production of bispecific IgG antibodies. In *Proc. Natl. Acad. Sci. U.S.A.* 108 (27), pp. 11187–11192. DOI: 10.1073/pnas.1019002108.

Schroeder, Harry W.; Cavacini, Lisa (2010): Structure and function of immunoglobulins. In *Journal of Allergy and Clinical Immunology* 125 (2), S41–S52. DOI: 10.1016/j.jaci.2009.09.046.

Schuurman, J.; Perdok, G. J.; Gorter, A. D.; Aalberse, R. C. (2001): The inter-heavy chain disulfide bonds of IgG4 are in equilibrium with intra-chain disulfide bonds. In *Mol. Immunol.* 38 (1), pp. 1–8.

Schuurman, J.; van Ree, R.; Perdok, G. J.; Van Doorn, H R; Tan, K. Y.; Aalberse, R. C. (1999): Normal human immunoglobulin G4 is bispecific: it has two different antigen-combining sites. In *Immunology* 97 (4), pp. 693–698.

Schweighofer, Carmen D.; Tuchscherer, Armin; Sperka, Sabine; Meyer, Thorsten; Rattel, Benno; Stein, Sandra et al. (2012): Clinical safety and pharmacological profile of the HLA-DR antibody 1D09C3 in patients with B cell chronic lymphocytic leukemia and lymphoma: results from a phase I study. In *Cancer immunology, immunotherapy : CII* 61 (12), pp. 2367–2373. DOI: 10.1007/s00262-012-1362-x.

Scott, Andrew M.; Allison, James P.; Wolchok, Jedd D. (2012a): Monoclonal antibodies in cancer therapy. In *Cancer Immun.* 12, p. 14.

Scott, Andrew M.; Wolchok, Jedd D.; Old, Lloyd J. (2012b): Antibody therapy of cancer. In *Nat Rev Cancer* 12 (4), pp. 278–287. DOI: 10.1038/nrc3236.

Scott-Taylor, Timothy H.; Axinia, Stefan-Claudiu; Amin, Sumeya; Pettengell, Ruth (2017): Immunoglobulin G; structure and functional implications of different subclass modifications in initiation and resolution of allergy. In *Immunity, inflammation and disease. DOI:* 10.1002/iid3.192.

Senter, Peter D.; Sievers, Eric L. (2012): The discovery and development of brentuximab vedotin for use in relapsed Hodgkin lymphoma and systemic anaplastic large cell lymphoma. In *Nature biotechnology* 30 (7), pp. 631–637. DOI: 10.1038/nbt.2289.

Sgro, C. (1995): Side-effects of a monoclonal antibody, muromonab CD3/orthoclone OKT3. Bibliographic review. In *Toxicology* 105 (1), pp. 23–29. DOI: 10.1016/0300-483X(95)03123-W.

Shefet-Carasso, LeeRon; Benhar, Itai (2015): Antibody-targeted drugs and drug resistance--challenges and solutions. In *Drug resistance updates : reviews and commentaries in antimicrobial and anticancer chemotherapy* 18, pp. 36–46. DOI: 10.1016/j.drup.2014.11.001.

Shteingauz, Anna; Ilan, Neta; Vlodavsky, Israel (2014): Processing of heparanase is mediated by syndecan-1 cytoplasmic domain and involves syntenin and α-actinin. In *Cellular and molecular life sciences : CMLS* 71 (22), pp. 4457–4470. DOI: 10.1007/s00018-014-1629-9.

Smyth, M. J.; Godfrey, D. I.; Trapani, J. A. (2001): A fresh look at tumor immunosurveillance and immunotherapy. In *Nat. Immunol.* 2 (4), pp. 293–299. DOI: 10.1038/86297.

Stackpole, C. W.; Cremona, P.; Leonard, C.; Stremmel, P. (1980): Antigenic modulation as a mechanism for tumor escape from immune destruction: identification of modulation-positive and modulation-negative mouse lymphomas with xenoantisera to murine leukemia virus gp70. In *J. Immunol.* 125 (4), pp. 1715–1723.

Sun, Ren-Xiao; Lu, Zhao-Yang; Wijdenes, John; Brochier, Jean; Hertog, Catherine; Rossi, Jean-François; Klein, Bernard (1997): Large scale and clinical grade purification of syndecan-1+ malignant plasma cells. In *J. Immunol. Methods* 205 (1), pp. 73–79. DOI: 10.1016/S0022-1759(97)00056-2.

Suresh, M. R.; Cuello, A. C.; Milstein, C. (1986a): Advantages of bispecific hybridomas in one-step immunocytochemistry and immunoassays. In *Proc. Natl. Acad. Sci. U.S.A.* 83 (20), pp. 7989–7993.

Suresh, M. R.; Cuello, A. C.; Milstein, C. (1986b): Bispecific monoclonal antibodies from hybrid hybridomas. In *Methods in enzymology* 121, pp. 210–228.

Szymczak, Andrea L.; Vignali, Dario A. A. (2005): Development of 2A peptide-based strategies in the design of multicistronic vectors. In *Expert Opin. Biol. Ther.* 5 (5), pp. 627–638. DOI: 10.1517/14712598.5.5.627.

Tao, M. H.; Smith, R. I.; Morrison, S. L. (1993): Structural features of human immunoglobulin G that determine isotype-specific differences in complement activation. In *J. Exp. Med.* 178 (2), pp. 661–667.

Tarhini, Ahmad; Lo, Ernest; Minor, David R. (2010): Releasing the brake on the immune system: ipilimumab in melanoma and other tumors. In *Cancer biotherapy & radiopharmaceuticals* 25 (6), pp. 601–613. DOI: 10.1089/cbr.2010.0865.

Teicher, Beverly A.; Chari, Ravi V. J. (2011): Antibody conjugate therapeutics: challenges and potential. In *Clinical cancer research : an official journal of the American Association for Cancer Research* 17 (20), pp. 6389–6397. DOI: 10.1158/1078-0432.CCR-11-1417.

Torre, Lindsey A.; Bray, Freddie; Siegel, Rebecca L.; Ferlay, Jacques; Lortet-Tieulent, Joannie; Jemal, Ahmedin (2015): Global cancer statistics, 2012. In *CA: a cancer journal for clinicians* 65 (2), pp. 87–108. DOI: 10.3322/caac.21262.

Torre-Amione, G.; Beauchamp, R. D.; Koeppen, H.; Park, B. H.; Schreiber, H.; Moses, H. L.; Rowley, D. A. (1990): A highly immunogenic tumor transfected with a murine transforming growth factor type beta 1 cDNA escapes immune surveillance. In *Proc. Natl. Acad. Sci. U.S.A.* 87 (4), pp. 1486–1490.

Traynor, Kate (2011): Ipilimumab approved for metastatic melanoma. In *American journal of health-system pharmacy : AJHP : official journal of the American Society of Health-System Pharmacists* 68 (9), p. 768. DOI: 10.2146/news110025.

van der Neut Kolfschoten, Marijn; Schuurman, Janine; Losen, Mario; Bleeker, Wim K.; Martínez-Martínez, Pilar; Vermeulen, Ellen et al. (2007): Anti-inflammatory activity of human IgG4 antibodies by dynamic Fab arm exchange. In *Science* 317 (5844), pp. 1554–1557. DOI: 10.1126/science.1144603.

Vanam, Ram P.; Schneider, Michael A.; Marlow, Michael S. (2015): Rapid quantitative analysis of monoclonal antibody heavy and light chain charge heterogeneity. In *MAbs* 7 (6), pp. 1118–1127. DOI: 10.1080/19420862.2015.1085145.

Vázquez-Rey, María; Lang, Dietmar A. (2011): Aggregates in monoclonal antibody manufacturing processes. In *Biotechnology and bioengineering* 108 (7), pp. 1494–1508. DOI: 10.1002/bit.23155.

Vidarsson, Gestur; Dekkers, Gillian; Rispens, Theo (2014): IgG subclasses and allotypes: from structure to effector functions. In *Frontiers in immunology* 5, p. 520. DOI: 10.3389/fimmu.2014.00520.

Walker, P. R.; Saas, P.; Dietrich, P. Y. (1998): Tumor expression of Fas ligand (CD95L) and the consequences. In *Curr. Opin. Immunol.* 10 (5), pp. 564–572.

Wan, Min; Wang, George Y. (1998): Enhanced aggregate removal from bulk biologicals using ion exchange chromatography. Applied for by TANOX INC [US] on 10/13/1998. App. no. US19980170411 19981013. Patent no. US6177548 (B1). C07K1/18;C07K16/06;C07K16/00. Priority no. US19970061842P 19971014;US19980170411 19981013.

Wang, Lintao; Amphlett, Godfrey; Blättler, Walter A.; Lambert, John M.; Zhang, Wei (2005): Structural characterization of the maytansinoid-monoclonal antibody immunoconjugate, huN901-DM1, by mass spectrometry. In *Protein science : a publication of the Protein Society* 14 (9), pp. 2436–2446. DOI: 10.1110/ps.051478705.

Wang, Lu; Hale, Geoff; Ghosh, Raja (2006): Non-size-based membrane chromatographic separation and analysis of monoclonal antibody aggregates. In *Anal. Chem.* 78 (19), pp. 6863–6867. DOI: 10.1021/ac060790g.

Wang, Wei (2005): Protein aggregation and its inhibition in biopharmaceutics. In *International journal of pharmaceutics* 289 (1-2), pp. 1–30. DOI: 10.1016/j.ijpharm.2004.11.014.

Wang, Xinhua; Mathieu, Mary; Brezski, Randall J. (2017): IgG Fc engineering to modulate antibody effector functions. In *Protein & cell. DOI:* 10.1007/s13238-017-0473-8.

Weill, Claire O.; Biri, Stephanie; Erbacher, Patrick (2008): Cationic lipid-mediated intracellular delivery of antibodies into live cells. In *BioTechniques* 44 (7), Pvii-Pxi. DOI: 10.2144/000112832.

Weiner, Louis M.; Surana, Rishi; Wang, Shangzi (2010): Monoclonal antibodies: versatile platforms for cancer immunotherapy. In *Nat. Rev. Immunol.* 10 (5), pp. 317–327. DOI: 10.1038/nri2744.

Weiskopf, Kipp; Weissman, Irving L. (2015): Macrophages are critical effectors of antibody therapies for cancer. In *MAbs* 7 (2), pp. 303–310. DOI: 10.1080/19420862.2015.1011450.

Wijdenes, J.; Dore, J. M.; Clement, C.; Vermot-Desroches, C. (2002): CD138. In *J. Biol. Regul. Homeost. Agents* 16 (2), pp. 152–155.

Wijdenes, J.; Vooijs, W. C.; Clément, C.; Post, J.; Morard, F.; Vita, N. et al. (1996): A plasmocyte selective monoclonal antibody (B-B4) recognizes syndecan-1. In *Br. J. Haematol.* 94 (2), pp. 318–323.

Williams, A. F.; Barclay, A. N. (1988): The immunoglobulin superfamily--domains for cell surface recognition. In *Annu. Rev. Immunol.* 6, pp. 381–405. DOI: 10.1146/annurev.iy.06.040188.002121.

Woof, Jenny M.; Burton, Dennis R. (2004): Human antibody–Fc receptor interactions illuminated by crystal structures. In *Nat Rev Immunol* 4 (2), pp. 89–99. DOI: 10.1038/nri1266.

World Health Organization (WHO) (2017): The top 10 causes of death. Edited by World Health Organization (WHO). Available online at http://www.who.int/mediacentre/factsheets/fs310/en/, updated on January 2017, checked on March, 2nd 2018.

Young, Elizabeth; Lock, Emma; Ward, Douglas G.; Cook, Alexander; Harding, Stephen; Wallis, Gregg L. F. (2014): Estimation of polyclonal IgG4 hybrids in normal human serum. In *Immunology* 142 (3), pp. 406–413. DOI: 10.1111/imm.12265.

Yu, Y.; Schurpf, T.; Springer, T. A. (2013): How Natalizumab Binds and Antagonizes 4 Integrins. In *Journal of Biological Chemistry* 288 (45), pp. 32314–32325. DOI: 10.1074/jbc.M113.501668.

Zheng, Kai; Bantog, Christopher; Bayer, Robert (2011): The impact of glycosylation on monoclonal antibody conformation and stability. In *MAbs* 3 (6), pp. 568–576. DOI: 10.4161/mabs.3.6.17922.

7 Appendix

7.1 Vector maps

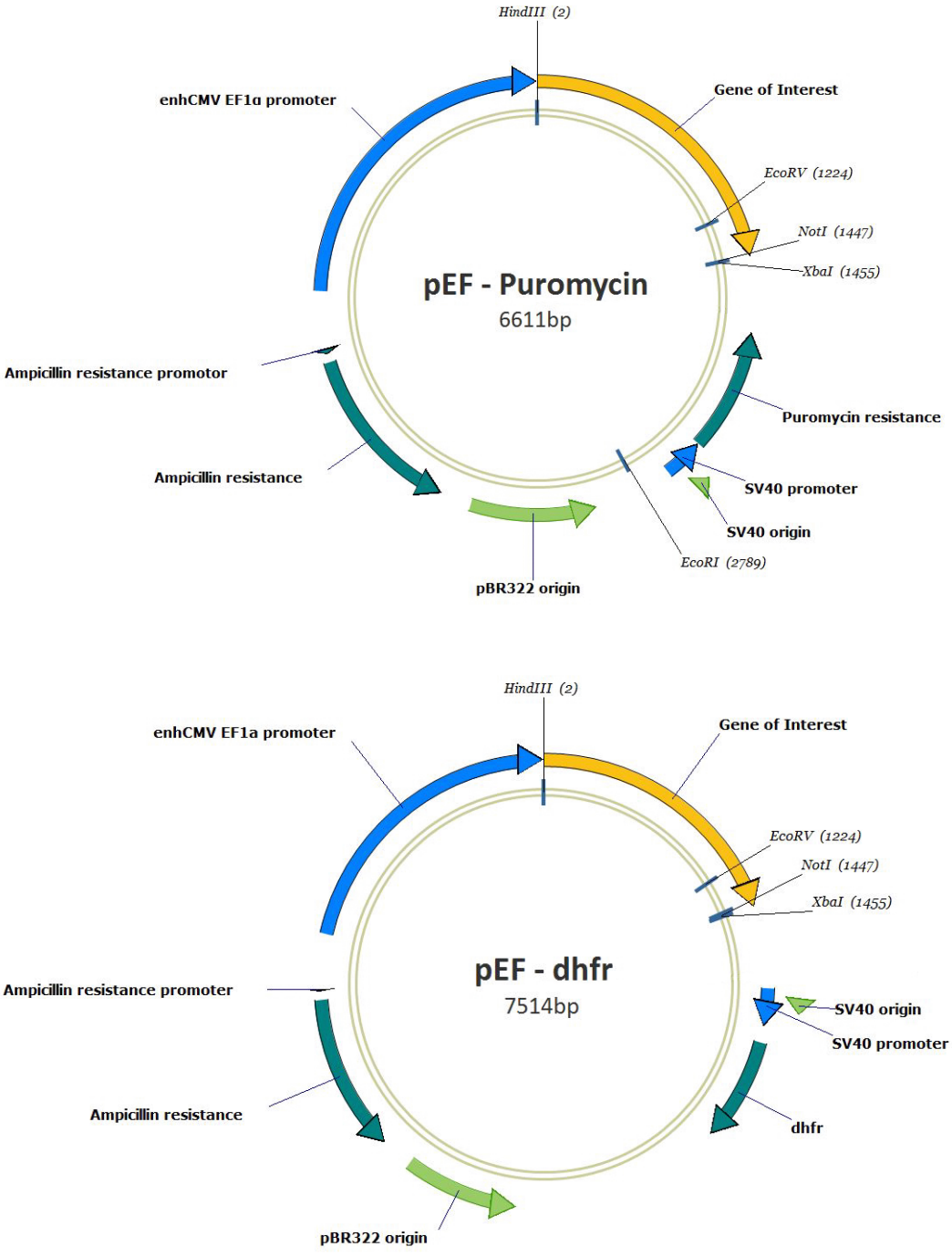

Figure 7-1: Vector maps for nBT062 variant expression.

The orientation of the genes is indicated by the arrow. *HindIII*, *NotI*, *XbaI* are the restriction sites used for cloning. enhCMV EF1α is the eukaryotic promotor for the gene of interest. Ampicillin resistance is used as prokaryotic selection marker. Puromycin or dhfr is used for eukaryotic selection. The SV40 origin provides the origin of replication for eukaryotes and the pBR322 origin provides the origin of replication for prokaryotes.

7.2 Markers for electrophoresis

SeeBlue Plus2 Protein Standard:

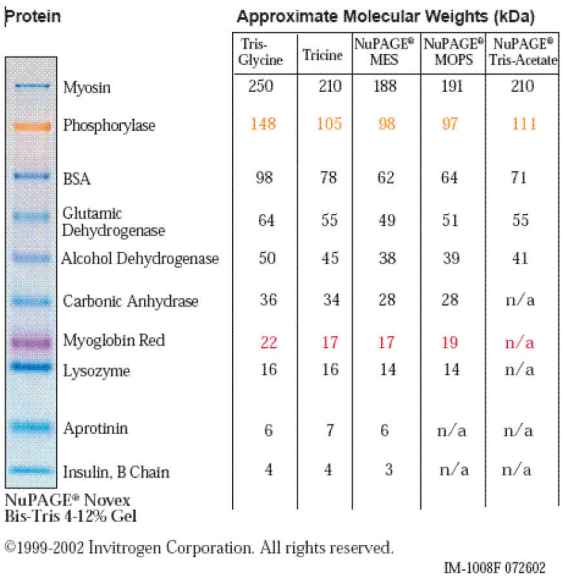

Protein	Approximate Molecular Weights (kDa)				
	Tris-Glycine	Tricine	NuPAGE® MES	NuPAGE® MOPS	NuPAGE® Tris-Acetate
Myosin	250	210	188	191	210
Phosphorylase	148	105	98	97	111
BSA	98	78	62	64	71
Glutamic Dehydrogenase	64	55	49	51	55
Alcohol Dehydrogenase	50	45	38	39	41
Carbonic Anhydrase	36	34	28	28	n/a
Myoglobin Red	22	17	17	19	n/a
Lysozyme	16	16	14	14	n/a
Aprotinin	6	7	6	n/a	n/a
Insulin, B Chain	4	4	3	n/a	n/a

NuPAGE® Novex
Bis-Tris 4-12% Gel

IM-1008F 072602

Source:
https://assets.thermofisher.com/TFS-Assets/LSG/figures/LC5925-chart.jpg-650.jpg

Serva IEF Marker pH 3-10:

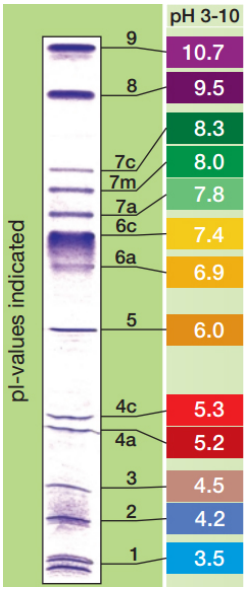

source:
http://tools.lifetechnologies.com/content/sfs/manuals/IEFmarker_card.pdf

7.3 Supplementary information for section 4.4.3

Table 7-1: Binding of nBT062 variants to Ba/F3-hCD138 cells - Statistical analysis.

Normalized nonlin fit: P-values of LogEC50 comparision	WT nBT062	Stable nBT062	Half nBT062	Bispecific nBT062-natalizumab	WT nBT062-DM4	Stable nBT062-DM4	Half nBT062-DM4	Bispecific nBT062-natalizumab-DM4
WT nBT062		0.2551	0.0013	<0.0001	0.1877	0.2733	0.0404	<0.0001
Stable nBT062			0.0139	<0.0001	0.7805	0.9443	0.2874	<0.0001
Half nBT062				<0.0001	0.0405	0.01	0.1432	<0.0001
Bispecific nBT062-natalizumab					<0.0001	<0.0001	<0.0001	0.1643
WT nBT062-DM4						0.7271	0.4731	<0.0001
Stable nBT062-DM4							0.2478	<0.0001
Half nBT062-DM4								<0.0001
Bispecific nBT062-natalizumab-DM4								

Significant values are shown in green.

Table 7-2: Binding of nBT062 variants to NCI-H929 cells - Statistical analysis.

Normalized nonlin fit: P-values of LogEC50 comparision	WT nBT062	Stable nBT062	Half nBT062	Bispecific nBT062-natalizumab	WT nBT062-DM4	Stable nBT062-DM4	Half nBT062-DM4	Bispecific nBT062-natalizumab-DM4
WT nBT062		0.195	0.0587	<0.0001	0.1116	0.0665	0.0259	<0.0001
Stable nBT062			0.5385	<0.0001	0.7467	0.5504	0.3295	<0.0001
Half nBT062				<0.0001	0.7768	0.9997	0.7151	<0.0001
Bispecific nBT062-natalizumab					<0.0001	<0.0001	<0.0001	0.5873
WT nBT062-DM4						0.7828	0.5214	<0.0001
Stable nBT062-DM4							0.7233	<0.0001
Half nBT062-DM4								<0.0001
Bispecific nBT062-natalizumab-DM4								

Significant values are shown in green.

Table 7-3: Binding affinities of unconjugated or DM4 conjugated nBT062 variants - individual experiments.

Cells	DM4-conjugate	WT nBT062				Stable nBT062				Half nBT062				Bispecific nBT062-natalizumab				natalizumab			
		1.	2.	3.	average	1.	2.	3.	average	1.	2.	3.	average	1.	2.	3.	average	1.	2.	3.	average
NCI-H929	No	1.13E-09	1.38E-09	9.84E-10	1.16E-09	1.56E-09	1.92E-09	1.24E-09	1.57E-09	2.12E-09	2.29E-09	1.22E-09	1.88E-09	1.07E-08	8.30E-09	8.71E-09	9.25E-09	4.73E-10	4.94E-10	4.03E-10	4.57E-10
NCI-H929	Yes	1.75E-09	2.00E-09	1.28E-09	1.68E-09	1.82E-09	2.14E-09	1.41E-09	1.79E-09	2.12E-09	2.44E-09	1.51E-09	2.02E-09	7.40E-09	8.87E-09	7.40E-09	7.89E-09				
BaF3-hCD138	No	5.10E-10	4.14E-10	7.13E-10	5.46E-10	5.71E-10	6.28E-10	9.17E-10	7.05E-10	9.91E-10	1.07E-09	1.30E-09	1.12E-09	2.78E-08	1.91E-08	2.08E-08	2.26E-08				
BaF3-hCD138	Yes	4.71E-10	6.34E-10	1.08E-09	7.28E-10	4.86E-10	6.24E-10	9.89E-10	7.00E-10	6.72E-10	7.89E-10	1.24E-09	9.00E-10	1.58E-08	1.53E-08	2.27E-08	1.79E-08				
Jurkat	No													2.16E-09	2.07E-09	1.93E-09	2.05E-09		3.03E-10	4.90E-10	3.97E-10

7.4 Supplementary information for section 4.5

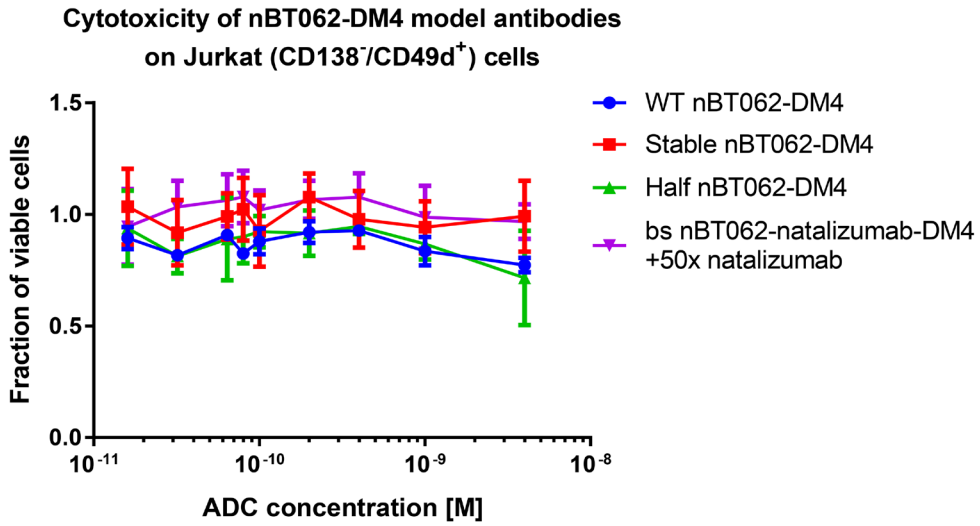

Figure 7-2: Cytotoxicity curves of Jurkat cells incubated with nBT062-DM4 variants.

Jurkat cells ($CD138^+/CD49d^+$) were incubated with different concentrations (4, 1, 0.4, 0.2, 0.1 0.06, 0.04, 0.02, 0.01, 0 nM) of WT nBT062-DM4, stable nBT062-DM4, half nBT062-DM4 or bispecific nBT062-natalizumab-DM4, as indicated in the presence or absence of an excess of natalizumab. After 5 days of incubation, a WST-1 assay was used to determine the viability. Concentration dependent inhibition curves are shown. No cytotoxicity was detected for the concentrations tested.

7.5 Supplementary information for section 4.6

Table 7-4: Body weight loss and survival rates from MAXF 1322 xenograft mouse experiment.

Group ID	Therapy	Dose Level [mg/kg/day]	Last Day of Group	Max. Median BWL [%] (Day) [1]	Overall Survival Rate [2]	Euthanasia for Tumor-Related Reasons (Day)	Adjusted Survival Rate [3]	Other Deaths / Euthanasia (Day)
1	Vehicle Control	10 ml/kg	51	1.0 (2)	0 / 5 (0%)	5 x ATV > 2000 mm³ (23,27,27,44,51)	100%	-
2	IVIg	10 ml/kg	37	0.3 (2)	0 / 5 (0%)	4 x ATV > 2000 mm³ (23,30,37,37) 1 x accessory tumor (23)	100%	-
3	WT BT062-DM4	4	86	1.9 (2)	4 / 5 (80%)	-	80%	1 x labored breathing (48); Necropsy
4	Stable BT062-DM4	4	86	0.3 (2)	5 / 5 (100%)	-	100%	-
5	Half BT062-DM4	4	86	n.r.	5 / 5 (100%)	-	100%	-
6	Bispecific BT062-natalizumab-DM4	4	71	n.r.	0 / 5 (0%)	4 x ATV > 2000 mm³ (27,37,41,71)	80%	1 x ongoing BWL >2 days (8)
7	IVIg // WT BT062-DM4	10 ml/kg // 4	86	0.6 (27)	5 / 5 (100%)	-	100%	-
8	IVIg // Stable BT062-DM4	10 ml/kg // 4	86	1.5 (2)	5 / 5 (100%)	-	100%	-
9	IVIg // Half BT062-DM4	10 ml/kg // 4	86	n.r.	4 / 5 (80%)	1 x ATV > 2000 mm³ (76)	100%	-
10	IVIg // Bispecific BT062-natalizumab-DM4	10 ml/kg // 4	44	1.3 (2)	0 / 5 (0%)	5 x ATV > 2000 mm³ (23,27,34,37,44)	100%	-
11	WT BT062-DM4	2	86	n.r.	4 / 5 (80%)	1 x ATV > 2000 mm³ (37)	100%	-
12	Stable BT062-DM4	2	86	n.r.	5 / 5 (100%)	-	100%	-
13	Half BT062-DM4	2	86	n.r.	3 / 5 (60%)	2 x ATV > 2000 mm³ (79,83)	100%	-
14	Bispecific BT062-natalizumab-DM4	2	37	n.r.	0 / 5 (0%)	4 x ATV > 2000 mm³ (27,27,37,37) 1 x ulcerating tumor (20)	100%	-
15	IVIg // WT BT062-DM4	10 ml/kg // 2	48	0.7 (2)	0 / 5 (0%)	5 x ATV > 2000 mm³ (23,27,44,48,48)	100%	-
16	IVIg // Stable BT062-DM4	10 ml/kg // 2	86	1.9 (2)	3 / 5 (60%)	2 x ATV > 2000 mm³ (23,55)	100%	-
17	IVIg // Half BT062-DM4	10 ml/kg // 2	76	9.4 (41)	0 / 5 (0%)	5 x ATV > 2000 mm³ (23,30,37,55,76)	100%	-
18	IVIg // Bispecific BT062-natalizumab-DM4	10 ml/kg // 2	48	1.1 (30)	0 / 5 (0%)	5 x ATV > 2000 mm³ (16,23,27,34,48)	100%	-

[1] Day on which the minimum median body weight was recorded; n.r., not relevant, no body weight loss recorded (i.e. group median RBWs always >100%). [2] Number of animals that would have survived beyond the last experimental day over total number of animals in the group. [3] Survival rate adjusted for (i.e. including) all animals that were euthanized for tumor-related reasons.

Table 7-5: Mantel-Cox statistical analysis of animal survival from MAXF 1322 xenograft mouse experiment.

Overall Comparison of Survival Curves
Log-rank (Mantel-Cox) Test

Chi square	89.46
df	17
P value	< 0.0001
P value summary	***
Are the survival curves sig different?	Yes

Mantel-Cox Test of individual groups	Vehicle control	IVIg	WT nBT062 4 mg/kg	stable nBT062 4mg/kg	half nBT062 4 mg/kg	bs nBT062-natalizumab 4 mg/kg	WT nBT062 4 mg/kg + IVIg	stable nBT062 4 mg/kg + IVIg	half nBT062 4 mg/kg + IVIg	bs nBT062-natalizumab 4mg/kg + IVIg	WT nBT062 2 mg/kg	stable nBT062 2 mg/kg	half nBT062 2 mg/kg	bs nBT062-natalizumab 2 mg/kg	WT nBT062 2 mg/kg + IVIg	stable nBT062 2 mg/kg + IVIg	half nBT062 2 mg/kg + IVIg	bs nBT062-natalizumab 2 mg/kg + IVIg
Vehicle control		0.4045 (ns)	0.0022 (**)	0.0018 (**)	0.0018 (**)	0.7891 (ns)	0.0018 (**)	0.0018 (**)	0.0018 (**)	0.5730 (ns)	0.0132 (*)	0.0018 (**)	0.0018 (**)	0.3726 (ns)	0.9787 (ns)	0.0277 (*)	0.2864 (ns)	0.4710 (ns)
IVIg			0.0025 (**)	0.0025 (**)	0.0025 (**)	0.3094 (ns)	0.0025 (**)	0.0025 (**)	0.0025 (**)	0.5918 (ns)	0.0079 (**)	0.0025 (**)	0.0025 (**)	0.9528 (ns)	0.1396 (ns)	0.0271 (*)	0.4479 (ns)	0.9400 (ns)
WT nBT062 4 mg/kg				0.3173 (ns)	0.3173 (ns)	0.0064 (**)	>0.9999 (ns)	0.3173 (ns)	0.9372 (ns)	0.0018 (**)	0.9372 (ns)	0.3173 (ns)	0.6071 (ns)	0.0026 (**)	0.0082 (**)	0.5203 (ns)	0.0127 (*)	0.0044 (**)
stable nBT062 4mg/kg					>0.9999 (ns)	0.0018 (**)	>0.9999 (ns)	>0.9999 (ns)	0.3173 (ns)	0.0018 (**)	0.3173 (ns)	>0.9999 (ns)	0.1343 (ns)	0.0026 (**)	0.0027 (**)	0.1343 (ns)	0.0018 (**)	0.0018 (**)
half nBT062 4 mg/kg						0.0018 (**)	>0.9999 (ns)	>0.9999 (ns)	0.3173 (ns)	0.0018 (**)	0.3173 (ns)	>0.9999 (ns)	0.1343 (ns)	0.0026 (**)	0.0027 (**)	0.1343 (ns)	0.0018 (**)	0.0018 (**)
bs nBT062-natalizumab 4mg/kg							0.0018 (**)	0.0018 (**)	0.0018 (**)	0.5670 (ns)	0.0143 (*)	0.0018 (**)	0.0018 (**)	0.2916 (ns)	0.8596 (ns)	0.0607 (ns)	0.5852 (ns)	0.4412 (ns)
WT nBT062 4 mg/kg + IVIg								>0.9999 (ns)	0.3173 (ns)	0.0018 (**)	0.3173 (ns)	>0.9999 (ns)	0.1343 (ns)	0.0026 (**)	0.0027 (**)	0.1343 (ns)	0.0018 (**)	0.0018 (**)
stable nBT062 4mg/kg + IVIg									0.3173 (ns)	0.0018 (**)	0.3173 (ns)	>0.9999 (ns)	0.1343 (ns)	0.0026 (**)	0.0027 (**)	0.1343 (ns)	0.0018 (**)	0.0018 (**)
half nBT062 4 mg/kg + IVIg										0.0018 (**)	0.9372 (ns)	0.3173 (ns)	0.6071 (ns)	0.0026 (**)	0.0027 (**)	0.4261 (ns)	0.004 (**)	0.0018 (**)
bs nBT062-natalizumab 4mg/kg + IVIg											0.0088 (**)	0.0018 (**)	0.0018 (**)	0.5952 (ns)	0.2077 (ns)	0.0273 (*)	0.2799 (ns)	0.9307 (ns)
WT nBT062 2 mg/kg												0.3173 (ns)	0.6071 (ns)	0.0084 (**)	0.0251 (*)	0.5203 (ns)	0.0143 (*)	0.0064 (**)
stable nBT062 2 mg/kg													0.1343 (ns)	0.0026 (**)	0.0027 (**)	0.1343 (ns)	0.0018 (**)	0.0018 (**)
half nBT062 2 mg/kg														0.0026 (**)	0.0027 (**)	0.7987 (ns)	0.0018 (**)	0.0018 (**)
bs nBT062-natalizumab 2 mg/kg															0.1368 (ns)	0.0348 (*)	0.2151 (ns)	0.9371 (ns)
WT nBT062 2 mg/kg + IVIg																0.0346 (*)	0.4644 (ns)	0.3702 (ns)
stable nBT062 2 mg/kg + IVIg																	0.0768 (ns)	0.0206 (*)
half nBT062 2 mg/kg + IVIg																		0.1642 (ns)
bs nBT062-natalizumab 2 mg/kg + IVIg																		

ns= not significant

8 Acknowledgment

Removed for privacy reasons.

Curriculum vitae

Removed for privacy reasons.

Removed for privacy reasons.

ERKLÄRUNG

Ich versichere hiermit, dass ich meine Dissertation

„**Influence of the *in vivo* half-antibody exchange on the therapeutic efficacy of an IgG4 antibody-drug conjugate"**

selbstständig, ohne unerlaubte Hilfe und mich dabei keiner anderen als der von mir ausdrücklich bezeichneten Quellen und Hilfen bedient habe. Die Dissertation wurde in der jetzigen oder einer ähnlichen Form noch bei keiner anderen Hochschule eingereicht und hat noch keinen sonstigen Prüfungszwecken gedient.

Marburg, _____ _____

Ort, Datum Peter Herbener